EXPERIMENTAL AND THEORETICAL INVESTIGATION OF SHALE-FLUID INTERACTIONS FOR DRILLING APPLICATIONS

BY

MOHAMMED KHALID AL-ARFAJ

A Dissertation Presented to the

DEANSHIP OF GRADUATE STUDIES

KING FAHD UNIVERSITY OF PETROLEUM & MINERALS

DHAHRAN, SAUDI ARABIA

In Partial Fulfillment of the

Requirements for the Degree of

DOCTOR OF PHILOSOPHY

In

PETROLEUM ENGINEERING

MAY 2017

KING FAHD UNIVERSITY OF PETROLEUM & MINERALS

DHAHRAN- 31261, SAUDI ARABIA

DEANSHIP OF GRADUATE STUDIES

This thesis, written by Mohammed Khalid Al-Arfaj under the direction of his thesis advisor and approved by his thesis committee, has been presented and accepted by the Dean of Graduate Studies, in partial fulfillment of the requirements for the degree of **DOCTOR OF PHILOSOPHY IN PETROLEUM ENGINEERING.**

Dr. Abdulazeez Abdulraheem
(Advisor)

Dr. Dhafer Al-Shehri
Department Chairman

Dr. Abdullah Sultan
(Co-Advisor)

Dr. Salam A. Zummo
Dean of Graduate Studies

Prof. Ibnelwaleed Hussein
(Member)

25/9/17
Date

Prof. Sidqi Abu-Khamsin
(Member)

Dr. Md. Amanullah
(Member)

Dedicated to my Father, Mother and Wife

ACKNOWLEDGEMENTS

First, all praise and sincere thanks to the Almighty ALLAH, the most gracious the most merciful for all the blessings, all the support and all the patience that ALLAH empowered me with to survive this long journey of study and research. Second, peace and blessings be upon Mohammed, the messenger of ALLAH who encouraged everyone to learn and said: "He who shall *pursue* the *path* of knowledge, ALLAH will direct *him* to the *path* of *Paradise*".

I would like to express my sincere gratitude to my parents for the support and guidance through my early and current studies. I wish to thank my thesis advisor Dr. Abdulazeez Abdulraheem for his involved supervision and valuable feedback. Special and exceptional thanks to my thesis co-advisor Dr. Abdullah Sultan for his complete support and time in every aspect of this research whether it is experimental or molecular simulation. I would like to thank Prof. Ibnelwaleed Hussein for his time and critical feedback that significantly improved and enhanced the outcomes of this work. Thanks to Dr. Amanullah for all the knowledge and experience he shared with me during this study to achieve my objectives. Many thanks also go to Prof. Sidqi Abu-Khamsin for his thorough feedback and guidance that helped to complete this work.

Thanks to my wife, children, brothers and all family members for their patience and support throughout this seven-year journey. I would like also to thanks my colleagues in KFUPM and Saudi Aramco who helped me in different aspects of this work. Special thanks go to Hamad Al-Kharaa, Saad Al-Mutairi, Khalid Zidan, Abdulkareem Al-Sofi, Syed Rizwanullah, Mohammed Al-Tahir, Zaid Janghda and many others to whom I owe a debt of gratitude for all their help and valuable cooperation.

TABLE OF CONTENTS

LIST OF TABLES

LIST OF FIGURES

LIST OF ABBREVIATIONS

CEC	:	Cation Exchange Capacity
CST	:	Capillary Suction Time
CT	:	Computed Tomography
MD	:	Molecular Dynamics
NMR	:	Nuclear Magnetic Resonance
NPT	:	Constant particles number, pressure and temperature ensemble
SEM	:	Scanning Electron Microscopy
TGA	:	Thermogravimetric Analysis
XRD	:	X-ray diffraction
XRF	:	X-ray fluorescence

ABSTRACT

Full Name : [Mohammed Khalid Al-Arfaj]

Thesis Title : [Theoretical and Experimental Investigation of Shale-Fluid Interactions for Optimized Drilling Practices]

Major Field : [Petroleum Engineering]

Date of Degree: [May 2017]

Problems and challenges encountered while drilling through shale are well documented in literature. Shale formations with high content of clay are highly reactive in water-based drilling fluids. The use of water-based drilling fluids to drill shale formations can cause wellbore instability problems as a result of the reaction of water with clay minerals. Examples of wellbore instability problems include shale disintegration, swelling and sloughing. Consequently, there will be higher solids loading in the wellbore. Hence, the chance to get pipe stuck increases and the hole cleaning efficiency of drilling fluid decreases significantly. In this work, one laterally-extensive shale formation in the Kingdom of Saudi Arabia is studied utilizing experimental and modeling techniques. Four samples from different locations were collected and analyzed and results showed significant heterogeneity in that formation. Characterization scheme consisted of three stages: (i) imaging and topographical studies, (ii) mineralogical, elemental and organic content studies and (iii) shale reactivity studies. This was supported by investigating the moisture content and adsorption potential of the samples. Imbibition study was carried out using Nuclear Magnetic Resonance (NMR) to explain the imbibition of different fluids into shale pore network. In addition, inhibition performance testing was carried out to study the swelling and dispersion characteristics of the shale samples. It was found that the main clay type in downhole samples is

illite and illite-smectite mixed layer. While illite does not have strong tendency to swelling, illite-smectite showed high level of swelling when tested experimentally. Moreover, Molecular modeling technique was utilized to provide theoretical background on the rock-fluid interactions at molecular scale. Molecular dynamics simulation was conducted to study the behavior of illite-smectite mixed layer that exists in abundance in the tested shale formation samples. Results of total energy simulated values showed agreement with those that were generated using first principle calculations. Also, modeling the interlayer spacing revealed the swelling behavior of this mixed layer upon hydration. The approach used in this study provides a basis upon which the design of drilling fluids can be optimized to mitigate wellbore instability issues.

ملخص الرسالة

الاسم الكامل: محمد بن خالد العرفج

عنوان الرسالة: دراسة نظرية ومختبرية للتفاعلات بين التربة الطينية والسوائل لحل مشاكل حفر الآبار

التخصص: هندسة البترول

تاريخ الدرجة العلمية: مايو 2017

تعتبر مشاكل الحفر لطبقات الصخور الطينية، القابلة للانتفاخ أو التحلل والذوبان، من المواضيع المهمة التي تم بحثها بشكل مكثف. هذا النوع من الصخور قابل للتفاعل بشكل كبير عند تعرضه لسوائل الحفر المائية. ونتيجة لهذا التفاعل، تحدث مشاكل في ثبات الصخور المحفورة بسبب انتفاخها أو تحللها وذوبانها. وبالتالي، يكون هناك تركيز عال من فتات الصخور في البئر مما يؤدي إلى زيادة احتمالية حدوث انحشار لعمود الحفر. في هذا البحث، تمت دراسة طبقة صخور طينية متواجدة في المملكة العربية السعودية بشكل ممتد أفقيا ليشمل مناطق نشطة في الحفر والإنتاج. تم أخذ أربعة عينات من طبقة "قصيباء" وعمل اختبارات عدة لتشخيصها وتوصيفها مما يساعد في اقتراح حلول عملية لمشاكل الحفر فيها. احتوى الجزء التوصيفي من هذه الدراسة على ثلاثة مراحل مختبرية: دراسة تصويرية للسطح والتضاريس، ثم دراسة التكوين العنصري والمعدني، وأخيرا دراسة مدى القابلية للتفاعل. بعد ذلك تم استخدام جهاز الرنين المغناطيسي لدراسة كيفية انتشار وتقدم السوائل داخل الفراغات الصخرية. وفي مرحلة لاحقة تم إجراء الاختبارات لقياس مدى انتفاخ أو تحلل العينة الصخرية عند تعرضها للسوائل المائية. من ناحية أخرى، فقد تم عمل المحاكاة الجزيئية للمعادن الفعالة المكونة لهذه الصخور من أجل فهم كيفية تفاعلها مع الماء على مستوى الجزيئات. هذه المحاكاة تعطي فهما أفضل لطبيعة التفاعلات من ناحية نظرية لشرح أسباب فعالية مادة كيميائية معينة في مقاومة مشاكل الحفر لنوع معين من الصخور. بعد

دراسة العينات الصخرية، تبين أن نوع الطين الرئيسي المتواجد هو (illite) و (illite-smectite). بينما لا يبدي الـ (illite) قابلية للانتفاخ، فإنه وعلى العكس من ذلك يظهر الـ (illite-smectite) قدرا أعلى من الانتفاخ تحت الدراسة المختبرية. ولذلك تم عمل المحاكاة الجزيئية للـ (illite-smectite) لدراسة كيفية تفاعل وانتفاخ هذا المعدن الطيني المتواجد بنسب كبيرة في العينات المختارة. إن المقاربة المتبعة في هذا البحث تقدم أرضية مناسبة لتحسين طرق الحفر في المستقبل لتقليص فرص حدوث مشاكل في ثبات الصخور والآبار.

CHAPTER 1

INTRODUCTION

Interactions of reactive shales with the fluid phase of conventional water-based muds usually causes serious changes in physio-chemical and mechanical properties of the shale due to the degradation of the fabrics and structures of the shale matrix. Therefore, conventional water-based drilling muds usually create different types of problems when drilling shale formations (Chenevert 1970, Kendal and Norton, 1974, Wilcox et al. 1987) leading to an increase in mud and mud management cost. It was estimated that 10 to 20 % of the total well drilling cost is lost due to wellbore instability problems and 80 to 90 % of instability problems are encountered when drilling shale formations (Santarelli et al., 1992).

A quite high percentage of the formations drilled worldwide are shale formations with a high sensitivity to water-based muds. These formations contain high clay content and, therefore, associated wellbore instability problems are triggered (Steiger, 1992). While conventional shale formations are the source rock for oil and gas, unconventional shale formations are the source rock and the reservoir at the same time. The well is drilled and completed into the shale zone.

Excessive non-productive time associated with drilling problematic shale zones necessitates the efforts and studies to overcome drilling challenges. Numerous attempts have been carried out in the past to solve and mitigate shale drilling problems especially those shales with high clay content. Different approaches have been used ranging from characterizing shale samples and testing different shale inhibitors and stabilizers, to studying the chemistry of reactive clays and geological structures and also fluid diffusion into shale pore network while other researchers, more recently, have been utilizing molecular modeling software to study the

theory behind shale-fluid interactions. Integration of these different approaches, where results from modeling are combined and validated with the results from laboratory, can help in comprehensive understanding of the shale-fluid interactions.

Depending on the types of clays present in a shale rock and the type of contacting fluid, the shale sample may behave in different manners. There are four main clay groups that are found frequently in shale formations: kaolinite, smectite, illite and chlorite. In general, shales with high percentage of kaolinite tend to disperse and disintegrate while those with high percentage of smectite tend to swell and increase in volume when they come in contact with the fluid, especially fresh water. Factors playing role include but not limited to: clay structure, cation exchange capacity, fluid type and salinity, cations types and positions, as well as geomechanics from mechanical point of view.

1.1 Background

As a solution to the high reactivity of shale with water-based muds, oil-based muds have been used to achieve more stable boreholes. Different types of oil-based muds such as invert emulsion and all-oil muds have been used to drill these formations with minimal instability problems. Oil-based muds work by wetting of the wellbore with an oil film to prevent interaction with the surrounding or internal water phase. Due to negative osmotic effect of the salinity of water phase in the invert emulsion mud, the diffusion of water into the shale formation is prevented or reduced significantly. This is due to the flow of water from the shale matrix to the wellbore as a result of the osmotic effect that hinders the flow of fluid from the wellbore to the shale matrix under the action of capillary suction and overbalance pressure (Tan et al. 2002). Hence, hydration of reactive shales will be significantly reduced in the presence of OBMs

(Chenevert, 1969). However, several factors limited the application of oil-based muds such as environmental impact, disposal cost, handling problems, formation evaluation tools compatibility and the high cost of oil-based muds. Moreover, when loss circulation is anticipated while drilling, the use of OBMs can not usually be justified. Furthermore, the increasingly strict environmental rules and regulations to protect the global environment make the use of oil-based mud very limited for sensitive environments.

While OBM is rarely acceptable for sensitive environments, conventional water-based drilling fluids do not perform well when drilling problematic geological formations (Amanullah, 2007, Chenevert 1970, Simpson et al. 1989, Ballard et al., 1992). Especially designed inhibitive water-based muds are used to mitigate the problems encountered while drilling these formations. These drilling fluids contain different shale inhibitors to isolate the reactive shale surfaces or prevent the infiltration of water into the shale matrix or neutralize the negative and/or positive charges of reactive clay surfaces. Hence, when drilling clay-rich formations, such as shale, these water-based drilling fluids prevent swelling of clays and loss of shale matrix compressive strength by eliminating or minimizing the shale-drilling fluid interactions.

The severity and frequency of borehole instability problems are governed by the degree of clay sensitivity and the performance of the inhibitive mud to avoid short as well as long term shale-drilling fluid interactions. Inhibitive drilling muds that are able to prevent the swelling, hydration, degradation of mechanical properties of shale formation for a short period are not necessarily effective in providing long term stability of reactive shale. Amanullah (1993) highlighted the importance of long term inhibition potential of shale inhibitors in avoiding time dependent borehole instability problems. Highly durable shale inhibitors can protect the shale matrix from the detrimental action of drilling mud for a long time and thus can prevent time-

dependent borehole instability problems.

When clay-rich rocks are exposed to water, they start to react and behave like unconsolidated rocks. The extent of reaction, the mechanism and the consequences differ from one type of clay to another. Kaolinite clay has more tendency to dispersion while smectite clay has more tendency to swelling. Depending on the clay mineralogy, the response of every shale zone is usually different when exposed to water.

It is important to characterize shales in terms of morphology and mineralogy in order to understand the mechanisms of shale-drilling fluid interactions when exposed to water-based drilling muds. Evaluation of shale-drilling fluid interactions is essential in mitigating wellbore instability problems attributed to shale reactivity and sensitivity. Different standard and non-standard experimental methods are available in the industry to assess shale reactivity and predict potential problems in advance. Based on this, inhibition mechanisms can be utilized to inhibit shale-water interaction and reduce the non-productive time associated with reactive shale formations.

This study is carried out on four different shale samples from Qusaiba formation which is main shale formation encountered in drilling unconventional resources. Qusaiba formation is part of the Qalibah group from the Silurian period, Figure 1. Lithology mainly consists of clay, sand and silt. The formation has five cartographic units, Figure 2. (Halawani, 2013) The first unit from the bottom is about 82 feet composed of pale-gray and white to pink clayey siltstone, fine-grained micaceous sandstone with interbeds of siltstone. The second unit is 233 feet composed of clayey siltstone, micaceous siltstone and fine-grained sandstone interbedded with silty claystone. The third unit is 131 ft composed of homogeneous dark micaceous/silty claystone with minor fine-grained sandstone which is in parallel bedding, fine to medium-grained sandstone

interbedded with clayey siltstone. The fourth unit is 82 feet composed of silty claystone interbedded with fine-grained sandstone. The fifth unit is 360 feet composed of clayey siltstone, clayey sandstone and fine-grained sandstone.

While depositional environment of the fifth unit has four thinner cycles where the distal clayey siltstone is less extensively developed and the proximal sandstone is from the middle-to-upper shore face domain, the first four units consist of cycles of transgression and regression. Composed of clayey siltstone deposits, the transgressive cycle developed in distal, lower-to-upper offshore domain while the regressive cycle is composed of deposits existing as upper-middle to proximal offshore sandstone facies. The regressive character of Qusaiba is shown by the regressive facies and the decrease in cycle thickness. (Zalasiewicz, 2007)

1.2 Research objectives

Understanding shale-fluid interactions is a crucial element in the pursuit to tackle and mitigate shale drilling problems. Different approaches and methods have been implemented to give insights into the adsorption, swelling and dispersion of shale particles when exposed to aqueous fluids. It is essential to investigate the behavior of pure clays and how they can impact the shale-fluid interactions as the clay particles are the main active ingredients in the shale rocks.

Previous work in the area of mitigating shale drilling problems mainly concentrated on the shale inhibition performance of several shale inhibitors using laboratory testing methods for evaluation of shale swelling, dispersion and hardness. In addition, for shale formations in Saudi Arabia, there is lack of shale characterization studies for drilling applications.

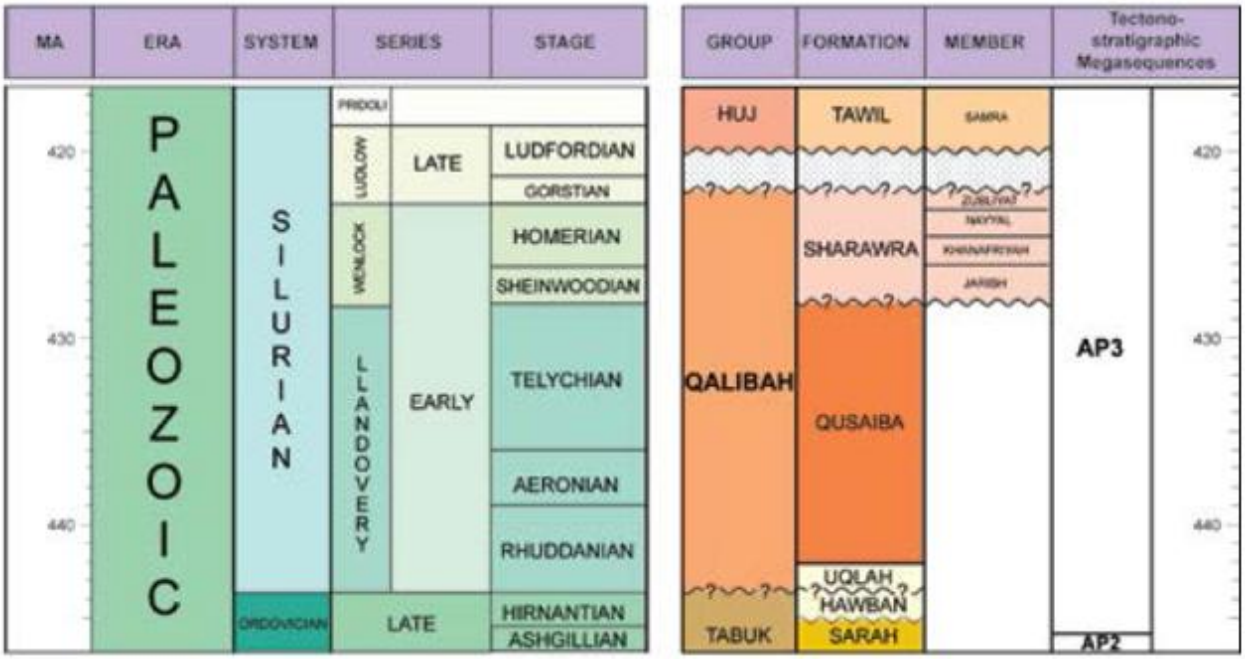

Figure 1: Geological time and lithostratigraphy of Qalibah group (After Halawani, 2013)

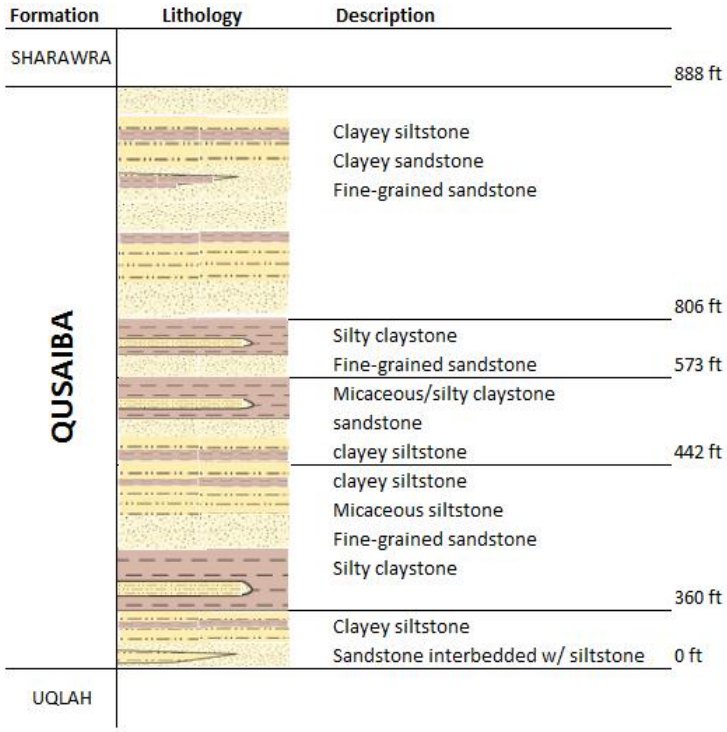

Figure 2: Composite section Qusaiba formation

For molecular modeling part, extensive research has been carried out on pure types of clays, especially montmorillonite. However, clay mixed layers such as illite-smectite did not receive the same attention although they are available in abundant amounts in shale formations and encountered frequently while drilling. This work investigates the swelling behavior and interlayer structure of K-rectorite with different levels of hydration.

The objectives of this study include:

1) Characterization of four shale samples in terms mineralogy, petrography and reactivity
2) Experimental Investigation of shale-fluid interactions:
    a. Investigation of shale inhibition additives to inhibit swelling and dispersion for each type of shales
    b. Studying the fluid imbibition into shale pore system using nuclear magnetic resonance
3) Understanding shale-fluid interactions using molecular simulation techniques

1.3 Research plan

The research plan covers: studying and characterizing one laterally-extensive shale formation in the kingdom of Saudi Arabia utilizing four samples collected from different locations and depths, conducting shale inhibition performance testing after exposing the shale samples to different types of aqueous fluids and finally performing molecular dynamics modeling to theoretically comprehend the shale-fluid interactions. The proposed activities include the following:

- Characterization scheme consisting of three stages: imaging and topographical studies, then, mineralogical, elemental and organic content studies and finally, shale reactivity studies. Imaging analysis at three different levels was used to study

the shale topography, pore network and the presence of micro-fractures. Furthermore, Initial moisture content is one of the factors controlling the swelling behaviour of shales. Correlating the ultimate swelling percentage to moisture content and other parameters can help in predicting the swelling potential and mitigating any associated problems.

- It is essential to assess the shale samples and their adsorption and swelling potential in order to be proactive and mitigate the scope of shale drilling problems. In addition, assessing the durability of shale inhibition is important to overcome operational drilling problems and avoid the usage of excessive amounts of expensive shale inhibitors. Moreover, the study of diffusion process in shales is essential to understand the special progression of fluids inside shale pore network.
- The clay-fluid interactions of two different models of potassium illite-smectite are investigated by molecular simulation techniques. The parameters that were studied include: total energy, swelling behavior, interlayer structure and the interactions on the atomic level utilizing the distance analysis technique. One advantage of using molecular modeling in this context is to gain better understanding of the rock-fluid interactions from theoretical point-of-view in order to explain why one shale inhibitor works and provide adequate inhibition with one shale sample but does not work properly with another sample. The second advantage is that having insights into the potential rock-fluid interactions can guide the research to include or exclude certain types of shale inhibitors to shorten the trial and error procedure. These advantages provide a basis upon which future drilling fluids planning can be optimized to mitigate wellbore stability issues.

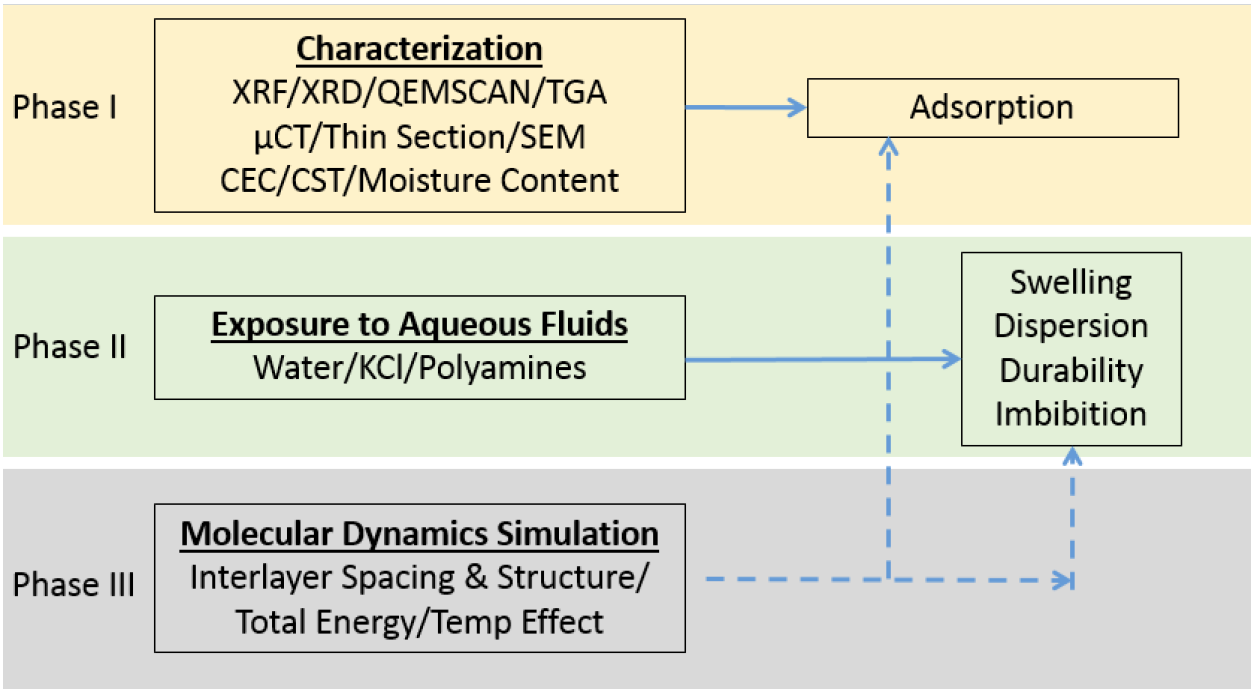
Phase I
Characterization
XRF/XRD/QEMSCAN/TGA
µCT/Thin Section/SEM
CEC/CST/Moisture Content
Adsorption
Phase II
Exposure to Aqueous Fluids
Water/KCl/Polyamines
Swelling
Dispersion
Durability
Imbibition
Phase III
Molecular Dynamics Simulation
Interlayer Spacing & Structure/
Total Energy/Temp Effect

CHAPTER 2

LITERATURE REVIEW

2.1 Shale characterization

Comprehensive characterization of shale samples is necessary to understand and predict their interactions with fluids. It is critical to study the pore structure and shale matrix to explain fluid diffusion into the porous network. Shale characterization includes mineralogy and elemental determination using techniques such as X-ray diffraction (XRD), X-ray fluorescence (XRF) and Quantitative Evaluation of Minerals by Scanning Electron Microscopy (QEMSCAN). In addition, Thermogravimetric Analysis, TGA, is conducted to give indication of the total carbon content, TOC. Characterization also includes the use of imaging techniques such as micro-computed tomography (micro-CT) to look for possible micro-fractures and other features. It also includes thin section analysis and Secondary Electron Microscopy (SEM) to confirm mineralogy, crystal structure and visualize layering and the shape of the clay sheets. Also included in the shale characterization is reactivity measurement based on cation exchange capacity (CEC) and capillary suction time (CST) testing to predict the response of clay to different types of fluids. Adsorption isotherms can be integrated into the characterization scheme to predict the water uptake of shale samples as this has implications on d-spacing between clay sheets and, in turn, on shale swelling.

Micro-CT has being used to visualize the rock sample for the presence of fractures, to study the bedding, if any. It is also conducted for samples prepared to be tested for special core analysis (Josh et. al., 2012). Thin section analysis is the technique utilized to prepare and visualize rock samples under petrographic microscopes. It is mainly carried out to study the petrology of the rock and identify rock forming minerals (Adams, 1984; Scholle, 2003; Loucks,

2007). SEM is used to examine three-dimensional grain relationships, help identify the minerals present and study the distribution of the minerals throughout the rock matrix (Chalmers, 2012; Keller, 2011; Rodriguez, 2014; Chen, 2015; Hazra, 2016). X-ray diffraction has been extensively used to study the mineralogy of shale rocks. (Mooney et al., 1952; Norrish, 1954) The presence of different types of clays gives rise to peaks of different intensities and positions on the 2θ axis. On the other hand, X-ray fluorescence can estimate the elemental composition that can help in interpreting XRD patterns (Tour, 1989). QEMSCAN is the technique used to scan the surface of the sample and generate the mineral composition (Goodall, 2008; Mackay, 2016). Thermogravimetric Analysis (TGA) is used to have indication about the total organic content. Weight loss is monitored while increasing the temperature to study the decomposition of the sample (Awaja and Bhargava, 2006).

There are five main groups of clays: kaolinite, smectite, illite, chlorite and vermiculite with the first three groups being the most relevant groups to the drilling activities. Clay structure consists of sheets containing planes of atoms. These sheets can be tetrahedral or octahedral. In the case of kaolinite, the structure is arranged so that one tetrahedral sheet is followed by one octahedral sheet in a ratio of 1:1. For other types of clays, every octahedral sheet is sandwiched between two tetrahedral sheets in a ratio of 2:1. The clay should be neutral, i.e. number of anions is equal to the number of cations to avoid any interaction with water or water-based muds. If this is not the case, interlayer materials such as individual cations or hydrated cations work to neutralize the clay (Brindley and Brown, 1980). The variation in clay structure can be one of the factors governing the response of each clay type to the hydration process when exposed to water. Every shale sample has some percentage of one or more types of clay in addition to quartz and other minerals. Therefore, the mineralogy of the shale sample determines its response when it

comes in contact with water. While the permeabilities of sandstones, for example, are in the range of Darcy to millidarcy, typical permeabilities of clays are in micro or nano-Darcy range (Deville et. al., 2011).

Understanding adsorption of water molecules onto clay surfaces is essential to explain clay hydration process. Adsorption is the adhesion of atoms, ions and molecules of one phase to a surface. One or more than one layers of hydrate can adhere to surfaces that has bond deficiency.

Johansen and Dunning (1959) studied the water-vapor adsorption on clays. They utilized standard clay samples as well as oil-producing shale samples. It was found that the behaviors of montmorillonite, kaolinite and illite are distinctive and can be used as a characteristic feature for each type of clay. They found strong hysteresis behavior between the adsorption and desorption isotherms for montmorillonite, intermediate hysteresis for illite and no hysteresis for kaolinite, Figure 3. For shale samples, the behavior was dependent on the swelling clays content and water sensitivity.

Parfitt and Greenland (1970) analyzed the adsorption of water by montmorillonite with the presence of polyethylene glycol in terms of the increase in basal spacing and adsorbed water amount. They compared the behavior of calcium montmorillonite and sodium montmorillonite with different concentrations of poly ethylene glycol and found that this additive could not prevent this type of clay from extensive swelling.

Chenevert (1970) conducted a laboratory work utilizing the drilled cuttings to measure the water activity of different shales based on the adsorption characteristics. Isotherms for adsorption and desorption were established after drying and placing shale drilled cuttings in a desiccator and allowing them to reach equilibrium, Figure 4. Based on the isotherms and the weight percentage of water in the shale, a scale from 0.1 to 1.0 was suggested for the water activity.

Wilcox and Fisk (1983) characterized shale samples based on their behavior upon hydration using sorption meter, Figure 5, and capillary suction time that represents filtration characteristics. Shale samples were classified according to their tendencies towards swelling and dispersion. According to Wilcox and Fisk classification, shales with hydration rates equal to or greater than 0.15 were classified as high swelling shales, those with hydration rates ranging from 0.06 to 0.15 were classified as medium swelling shales and low-swelling shales are those with hydration rates values lower than 0.06. In addition, CST is used to characterize shale based on filtration.

2.2 Imbibition of aqueous fluids into shale pore system

Comprehensive understanding of the imbibition and propagation process into shale matrix is important in order to tackle shale-fluid interactions. The starting point of shale-fluid interactions is when drilling fluids are introduced and used to drill shale formations where water filtrate invades and starts to imbibe into shale pore network. As water molecules advance and propagate into shale pores, they contact an increasing number of clay particles and start to interact. Water molecules start to adsorb on clay surfaces and different clay types have different responses when get exposed to water.

Imbibition and diffusion involves the mass transfer of fluid molecules into micro, meso as well as macro pores. Fick's first law defines the diffusion flux as (Karger and Freude, 2002):

$$j = -D_T \frac{\partial c}{\partial z}$$

Where j is the diffusion flux, D_T is the transport diffusivity, c is the concentration of the diffusing species and z is the space coordinate in the direction of the concentration gradient. The

diffusion process is monitored using mean square displacement and pore sizes.

Spontaneous imbibition can be defined as the ingress and propagation of a wetting phase to into porous material to displace a non-wetting phase without external driving force. Here, only capillary forces play role in the imbibition process (Ding and Kantzas, 2004). There exist several models for spontaneous imbibition process that mainly depend on the chemical composition of the imbibed fluid and rock properties of the invaded formation.

Handy (1960) utilized differential equations that describe the oil-water displacement but using some assumptions that are applicable to air-water system. He found a linear relationship between the square of imbibed fluid volume and the imbibition time assuming a piston-like displacement.

$$Q_w^2 = \left(\frac{2P_c \emptyset k_w A_c^2 S_w}{\mu_w}\right) t$$

where: Q_w^2 is the square of the imbibed water volume, P_c is the capillary pressure, $\emptyset$ is rock porosity, k_w is the relative permeability to water, A_c^2 is the square of contact surface area, S_w is the water saturation, μ_w is the water viscosity and t is the imbibition time.

A quantity called "imbibition potential" was suggested as a measure to predict the degree of imbibition when different types of shale rocks and fluids are combined. Mathematically, the imbibition potential is the product of capillary pressure, relative permeability to water and water saturation. This quantity is useful especially in the case of constant rock porosity and surface area given the fluid is water with constant viscosity (Makhanov, 2012).

Li and Horne (2000) modeled the water spontaneous imbibition into gas-saturated rocks. They assumed the applicability of Darcy's law with upward water imbibition and started to

derive the water imbibition velocity as:

$$v_w = \frac{k_w}{\mu_w}\left(\frac{\partial p_w}{\partial x} + \rho_w g\right)$$

Upon mathematical manipulation and then calculating the water imbibition rate as the product of the contact surface area and water imbibition velocity ($A\ v_w$):

$$Q_w = \frac{dN_{wt}}{dt} = a\frac{1}{-} - b$$

where:

$$a = \frac{Ak_w(S_{wf} - S_{wi})}{\mu_w L} P_c$$

$$b = \frac{Ak_w}{\mu_w}\Delta\rho g$$

$$= \frac{N_{wt}}{V_p}$$

The most frequently used method to analyze spontaneous imbibition is to introduce the imbibing fluid and allow it to contact the rock while measuring and monitoring the weight of the rock using an analytical balance. The shale sample is protected and covered with epoxy resins from all the sides except the side where imbibition is to be allowed. Then, it is hanged below the analytical balance and immersed into the imbibing fluid where the changes in weight and quality are monitored with time.

Makhanov (2012) studied shale samples from Horn River and Fort Simpson formations. With clay content in the range of 22 to 51% composing mainly of illite as well as chlorite in some samples, porosity values were found to be between 7.8 and 10.9%. Contact angle measurements have been carried out to analyze the wettability that play a major role in mass

transfer that takes place in the imbibition process. All samples were found to have smaller contact angles when tested with mineral oil compared to the results of deionized water or 2% KCl brine suggesting the rocks to have more oil wettability. After that, imbibition testing started using an analytical balance and the effect of anisotropy was investigated by conducing the imbibition tests parallel as well as orthogonal to the bedding planes. The imbibition has been carried out in counter-current mode on rectangular shale samples that have been already cleaned, dried and analyzed for surface area and volume.

Yang (2015) conducted spontaneous imbibition testing on a shale sample from Lujiaping formation in the Sichuan basin whose porosity was 1.02% and permeability was 0.0021 mD. X-ray analysis revealed that total clay content was 23% composing mainly of illite and illite-smectite mixed layer with minor presence of smectite, chlorite and kaolinite. The samples were coated with epoxy to perform the test in counter-current condition. Then, the samples were dried at 105 °C for 24 hours before starting the imbibition testing.

Zhou and Zhang et. al. (2016) carried out spontaneous imbibition test for shale outcrop samples from four different formations in the Sichuan Basin. The samples were characterized first for porosity, permeability and mineralogy using helium porosimeter, pulse decay permeameter and X-ray diffraction respectively. Porosity values were in the range of 1.1 to 2 % with clay content varying from 14.3 to 41.5% (mainly: swelling illite-smectite mixed layer) and high percentage of quartz (40.5 to 68.1%). After that, disc slices of 50 mm in diameter and 5 mm in thickness where utilized to conduct the spontaneous imbibition test at constant temperature of 60 °C.

Shen (2016) examined shale samples from two different formations: Longmaxi marine shale in Sichuan basin with average porosity of 3.5% and TOC of 5.2% and Chang-7 continental

shale in Erdos basin with average porosity of 2.37% and TOC of 4.7%. Permeabilities were in the order of 10-3 mD. Clay content of the Longmaxi shale was estimated to be 28% while it was 49% for Chang-7 shale sample with illite and illite-smectite being the main clay types for both samples. They utilized analytical balance and distilled water to study the liquid imbibition capacity and liquid diffusion ability. They allowed the imbibition process to take place on all sides of the samples.

Zhou and Abbas et. al. (2016) conducted imbibition testing on Horn River, Woodford and Niobrara shale samples. After determining the permeability, porosity, initial water saturation, contact angle and salinity, the samples were immersed in the imbibing fluid and under-weighing approach was used to monitor the weight changes with time.

Another tool used for monitoring imbibition is X-ray tomography where different variations of have been used ranging from CT, micro-CT to nano-CT. The principle is to scan small pieces of the shale sample and then introduce the imbibing fluid to the sample while taking images at every step.

Akbarabadi and Piri (2014) utilized nano-CT to analyze one shale reservoir sample whose porosity and permeability were 1.43% and 21 μd respectively using nano-CT segmentation method and 1.2% and 5.82 μd respectively using scanning electron microscopy method. Three fluids have been used: 25% sodium iodide brine, surfactant/brine mixture and oil. Pore size distribution was also analyzed using the segmentation method where the pore size range was 0.03 to 1 μm with majority of the pores were in the range from 0.03 to 0.2 μm.

Chakraborty et. al. (2017) extended their study to cover utilization of micro-CT in order to generate spatial saturation profiles as a function of time. A jacketed shale sample was placed in a glass container and scanned in the dry state. After that, water column was placed above the

sample and the spontaneous imbibition started. Micro-CT scans have been taken after 5 hours, 48 hours and 7 days.

NMR has been used to generate water imbibition and saturation profiles. One approach was to plot T2 relaxation time curve and analyze the incremental and cumulative increases in porosity. Another approach was to plot water saturation and amplitude as a function of the position and distance from the wetting rock surface.

Gomaa (2014) generated the T2 relaxation time profiles for three types of shale formations before and after imbibition: Eagle Ford, Marcellus and Mancos shales. Although their experimental work was not spontaneous imbibition since they applied injection pressures of 500 and 1000 psi, the approach of their work is useful to be applied at conditions of no injection pressure. Based on the T2 distributions before and after imbibition, they drawn some conclusions about the preferential imbibition.

Meng (2015) performed the analysis on shale samples collected from Longmaxi formation with total clay content ranging from 31 to 51% with illite, illite-smectite and chlorite being the main clay types present. The spontaneous imbibition was established in co-current mode as well as counter-current mode for replicate samples. For co-current mode, samples were immersed in 2 mm deep water, while for counter-current mode, samples were immersed completely. Several NMR T2 curves were generated for different intervals of imbibition. As water imbibed and propagated, the amplitude of the T2 curves increased and preferential imbibition can take place based on the pore size range.

Zhou and Zhang et. al. (2016) utilized NMR imager to generate NMR spectral lines to study the distribution of water saturation along the length of the shale core plug. Shale samples were analyzed before and after immersion in water for seven days. Slicing procedure has been carried

out using NMR imager to determine the water saturation at every single point. Results were plotted as amplitude on the y-axis against distance from the imbibition surface on the x-axis.

NMR can be a useful tool that can be also used to have insights into the diffusivity of different types of fluids into porous media. Relaxation times (T1 and T2) and diffusivity measurements can be used to describe the diffusion process and evaluate the diffusivity of the imbibed fluid. The diffusivity depends on several factors such as fluid viscosity and pore size.

After understanding the diffusion process, ways to reduce the diffusivity of water into shale matrix can be recommended and, as a result, negative impact of shale-fluid interactions can be minimized. In literature, there exist several studies to analyze shale porosity and the imbibition of different fluids into shale pore network. They are carried out using NMR to study the fluid flow through porous media and the effect of movable fines on oil production. (Appel, 2004; Washburn et. al., 2014; Xu et al., 2015)

T_2 relaxation time can be calculated using the following equation (Gomaa et. al., 2014):

$$\frac{1}{T2} = \rho_2 \frac{S}{V} + \frac{1}{T_2^{bulk}} + \frac{1}{T_2^{diff}}$$

Where ρ_2 is the surface relaxivity, S is the surface area of the pores and V is the volume of the pores. The first term on the right hand side is the major contributing term to T_2 values while the other two terms can be neglected for shale formations give that they have long bulk relaxation times and assuming the internal gradient is low.

Chitale et. al. (2000) investigated the clay typing in formation evaluation using NMR. They utilized the NMR T_2 distribution to study the clay-bound water in water saturated as well as vaporized montmorillonite clay. It was observed that T2 distribution was uni-modal for hydrated clay samples at less than the critical saturation, 500 mg of water per gram of dry clay. However, the T2 exhibited bi-modal distribution at higher saturation values.

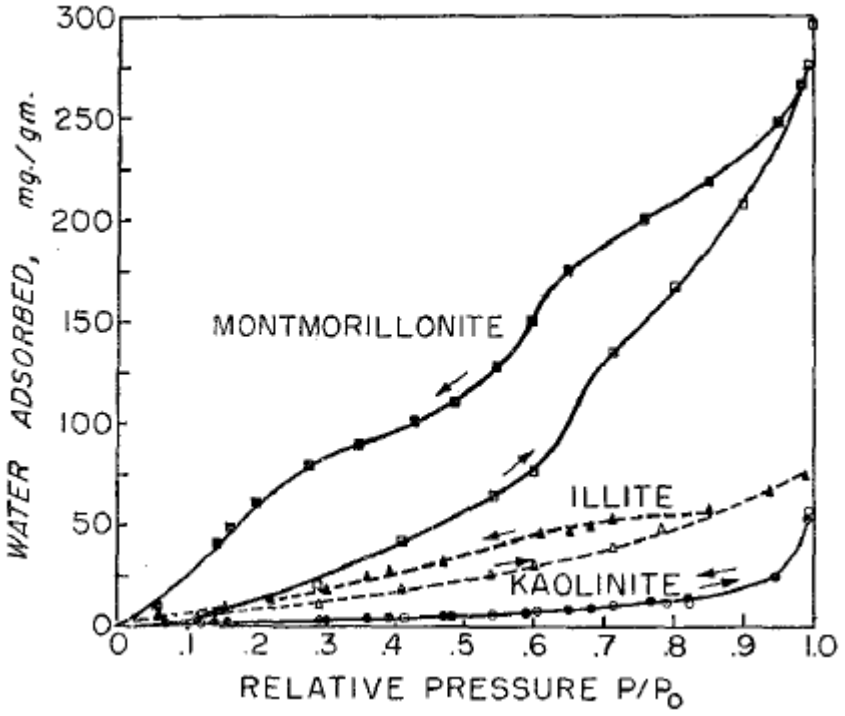

Figure 3: Water-vapor adsorption of clay samples (After Johansen, 1959)

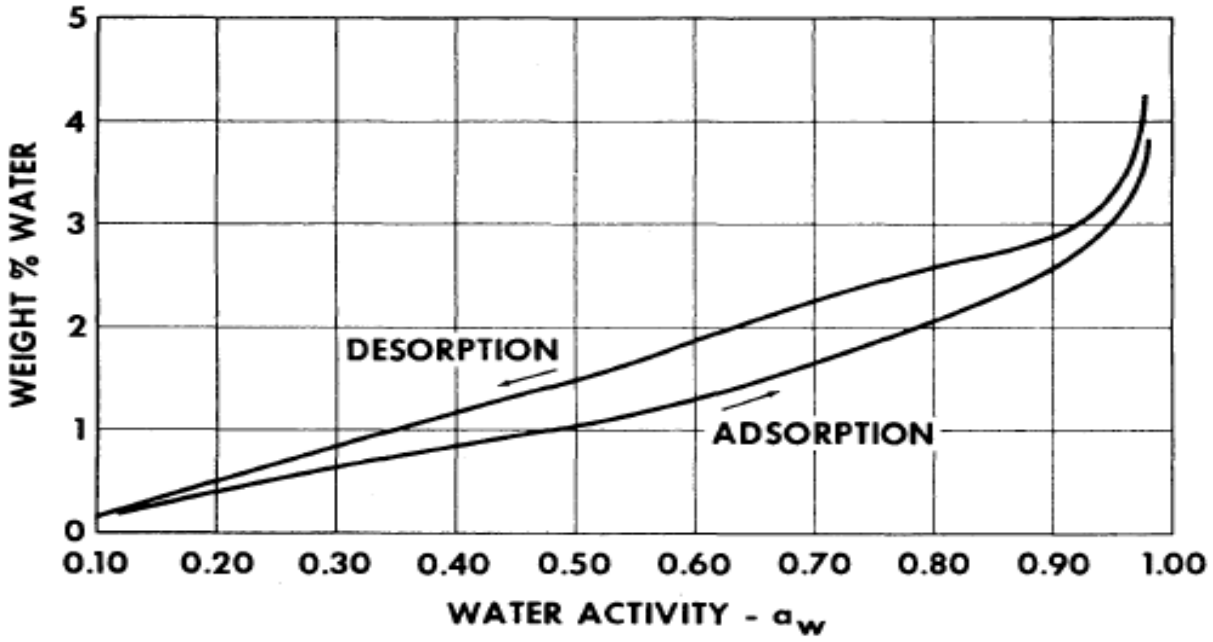

Figure 4: Adsorption and desorption isotherms for one shale sample (After Chenevert, 1970)

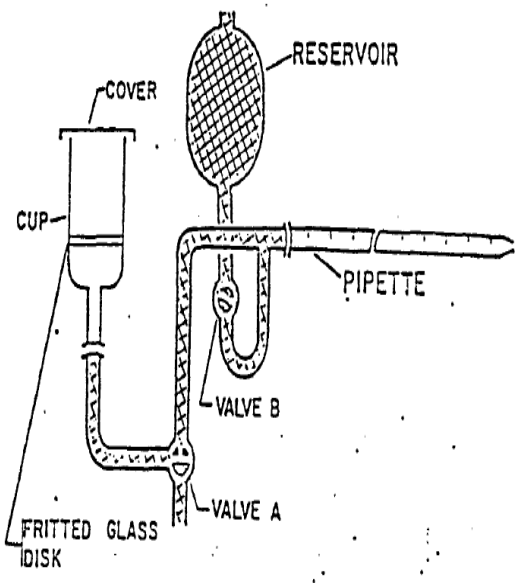

Figure 5: Sorption meter used to measure hydration (After Wilcox and Fisk, 1983)

Meng et. al. (2015) investigated the mechanism by which spontaneous imbibition takes place in shale reservoirs. Their work aim was to explain preferential imbibition of fluids into small and large pores for two scenarios: co-current and countercurrent. Unlike the case of sandstone and volcanic rock, they found preferential imbibition in the case of shale where micro pores have the ability to imbibe more than large pores.

There exist several mechanisms by which fluids imbibe into shale rocks. Previous studies revealed that capillarity, osmosis diffusion and water adsorption are the three driving forces of spontaneous imbibition in shale matrix. (Zhou and Abbas, 2016; Yang et. al., 2017)

Capillary pressure is the general driving force for all types of rocks including sandstones and shales. It is equal to the difference in pressures of the wetting and not-wetting phases. This amount of pressure is necessary to initiate the flow and displacement. Capillary pressure (for: n = non-wetting phase and w = wetting phase) is calculated using the following equation:

$$P_{cnw} = P_n - P_w = \sigma_{nw}\left(\frac{1}{R_1} + \frac{1}{R_2}\right)$$

where: σ_{nw} is the interfacial tension between the two phases, R1 and R2 are the radii of curvature.

Osmosis diffusion is the driving force that takes place when the salinity of the imbibing fluid is lower than the salinity of the shale pore fluid. The fluid flows from the low-salinity to the high-salinity environments in an attempt to balance the salinities on both sides. It can be investigated by running spontaneous imbibition experiments with the use of high-salinity imbibing fluid. In this case, a reduction in the amount of imbibed fluid should happen since water starts to leave the shale rock and flows into the imbibing fluid.

Water adsorption is considered one of the imbibition driving forces due to the presence of clay minerals that possess high affinity to adsorb water. For shale samples with high clay

content, increased water imbibition has been observed. This was attributed to the direct water adsorption on clay surfaces as well as the microfractures that are induced by the enhanced shale permeability due to water adsorption. Hatch et. al. (2012) conducted a study to understand the water adsorption behavior of three types of clay: kaolinite, illite and montmorillonite. Water content measurements revealed that with increasing relative humidity, there was an increase in water quantities as well as water content in the clays. However, kaolinite showed the lowest amount of water adsorption. Illite had showed slightly higher water adsorption tendency. Montmorillonite which is an expandable clay, showed a significant increase in water adsorption compared to the other non-expandable clays: kaolinite and illite.

When imbibed water volume was plotted against time, (Ge et. al. ,2015), three regions were identified: early, middle and late time regions. For the early time region, the high imbibition rate was attributed to capillarity. With the increase in water saturation, the imbibition went under transition phase where capillarity effect and the imbibition rate decreased. The late time region was dominated by diffusion which is a distinctive feature of tight rocks such as shales. Water adsorption on clay surfaces started in the transition region and continued into the diffusion region as well.

Related to diffusion and fluid flow through shale pore network, water activity, or salinity, of the mud compared to that of the pore fluid is one of the factors to be considered in controlling shale reactivity. For a drilling fluid with a high water activity, i.e. low salinity, water will be driven from the drilling fluid into the shale formation with the aid of osmosis phenomenon. As a result, pore pressure increases, confining pressure decreases, shale starts to swell and willbore will be destabilized. Because water activity is inversely related to salinity, raising salinity of drilling mud can enhance wellbore stability (Chenevert, 1970). However, previous experimental

work showed that increasing salinity above an optimum value can have adverse effects due to the possibility of fracturing the shale and thus can cause wellbore instability. This is because too high salinity will cause pore pressure to drop down significantly due to water movement from formation into the wellbore leading to the formation of cracks and fissures within the shale matrix.

Sometimes mud weight is increased for mechanical stabilization of the borehole wall. Because the effect of high mud weight is time-dependent, it is usually increased step-wise, e.g. mud weight is increased by 0.5 ppg for every step. The mud weight is increased until the weight that is capable of stabilizing the shale is reached. Breakout widths can be significantly reduced when the mud weight is increased for a constant mud activity (Zoback, 2007). Raising mud weights can stabilize wellbore by reducing the wellbore stresses below the shale strength. However, excessive increases in the mud weight can result in low rate of penetration and can create induced lost circulation problems. Therefore, mud weight should be optimized to the minimum that is just sufficient to achieve wellbore stability without inducing mud losses or causing other drilling problems (Steiger and Leung, 1992)

An equation was developed by Mody and Hale (1993) to determine the pore pressure increase as a function of water activity. Parameters considered in this equation include: membrane efficiency, temperature, molar volume of water and the activities of both the pore fluid and mud. However, time was not considered although shale instabilities are dependent on time in many cases. Time was considered as a factor in other models. These models allow the estimation of the time duration that a mud with a known activity can support the wellbore formation with a known pore fluid activity before failure. As a result, plot of failure vs. time can be generated and based on these plots, mud chemistry can be adjusted to enhance the wellbore

stability.

Cohesive forces are the forces that keep the rock particles sticking to each other. When the filtrate, i.e. water, penetrates shale rocks, cohesive forces will be broken, reduced or damaged. Thus, there will be a decrease in the shear stress that is required for failure to occur. This results in movement along the existing fracture or along the weak planes leading to hole enlargement problem. Furthermore, when the filtrate invades the shale and the osmotic swelling starts, the rock will be softened and an increase in the rock volume is noticed because osmosis triggers swelling of particle surface as well as the shale layers (Hayatdavoudi and Apande). Another effect of osmosis is the pressure created in the rock due to the flow of fluid into the shale matrix. This will weaken the cohesive structure further.

Interactions between the shale rock and the mud have various effects on different properties related to rock strength. The friction between the rock particles increases the amount of shear required to cause rock failure. However, due to rock-fluid interactions, this amount of shear is significantly reduced making the rock more prone to shear failure. Amanullah (1993) discussed one factor that controls the cohesion other than the water content. Upon entering the invaded shale rock, filtrate reduces the surface free energy. This reduction causes the cohesion to decrease as well. Due to the reduction in both the friction between the rock particles and the inter-particle cohesion, the resistance of the rock to shear is reduced.

Rock-fluid interactions cause tensile strength to decrease and consequently, may lead to fracturing of borehole walls. Similarly, these interactions reduce the compressive strength of the rock. This is due to the effect of swelling and associated high pore pressure.

Another concept to be discussed in this context is the mud pressure penetration. Due to capillary suction effect of shale matrix, there will be mud pressure penetration into the shale

rock. A small amount of filtrate can penetrate due to the low permeability and high capillary suction of shales. This pressure penetration causes the pore pressure to increase and destabilizes the wellbore (Riley et. al. 2012). The mud pressure penetration mechanism was supported by an experiment carried out by exposing one shale sample to water. The shale sample contained 4% smectite and 25% illite with a low cation exchange capacity (CEC) value of 3 meq/100 grams. After several days, instead of swelling or dispersing in water, the shale sample developed fractures along the bedding planes with widths ranging from 5 to 45 µm. As fractures get wider with time, wellbore instability will be triggered in this type of shales.

2.3 Shale swelling and dispersion

Shale swelling is the increase in shale volume when exposed and hydrated by water. Hydration is an equilibrium process which depends on parameters such as shale composition, fluid composition, pressure and temperature. Since pressure is the only varying property while drilling a well, it controls the equilibrium water content of the shale.

Roehl and Hackett (1982) described three mechanisms of swelling: surface hydration, ionic hydration and osmotic hydration. Surface hydration usually occurs in clays with low CEC such as illite. Although illite has relatively a large number of compensating ions, it does not show high tendency to swelling. This is because the cations substitution takes place in the outer tetrahedral layer, Figure 6. Therefore, they are more difficult to exchange due to their interactions and attractive forces to the negative charges of the clay. The second mechanism is the ionic hydration where hydration shells are formed around the compensating ions that contribute to the lattice substitutions in the clay structure. This mechanism only occurs in clay types of high CEC values where ionic hydration takes place because of the presence of the cations in the octahedral sheet.

This gives the cations freedom to exchange with those present in the fluid depending on several factors such as the concentration location and types of compensating ions. The third mechanism is the osmotic hydration that is basically due to the difference in salinity of the shale rock fluid and the drilling fluid. If the salinity of the drilling fluid is lower than that of the shale rock fluid, water tends to move and diffuse into the shale rock and hydrate shale particles. The water adsorption causes the shale to behave as two layers with repulsive potential leading to the expansion of the clay matrix.

Amorim et. al. (2007) classified shale swelling into crystalline and osmotic swelling. Utilizing XRD, they relied on the d-spacing between the sheets of the clay to distinguish between the two classes. They conducted experiments on sodium bentonite with NaCl, KCl and CaCl2. For example, they found that when Na-bentonite is treated with 1 M KCl, the d-spacing increased from 12 Å to 16 Å, Figure 7. This limited d-spacing increase was classified as crystalline swelling. However, when the concentration of KCl was reduced to 0.2 M, there was a significant d-spacing increase, 52 Å. They classified this as osmotic swelling. Also, they carried out swelling tests on several polymers. Some polymers were based on polyacrylamide and the others were based on cellulose and xanthan gum. They modified those polymers by adding and increasing the concentration of KCl and measuring the effect on swelling for every polymer, Figure 7. They concluded that there is an optimum concentration of KCl beyond which any addition in the concentration did not result in further improvement.

Shale dispersion is the erosion and progressive disintegration of shale cuttings where micro shale particles start to break down into smaller particles when they are subjected to shear or fluids with different ionic content. Dispersion depends on the stresses around the borehole, degree of hydration, shale composition, annular velocity and brittleness degree of the shale rock.

Bol (1986) suggested that rocks behave in brittle mode are prone to disintegration more than ductile rocks. Also, the sedimentation history and the heterogeneity of the shale rock can play an important role.

2.4 Shale inhibition mechanisms

Different proactive and reactive solutions to mitigate shale reactivity problems have been identified and used in the field. One solution is to increase the weight of the drilling fluid to mechanically stabilize shales. However, excessive increases in the weight of the drilling fluid result in decreasing the penetration rate and increasing the drilling costs. Another solution to retard shale inhibition is to reduce fluid loss. Reducing fluid loss minimizes the water invading the formation and, as a result, minimizes shale contact with water. Also, several salts such as KCl were used to minimize shale swelling. Although they can provide good shale inhibition, they have the disadvantages of causing corrosion to the pipe and the difficulty to dispose of waste due to high salt content. (Myers, 1993, Stephens et. al., 2013)

In literature, there are several mechanisms by which shale inhibition can be achieved chemically. One mechanism is to reverse the osmosis phenomenon by adding salts to the drilling fluid such as KCl. In the osmosis theory, the electrical field around the clay particle acts as a semi-permeable membrane and water in the drilling fluid tends to pass the membrane into the clay matrix and hydrate it. Adding salt to the drilling fluid makes it more concentrated with ions and, now, water from the clay matrix flows in the opposite direction, i.e. from clay to drilling fluid. This hinders the contact and hydration of clay particles with water and provides inhibition. Similarly, in the case of invert emulsion mud, due to negative osmotic effect of the salinity of water phase, the diffusion of water into the shale formation is prevented or reduced significantly.

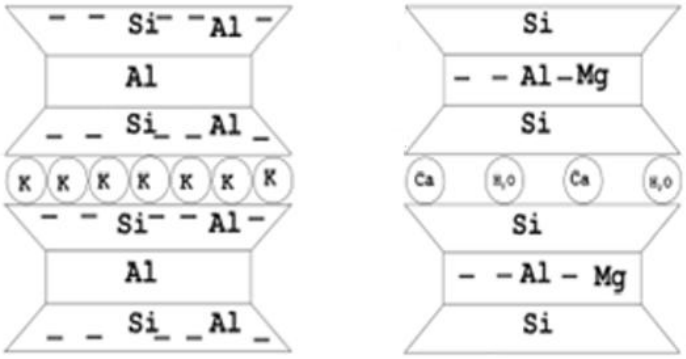

Figure 6: Structures of Illite and Smectite

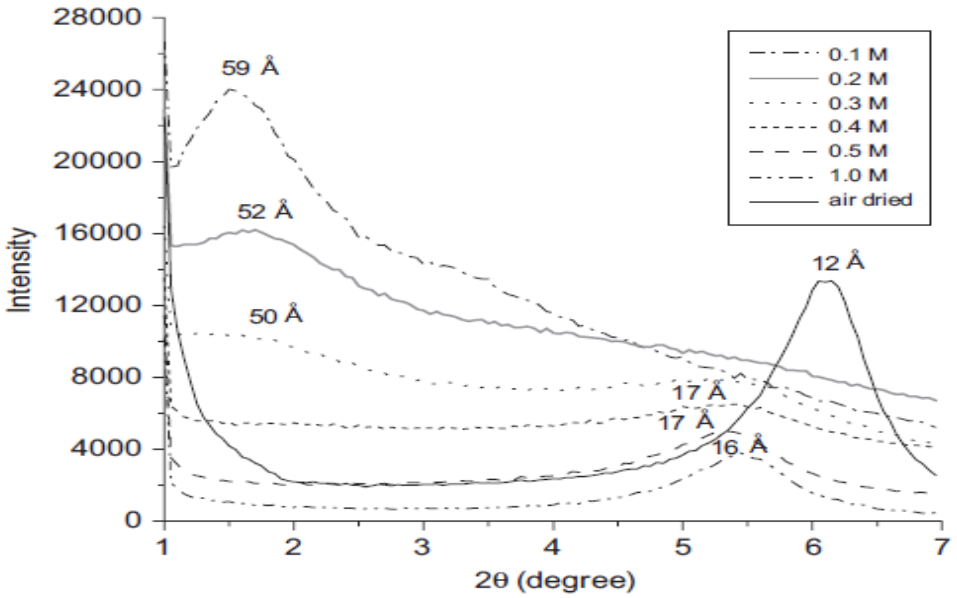

Figure 7: XRD patterns for sodium bentonite exposed to KCl solutions (After Amorim et. al., 2007)

That effect is due to the flow of water from the shale matrix to the wellbore as a result of the osmotic effect that hinders the flow of fluid from the wellbore to the shale matrix under the action of capillary suction and overbalance pressure (Tan et al. 2002). Another shale inhibition mechanism is by reducing the porosity and permeability to drilling fluid filtrate. Sodium and potassium silicate fluids, composed of silica, alkali and water, have the ability to physically plug the shale pores through a process of polymerization and precipitation. This is a result of the silicate fluid being mixed with the low-pH pore fluid that contains calcium and magnesium ions. Reduced shale permeability results in the improvement of membrane characteristics and thus decreases the hydration tendency of clay as the scope of diffusion of water into shale matrix reduces significantly. They also strengthen the shale formation through cementing the grain contacts by precipitate. The cementing action of precipitated materials works as a second shale stabilization mechanism. Furthermore, this porosity and permeability reduction can even facilitate the first mechanism and enhance the osmotic effect. Therefore, silicates can work effectively by these mechanisms to provide the required shale inhibition (Bailey et. al., 1998).

Chrome and ferrochrome lignosulfonate are also used to develop inhibitive muds. These mud additives have high tolerance to sodium and calcium ions and thus able to tolerate salt contamination while drilling subsurface formations containing brine or these salts. However, the concentration of chrome lignosulfonate decreases significantly due to thermal degradation of these additives at temperature above 300 ^{o}F. Hence, these additives are not suitable for high temperature application. Another mechanism of converting reactive shale to low or non-reactive shale is the cation exchange reaction. For example, the replacement of Na+ ions of smectite shale by the calcium ions of a mud can turn a high swelling shale to a low swelling shale. That's why conversion of sodium montmorillonite to calcium montmorillonite reduces the hydration

tendency of the shale (Bourgoyne, 1986).

Saltwater muds have the capability of reducing the reaction between clay and water. It was shown that bentonite viscosity decreases exponentially as the salt concentration increases. That is why bentonite is usually prehydrated with water to have a reasonable viscosity when using sea water or salt water as the fluid phase. Potassium chloride salt is frequently used in water-based mud design to inhibit reactive shale due to the ability of K^+ ions to replace the sodium ions of smectite clays. The clay fixation property of K^+ cation ions along with its ability to lower hydration tendency of smectite shale reduces the swelling of shale significantly. The K^+ ions induced inhibition is attributed to the small size of potassium ions that fits into the montmorillonite structure (Bourgoyne, 1986). Another inhibition mechanism, usually used for smectite clay, is to increase the water phase ionic concentration using heavy brines. This high ionic concentration hinders the osmotic effect and reduces the hydration (Gomez and Patel, 2013).

From the organic chemistry, amines and polyamines have been frequently used as shale inhibitors. The positively charged amine attaches strongly to the negatively charged faces of the clays of the shale matrix and thus dramatically reduces the water affinity of the shale. The low molecular weight and smaller size make it possible for these molecules to enter into the clay structure and inhibit both the internal and external hydration of reactive shale (Amanullah 1993). The inhibition mechanism of polyamines is similar to the inhibition mechanism of amines. However, polyamine performs better in preventing the water adsorption due to the presence of multiple active sites in the long chain to neutralize clay charges in shale matrix (Patel et al., 2007). Due to the ability to inhibit both the internal and the external surfaces of reactive shales and clays, polyamine is a better shale stabilizer. Hence, this inhibitor may have higher duration

of inhibition compared to others.

Methyl glucoside works by reducing the water activity. It differs from other commonly used salts by forming a semi-permeable membrane inside the shale matrix. This is a result of its particle size that makes it possible to diffuse into shale pores and allows hydroxyls to adsorb on surfaces of clay. During the hydroxyls adsorption, ordered structures of methyl glucoside are formed after the water is displaced from the surfaces. (Ismail and Huang, 2009)

Based on the type of shale, amount of clay and types of clays present, a shale inhibitor can be identified, evaluated and compared to other inhibitors. When an inhibitive water-based mud is to be formulated for a shale formation, complete analysis and characterization need to be carried out on a shale sample from that formation. The analysis may include: shale mineralogy, morphology, reactivity, fracture development, capillary suction time and pore fluid salinity. Oil-based muds are well-known for their high performance in terms of shale stabilization, rate of penetration, lubricity, reduced torque and drag and tolerance to contaminants. Every attempt to develop an inhibitive water-based mud should achieve these excellent oil-based muds capabilities and, at the same time, avoid their drawbacks such as high cost and environmental concerns associated with base-oil transportation, cuttings transportation and disposal. Another consideration when formulating an inhibitive water-based mud is to overcome the inherited sensitivity to temperature, salinity, pH and different contaminants.

After comprehensive characterization of the shale sample, inhibition additives such as potassium chloride, silicates, polyamines and others can be utilized for this particular shale sample. Since every shale formation differs in mineralogy than other formations, customization of the mud is necessary to achieve best results. It is almost impossible to develop a universal inhibitive water-based mud that has high performance in all types of shales. (Deville et. al.,

2011)

Frieheim and Sartor (2003) developed a new inhibitive water-based mud in an attempt to achieve comparable performance to oil-based muds. Their approach was based on three mechanisms: shale hydration inhibition, shale dispersion inhibition and shale accretion inhibition. They identified and developed three additives to formulate an inhibitive mud with the desired properties. First, the hydration inhibitor polyamine-based additive was designed to fit between clay sheets and minimize the water imbibed into the shale formation. Second, the dispersion inhibitor was designed to effectively bind to clay surfaces and also tolerate high salinity and hardness. This additive was able to inhibit dispersion as well as swelling of the clays with no adverse effects on the mud rheological properties. Third, the accretion inhibitor was designed to coat drill cuttings and the metal surfaces of the drilling assembly so that the accretion tendency is reduced. Also, it helps in preventing the drill cuttings agglomeration and accumulation.

Recent developments in nanotechnology showed that nano-sized particles can play a vital role in shale stabilization through plugging the shale pores, reducing the permeability and minimizing water penetration into the shale structure. This is due to their small particle size that enables them to enter into the clay matrix and do the required inhibition both internally and externally. (Amanullah and Al-Tahini, 2009)

2.5 Shale inhibition testing

There exist several standard as well as non-standard testing methods for characterizing the shale and measuring its reactivity and sensitivity to drilling fluids. A representative shale sample should be acquired from the cores, drill cuttings or from the outcrops. The shale sample should

be characterized first by describing bedding and sedimentary structures, color and existing fractures, if any. The shale sample should be further characterized using different techniques such as X-ray diffraction, thin section method and scanning electron microscope. Furthermore, shale reactivity should be estimated using cation exchange capacity and water activity tests. After that a series of testing methods using different drilling fluids should be conducted to assess the shale-mud interactions.

Swelling test is carried out to measure swelling tendency of the shale sample after being exposed to a drilling fluid. In this test, a natural or outcrop shale sample of a specific dimensions or a reconstituted shale pellet can be placed into a linear swelling tester after filling the tester reservoir with the drilling fluid to be tested. When the shale pellet comes in contact with the drilling fluid, it starts to swell. Swelling is measured by measuring the increase in the sample volume or the linear expansion of the sample. The results are presented as a plot of swelling percentage against time. A high value of ultimate swelling percentage is indicative of poor inhibition quality of the drilling fluid against swelling (Stephens et al., 2009).

Dispersion test measures the dispersion tendency of the shale sample after being exposed to a drilling fluid. This test is carried out by rolling a pre-determined amount of sized shale cuttings in a hot-rolling cell with the drilling fluid to be tested. After hot-rolling the cell for 16 hours at 150 °F, the shale cuttings are recovered on a screen, washed and dried in the oven for 24 hours at 105 °C. Then, the sample is weighted to determine the cuttings recovery percentage. The results are presented as the percentage of cuttings recovery. A high value of cuttings recovery percentage is indicative of high quality inhibition against dispersion since a large amount of the cuttings does not disperse.

Slake durability test is similar to the dispersion test but carried out at more abrasive and

severe conditions. In this test, a pre-determined amount of sized shale cuttings is placed in a cage. The cage has a screen and it is immersed in the drilling fluid to be tested. Then, the cage is rotated and as the cuttings hydrate, they break down, disperse into the drilling fluid and pass through the cage screen. The results are presented as the percentage of cuttings recovery after a pre-determined period of time. A high value of cuttings recovery percentage is indicative of good inhibition against dispersion since a large amount of the cuttings does not disperse.

Shale membrane test is performed to measure the drilling fluid performance in plugging the shale pores to reduce the permeability and improving the membrane efficiency of the shale. The test is conducted by saturating the shale sample with a brine that has the same water activity (salinity) as that in the shale matrix fluid. The sample is confined in a test cell before starting the saturation phase of the test to simulate the subsurface confinement state. After saturation, the drilling fluid is circulated to inundate the bottom of the shale sample and produce the osmotic suction effect. The pressure drop due to the water expulsion from the shale matrix is measured. The results are presented in a plot of pressure vs. time. A significant decrease in shale matrix pressure indicates the formation of a good membrane effect at the shale-drilling fluid interface. During the test, the activity differential and the reduced poroperm characteristics allow the expulsion of water from the shale matrix and thus improve the mechanical stability of the shale.

Shale inhibition durability test is conducted to measure the durability of the inhibition, i.e. how long the shale inhibition lasts. Highly durable shale inhibitors can protect the shale matrix from the detrimental action of drilling mud for a long time and thus can prevent time-dependent borehole instability problems. In this test, 10 grams of sized shale cuttings is mixed with the drilling fluid to be tested and hot-rolled for 16 hours at 150 °F. Then, the recovered cuttings are washed and dried for 24 hours. After that, 5 grams of the recovered cuttings are mixed with fresh

water and hot-rolled at 150 °F for different periods of time, e.g. 1, 3, 5, 7 and 9 hours. The results are represented as a plot of the cuttings recovery percentage as a function of the hot-rolling time with fresh water, Fig 1. The inflection point indicates the inhibition break down time. The earlier is the inhibition break down point, the shorter-term is the inhibition which is indicative of limited inhibition quality (Al-Arfaj and Amanullah, 2014).

Huadi et al. (2010) performed different shale inhibition tests on two polyamine systems to compare with pure and modified KCl-based systems. The polyamine systems out performed two KCl systems while they gave comparable results to KCl/silicate systems in two tests: shale dispersion and shale bulk hardness tests, Figure 8.

Frenkel and Levy (1992) conducted a study to test kaolinite, illite and smectite for dispersion tendency. Clays were stacked in columns and drilling fluids were circulated through the clays. Drilling fluids containing anions play an active role in destabilizing and dispersing the clays in the water phase. The saturation of each clay type in the effluent is monitored. As the saturation increases, the clay type has higher tendency to dispersion. It was found that kaolinite was the most dispersive followed by illite while smectite did not show high tendency to disperse.

2.6 Molecular modelling and simulation

Numerous studies have introduced and tackled problems associated with drilling shale formations related to clay-fluid interactions. Different approaches have been used such as characterizing shale samples and testing different shale inhibitors and stabilizers (Tour, 1989; Smith, 1991; Awaja and Bhargava, 2006; Loucks, 2007; Keller, 2011; Shen, 2012; Chalmers, 2012). In addition, the chemistry of reactive clays as well as fluid diffusion into shale pore

network was studied (Mooney et al., 1952; Norrish, 1954). More recently, other researchers have utilized molecular modeling to study the theory behind shale-fluid interactions. Integration of these different approaches, where results from modeling are combined and validated with the results from laboratory, can lead towards a comprehensive understanding of the shale-fluid interactions. Molecular modeling has been used as a tool to study the microscopic rock-fluids interactions for a wide range of clay minerals including smectites and illites. Different parameters and factors can be investigated including interlayer structure, clay minerals dynamics, energy states, swelling potential and the effect of cations of different sizes and charges (Young and Smith, 2000; Abhijit et. al., 2005; Suter et. al., 2007; Anderson et. al., 2010; Tao et. al., 2010; Zhou et. al., 2014; Sun et. al., 2015).

Advantages of using molecular modeling to study clay-fluid interactions include, but not limited to, explaining the response of different clay types when exposed to fluids such as water-based drilling fluids. In addition, the simulations allow for conducting virtual experiments at elevated temperatures and pressures. Such experiments are difficult to maintain in the laboratory due to either equipment limitations or safety precautions. Having the ability to study clay-fluid interactions at downhole conditions can explain different field observations in order to suggest the required solutions and improve the current practices (Allen, 1987).

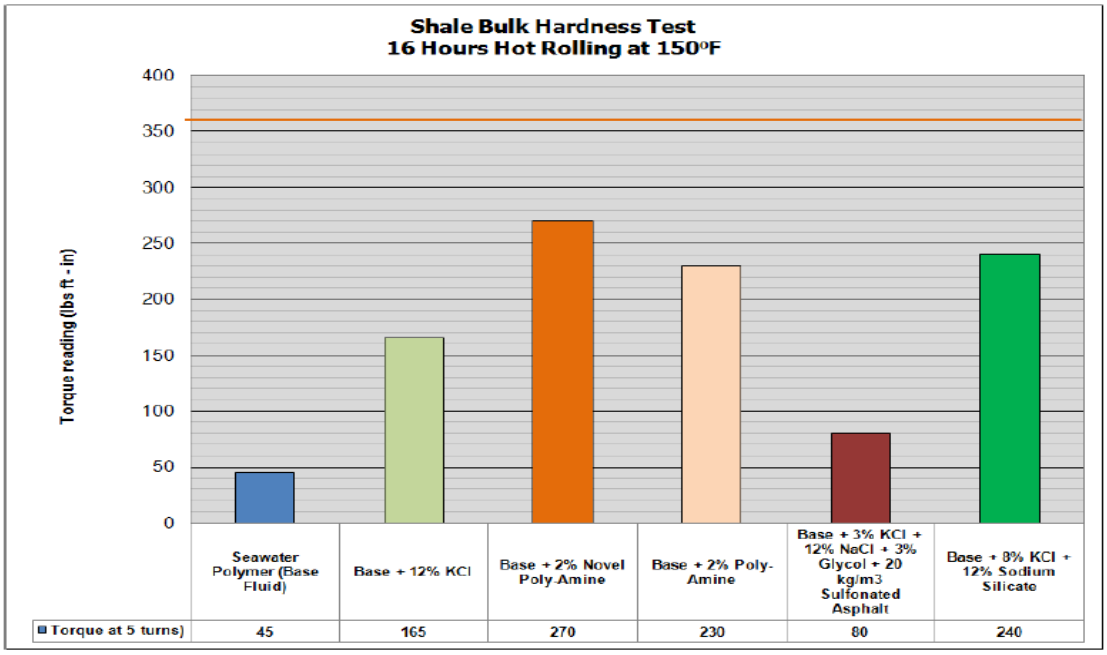

Figure 8: Dispersion test results with different types of fluids (After Huadi et. al., 2010)

Different types of shale inhibitors have been used in drilling fluid systems to mitigate shale-drilling problems. The selection of the inhibitors is a trial and error procedure where a series of laboratory experiments, such as swelling and dispersion tests, are carried out to investigate the effect of inhibitors on the clay types present in a shale sample. The inhibitors that are not capable of providing the required shale inhibition are screened out before further testing is conducted. Molecular modeling and theoretical understanding of the clay-fluid interactions can help in the screening process of the shale inhibitors and save time and resources.

Clays are generally divided into five main groups: kaolinite, smectite, illite, chlorite and vermiculite. Smectite and illite are layers composed of one octahedral sheet sandwiched between 2 tetrahedral sheets in a ratio of 2:1 (Worden, 2003). The tetrahedral sheet consists mainly of silicate while the octahedral sheet consists mainly of aluminum and hydroxyl groups. Clay layers are either neutral or have a negative charge. The negative charge arises when isomorphic substitution takes place. For smectites such as montmorillonite, the isomorphic substitution either takes place in the tetrahedral sheet where silicon atoms get substituted by aluminum or it takes place in the octahedral sheet where aluminum atoms are replaced by magnesium. However, for illite, only the tetrahedral isomorphic substitution occurs. As a result of the negative charge, clay surfaces get attracted to cations in order to be neutralized.

Mixed layer clay minerals form when more than one type of clay co-exist as interstratified vertical sequence in one structure (Brindley, 1980). The interstratified stacking can be ordered, partially ordered or random. An ordering scheme has been developed, the Reichweite parameter (R) with R0 indicating that the stacking is random and R1 indicating ordered stacking. R value can be greater than 1, which indicates that one layer is repeated more than one time for every cycle, e.g. AABAAB. (Bergaya, 2013). The ordered illite-smectite mixed layer is named

rectorite.

Boek et. al. (1995) conducted molecular simulation to explain quantitatively the significant swelling observed in sodium montmorillonite and the limited swelling of potassium montmorillonite, Figure 9. They plotted potential energy for both types against water content. At very low levels of water content, the potential energy for potassium montmorillonite was found to be higher than the bulk water internal energy, -28 kJ/mol and -42.3 kJ/mol respectively while the potential energy in the sodium montmorillonite case was much lower, -72 kJ/mol, Figure 10. This causes the swelling to start earlier when the interlayer cation is sodium and delayed hydration and swelling is observed in the case of potassium cation. That is because any system tends to move to the lowest possible potential energy to be in the most stable state.

Bains et al. (1999) investigated the inhibition mechanism provided by different organic inhibitors. They carried out molecular dynamics and Monte Carlo simulations on montmorillonite with polyalkylene glycols (polyethers) and polyhydroxyethers. They formulated different types of shale inhibitors and got positive results for highly-inhibited shale molecules when they design the molecule in a way to have two regions: hydrophobic region where advancement of water molecules is greatly reduced and hydrophilic regions to enhance binding of Na to clay surfaces which can reduce the interlayer spacing and shale swelling.

Liu et. al. (2006) carried out molecular simulation studies on Arizona Montmorillonites. They investigated the K-montmorillonite to find out the reason behind its inhibition ability compared to Na- montmorillonite. Their results showed the higher hydration energy required for the water to invade potassium montmorillonite compared to the hydration energy required to

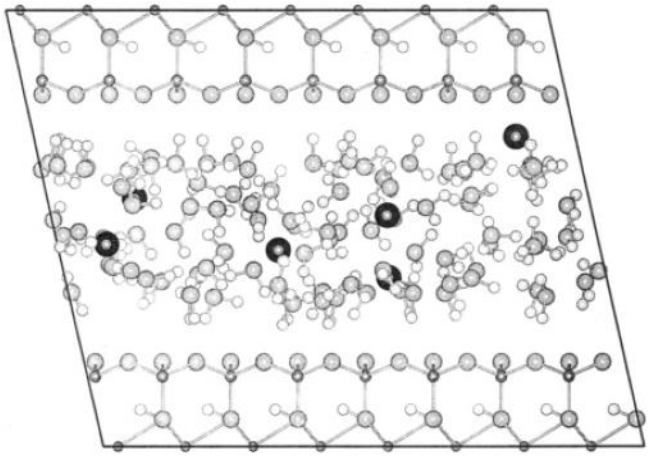

Figure 9: Molecular model of sodium montmorillonite (After Boek, 1995)

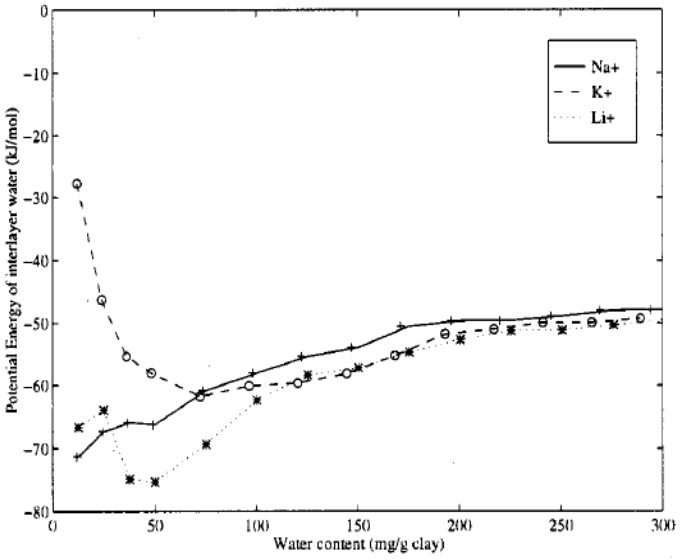

Figure 10: Potential energy of interlayer water in montmorillonite (After Boek, 1995)

invade sodium montmorillonite. Also they calculated the hydration energy, Figure 11, and another property called swelling immersion energy as:

$$\Delta U = \frac{\langle U(N) \rangle - \langle U(0) \rangle}{N} \tag{3}$$

$$Q = \langle U(N) \rangle - \langle U(N^0) \rangle - (N - N^0) U_{\text{bulk}} \tag{4}$$

When they plotted the immersion energy against water content, Figure 12, they found three local minima in the case of sodium cation and two local minima in the case of potassium ion. They concluded that three hydrate layers are formed in the former case and only two layers are formed in the latter case.

Tao et. al. (2010) run simulations for Na, K and Ca-montmorillonites and evaluated layer spacing as a function of water content. They found that layer spacing in Na is larger and therefore more swelling takes place, Figure 13. They concluded that valence of cations is the dominant factor. Sodium cation has an open structure while K and Ca have tighter structures when they are hydrated by water. As a result, potassium cation binds to clay surfaces and reduces d-spacing and shale expansion.

Stixrude and Peacor (2002) studied two models of illite-smectite mixed layer, namely: A and B, Figure 14. In model A, the mixed layer was built of fundamental particles by stacking layers of the end members. On the other hand, model B was built of structurally-unique crystallites that satisfy coherency and the local charge balance. They investigated the energetics and structures of the two models using first-principles density-functional theory (DFT) and found that model B is more stable since its total energy was 2.3 kJ mol-1 atom-1 lower than that of model A.

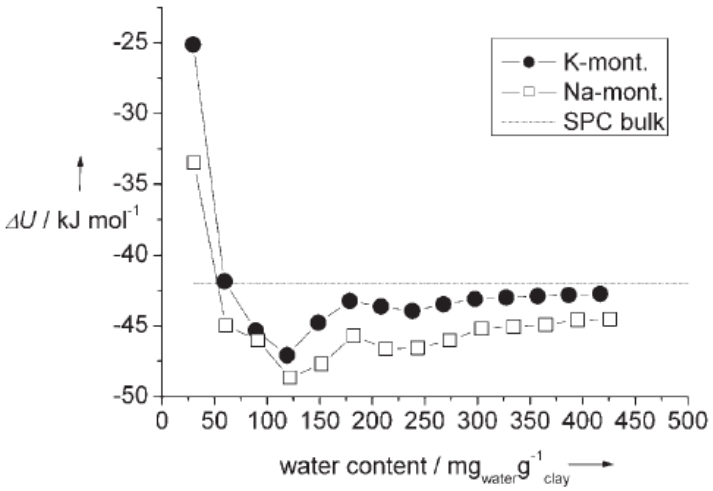

Figure 11: Hydration energy of montmorillonite with potassium and sodium cations (After Liu, 2006)

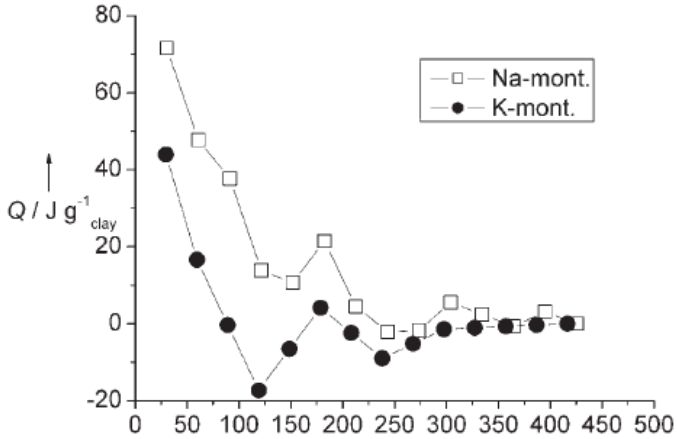

Figure 12: Swelling immersion energy of montmorillonite with potassium and sodium cations (After Liu, 2006)

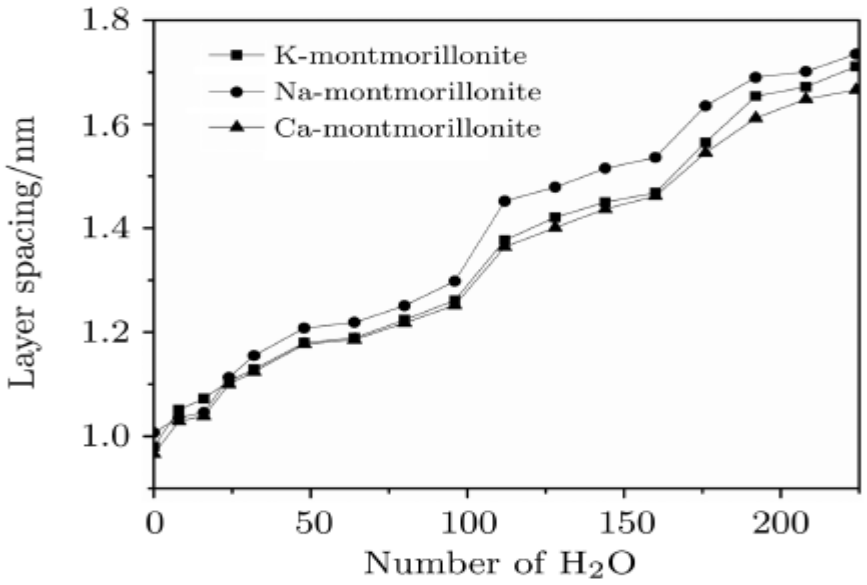

Figure 13: Layer spacing as function of water loading for montmorillonite (After Tao, 2010)

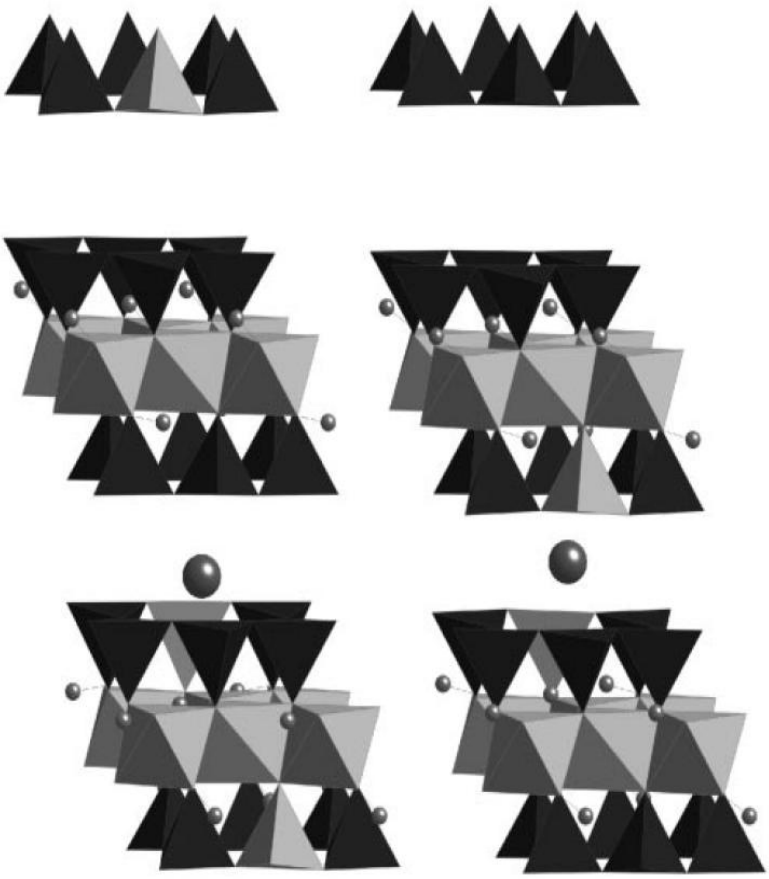

Figure 14: (Left) Illite-smectite model A, (Right) Illite-smectite model B (After Stixrude, 2002)

Tambach et. al. (2004) performed molecular simulations on montmorillonites from two regions: Arizona and Wyoming. They varied the d-spacing between 9 to 20 A and used relative humidity range of 0 to 100% to study the swelling behavior. They calculated the adsorption isotherms and free swelling energy of the two models by integrating the normal pressure to clay sheets. When they increased the d-spacing with constant/low relative humidity, they noticed an increase in the sorption of water molecules in the clay models. In addition, they used the minima of the pressure oscillations and obtained the lowest free energy to identify the stable states of the systems, Figure 15. They did the same calculations for lithium, sodium and potassium, Figure 16.

Militzer et. al. (2011) carried out first-principles calculations to model elastic moduli of illite-smectite and compared the results with muscovite. They used model B that was studied by Stixrude and Peacor since it is more stable in terms of energetics. On the other hand, muscovite is a sheet silicate that consists of one octahedral layer between two tetrahedral layers, Figure 17. It belongs to the mica group and exhibits similar feature of isomorphic substitution as illite and smectite clays do. They computed the elastic constants and found that illite-smectite has lower Young's modulus value than that of muscovite by half. This finding was attributed to the crystal structure differences. In muscovite, the negative charge and the potassium ions are present in all tetrahedral layers while this situation is alternating in illite-smectite case.

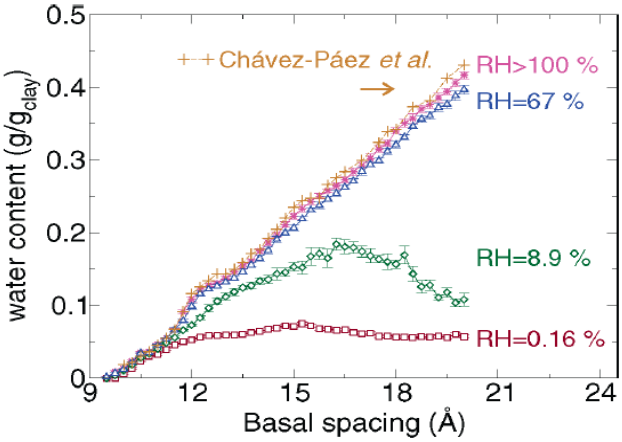

Figure 15: Water content as a function of basal spacing of montmorillonite (After Tambach et. al., 2004)

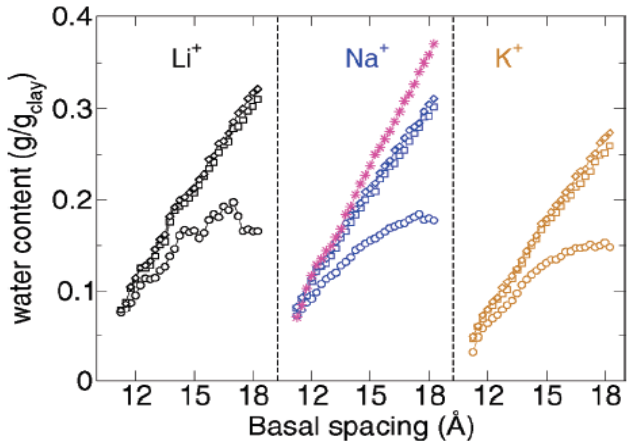

Figure 16: Water content as a function of basal spacing of montmorillonite (After Tambach et. al., 2004)

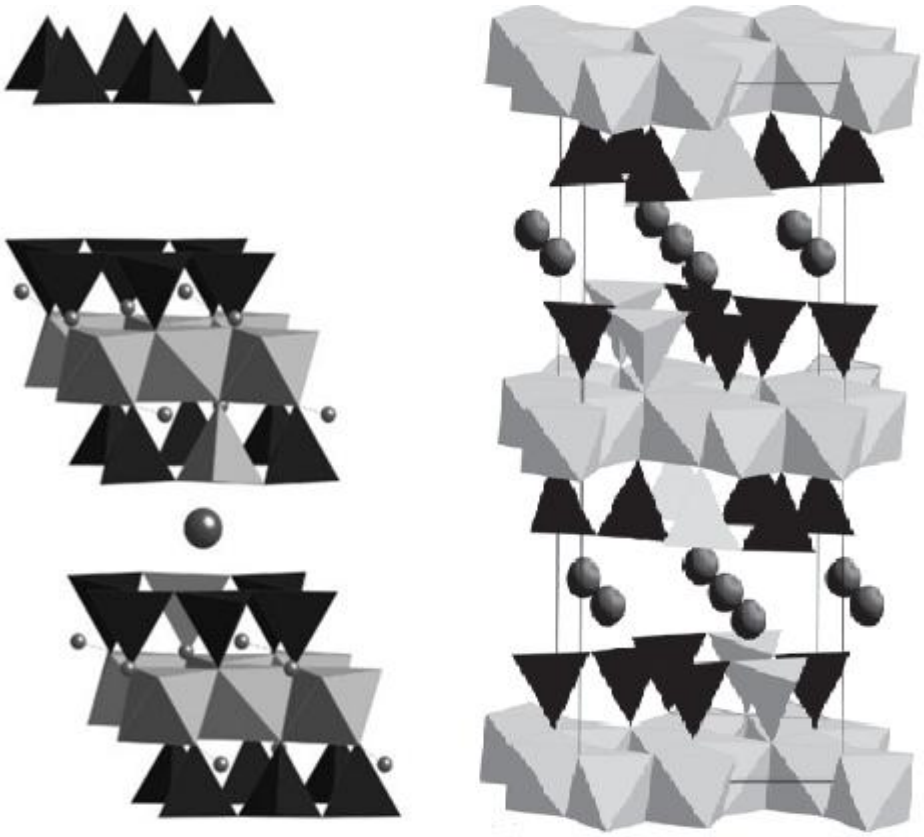

Figure 17: (Left) Illite-smectite model B (After Stixrude, 2002), (Right) Muscovite (After Militzer, 2011)

Zhou et. al. (2015) conducted a molecular simulation study on Na-rectorite to investigate the swelling behavior upon hydration. They utilized Molecular Dynamics (MD) and Monte-Carlo (MC) techniques to establish the swelling curves, swelling free energy curves and density profiles and then compared them with the case of montmorillonite. Similar to montmorillonite, rectorite with bi-layer hydrate was more stable than that with mono-layer hydrate. For interlayer sodium ions, they observed that, unlike in the case of montmorillonite, these ions showed asymmetrical distribution and migrated close to the illite part. This behavior was attributed to the unequal layer charges of the two constituents of rectorite: illite and smectite.

Mixed layers such as rectorite have unique characteristics as their structures are complex and their composition and properties are intermediate between the end-members. Illite and smectite clays are present as pure clays in the nature as well as mixed clays when there is transition from illite to smectite or vice versa. One of the most interesting features of the rectorite is the interstratification of expandable and non-expandable layers. The importance of studying this type of mixed layer comes from its abundance in shale formations and the significant swelling it experiences upon hydration (Ramseyer, 1986; Worden, 2003)

Molecular modeling studies of pure types of clays are well documented in literature. However, while there exist few studies on Na-rectorite, there is a lack in understanding and comprehending the behavior of K-rectorite. The objective of this work is to study the swelling behavior and interlayer structure of K-rectorite with different levels of hydration.

CHAPTER 3

METHODOLOGY

The methodology of this work consists of three phases to study shale-fluid interactions in the macro and micro-levels. The first phase characterizes the shale samples in depth using different testing techniques to be able, in a later stage, to understand their behaviors when coming in contact with fluids. Shale characterization was carried out to determine shale mineralogy, petrology, reactivity and adsorption potential.

The shale samples were taken in the second phase to analyze their behaviors when exposed to aqueous fluids. This was done using testing procedures for swelling, dispersion and diffusion. The performance of different shale inhibitors were assessed to help in identifying the appropriate fluid type to be used to drill similar types of shale formations.

The third phase consists of modeling different types of clays with the aid of molecular dynamics simulation software to comprehend the clay-fluid interactions on the molecular level. Two types of swelling clay: montmorillonite and rectorite (illite-smectite) were simulated and results were analyzed based on interlayer spacing, total energy, temperature sensitivity and interlayer structure. This chapter discusses the details of the materials used in this study and also the testing procedures and modeling schemes.

3.1 Materials

Four shale samples from the Lower Silurian period, Qalibah formation were collected from different fields and locations to be characterized; samples are denoted as A, B, C and D. Out of these four samples, three are downhole samples while one is an outcrop sample. The downhole samples were selected to represent three different cases: one silica-rich sample (A), one clay-rich

sample (B) and one sample that have comparable percentages of silica and clay (C). The outcrop sample is clay-rich shale (D) that was collected from outcrops close to Qusaiba village, 70 km northwest to Buraidah approximately.

For downhole samples A and C, the shale sections were drilled with water-based drilling fluids (KCl-Polymer mud) while an oil-based drilling fluid was used to drill the shale section of sample B. For outcrop sample D, the sample was extracted several feet into the outcrop to acquire fresh samples and minimize the effect of weathering. For samples A and C, plugging could be carried out and core plugs were cut and prepared for analysis. However, for sample B and due to the high clay content, no plugs could be extracted. Instead, small pieces from the core were taken at a single depth point. The samples were kept in sealed bags and envelopes until the tests were conducted. The samples were kept in sealed bags and envelopes until the tests were conducted.

Three clay samples were acquired from the Clay Mineral Society, namely: sodium montmorillonite SWy-3 (Crook County, Wyoming, USA), illite IMt-2 (Silver Hill, Montana, USA), illite-smectite ISCz-1 (Slovakia) and kaolinite KGa-1b (Georgia, USA). These clay samples were analyzed to aid in explaining and interpreting the results of the Silurian shale in study.

Six types of saturated salt solutions were used: potassium nitrate, potassium chloride, sodium chloride, sodium bromide, calcium chloride and sodium hydroxide were used to establish adsorption isotherms. For the shale dispersion, inhibition durability and swelling tests, de-ionized water, potassium chloride and polyamines solutions were utilized.

3.2 Micro-level imaging of fabric and structure

3.2.1 Micro-Computed Tomography

Micro-Computed Tomography is a non-destructive technique that uses x-rays to penetrate and take images of a sample by sections. The field of view and voxel for this technique are in the range of 10 to 0.5 micrometer. After processing, 2-D or 3-D images can be generated after reconstruction of the sections to produce multi-dimensional representations of the rock sample and allow the study of the pore space and internal matrix of the sample and the fluid flow behavior. In addition, using special software, rock porosity can be estimated including the isolated and fine pores as well as the connected pores. Statistical analysis can be conducted to estimate the percentage of each pore size in the rock matrix. However, since nano-pores can not be detected using Micro-CT, they are excluded and techniques with even higher resolutions should be used such as nano-CT.

Micro-CT system consists of an X-ray source and detector, a high-precision revolving stage, a mount for the rock specimen, a motor support, a mechanism for positioning the specimen, and a data acquisition and analysis system. The system utilized in this work is manufactured by Xradia, model No. VersaXRM-500. The X-ray source generates X-rays of voltages in the range of 30 to 160 kV to produce sample images and reference images with X-ray source filter holder. The X-ray detector picks up the X-ray samples images. The sample stage is a platform to mount the sample and prepare it for microscopy. Another component is the visual camera, which is located behind the sample stage, used to provide images to the visual light camera window (Xradia, 2011).

The working concept of micro-CT is to measure the linear attenuation coefficient defined by Beer's law. It calculates the fraction of X-rays passing through the sample and depends on the

effective atomic number and bulk electron density (Boruah, 2015). Micro-CT is utilized in this study to examine the structure heterogeneity of the shale sample, bedding and the presence of any fractures. Sample A is a cylindrical plug of 3 in height and 1.5 in diameter, sample B is irregular in shape since the attempt to produce a plug failed due to the instant reactivity with water, sample C is a cylindrical plug of 1.5 in height and 1 in diameter and sample D is irregular in shape as it is an outcrop sample and all attempts to get a cylindrical plug failed due to the high clay content. The test was carried out using an x-ray source with 80 kV/ 7 W while the exposure time was 1 second with 1601 projections. The instrument generated 2D slices then process them to reconstruct the 3D tomogram image. To reduce noise, a filter was used prior to segmentation step. CT numbers were utilized to process the images and differentiate between pores, matrix, organic content and minerals. In the image, they are differentiated with different colors. The darker regions are the regions that absorb more X-rays and the brighter regions are the regions that absorb less X-rays. The absorption intensity is controlled by several factors including: material density, thickness and also atomic number. The test is conducted under atmospheric pressure while the temperature can be changed.

3.2.2 Thin-section analysis

Thin section analysis was conducted to study petrography of the shale samples. The rocks were described in terms of textural relationships with mineralogy. For this analysis, the procedure to prepare thin sections started with a slab saw to cut the rock and produce small slabs. Then, the trim saw was used to cut the slab to the required dimensions. The sample was dried in an oven overnight. After that, the small sample was attached to a previously frosted glass slide using small quantity of a cold-setting epoxy resin. Then, most of the attached chip was cut off using saw motor leaving behind only a thin slice. The chip is further ground using vacuum and

grinding motor. Finally, the sample was covered with a cover slip to reduce the possibility of sample damage and improve the visual clarity under microscope.

3.2.3 Scanning Electron Microscopy

The third imaging technique used to characterize the shale samples was Scanning Electron Microscope (SEM). Using this technique, images of a sample are generated by scanning using a focused beam of electrons to study the topography of the sample. TESCAN instrument model MIRA3 was utilized to generate SEM images with resolutions in the range of 10 to 20 Kx. An SEM sample was prepared by grinding a small amount of the shale rock and fixing it to the sample holder. After that, the sample was coated with gold to make it conductive. Sample coating reduces the charging effect and thermal damage and enhances the secondary electron signal. The sample preparation started with cleaning the sample holder with ethanol and gluing 2-sided tape on it. The sample was placed on the tape and coated in the coating machine that contains a cathode, made of Gold, and an anode and the sample stage. When the inert gas, Argon, is energized, the Gold atoms start to deflect and collide in all directions with the gas atoms until they deposit on all inner surfaces of the machine including the sample. This technique is called sputter coating. (Mukhopadhyay, 2003)

3.3 Mineralogical composition and organic matter content

3.3.1 X-ray fluorescence

X-ray fluorescence experiment was conducted to determine the elemental composition of the samples. For this purpose, a PANalytical Epsilon3-XL was utilized with maximum voltage of 50 kV, current of 3 mA and tube power of 15 W, Figure 18 and Figure 19. For the elements fluorine through uranium, this instrument is sensitive to concentrations ranging from ppm to

100%. It has silver (Ag) anode with four tube filters for: Kapton, Titanium, Cupper, silver and two filters for aluminum. Compared to wet-chemical or atomic absorption, XRF is a rapid technique and required less amount of involvement of the analyst in the acquisition of the results (Timothy E. La Tour, The Rigaku Journal, Vol. 6/ No. 1/1989) The processing software can carry out qualitative and quantitative analysis. The measurements were taken using the Omnian method which is properly used for standard-less analysis.

Sample preparation started by grinding the sample to about 20 µm. A small plastic cylinder was covered on one end by a transparent film of specific properties. The sample holder was assembled by taking this small cylinder and inserting into another cylinder to fix the film and make it stable. Then, 4-5 grams of the sample was placed inside the inner cylinder and was covered by a tip. The sample holder was placed in one of the available positions in the XRF instrument and the test was run using a specialized software to analyze the sample and treat/interpret the results.

3.3.2 X-ray diffraction

X-ray diffraction was utilized to determine mineralogy of the shale samples. For this study, a Rigaku X-ray diffractometer was used with instrument settings of 45 kV and 40 mA, Figure 20 through Figure 25. Each sample was gently crushed using a mortar and pestle then a McCrone micronizing mill was used to further grind the samples to 10-20 µm with the aid of a grinding agent (isopropanol) added to cool down the cell while grinding. Then, the sample was filtered under vacuum for 16 hours. After that, powder samples were prepared and tested in the X-ray diffractometer for 2θ range from 4° to 75° with a step size of 1°/min.

Figure 18: XRF Device for elemental analysis (Outside)

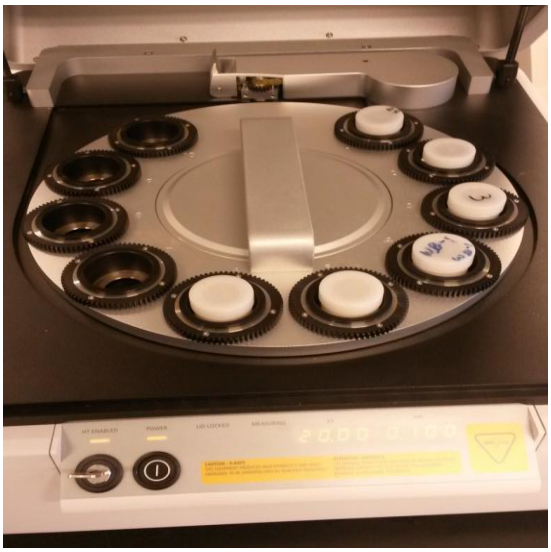
Figure 19: XRF Device (Inside)

Clay fraction from every sample was analyzed by preparing slide sample from clay slurries. The procedure started by weighing an empty glass tube then loading the tube with a small amount of the sample in fine powder form. Again, the weight for the glass tube with the sample was recorded. Then, few drops of sodium hexa meta phosphate (Calgon) were added to aid in dispersing the suspension after adding de-ionized water. The sample was then sonified for 15 minutes to further break the sample particles down. After centrifuging the sample for 5 minutes, the suspension that contained clay was poured in plastic tube containing few drop of 15% HCl to cause the clay minerals to flocculate. Then the plastic tubes are centrifuged again at the same settings. The excess clear water is carefully poured off from the plastic tube. A small amount of distilled water is added to the clay in the bottom of the plastic tube. A small amount of fine powder from the mineral fluorite is also added as an internal standard to correct d-spacings for possible sample displacement errors. The clay slurry is poured onto the glass slide and left to dry in air. After that, the slide sample was run in the XRD instrument for a 2-theta range of 2°-32° with a step size of 2°/min. Upon completion of XRD run, the slide was glycolated to analyze the presence of any expandable clays. It was glycolated using ethylene glycol vapor at 60 °C overnight. The remaining contents of the glass tubes were again mixed with de-ionized water and centrifuged several times until clear suspension was achieved. The contents were dried in a 100° oven for 24 hours then the weight was recorded to determine clay size fraction.

3.3.3 QEMSCAN

The accuracy of QEMSCAN results greatly depends on the quality of the sample preparation. To prepare the sample for testing, 5 grams of the rock was cut in a small piece and mounted in 5 mm of epoxy into a plastic sample cell. The rock sample was then covered completely with additional amount of epoxy. The cell was covered with a lid then placed in a

compactor at a temperature of 45 °C and a pressure of 8 bar for 5 minutes. After that, the sample was cut using sewing edge from the side that will be scanned by the machine until the rock sample surface is outside the epoxy. Then, it was polished from the same side with sandpaper, deionized water and acetone. The sample was dried in an oven at 60 °C for 10-15 minutes. Finally, the dried sample was coated with carbon as a thin electrically conductive layer, Figure 26.

After preparing the samples, QEMSCAN Wellsite device manufactured by FEI company, Figure 27. The testing was conducted with voltage of 15 kV, emission current of 49.5 µA, Tungsten filament and constant vacuum pressure. It was run under the mode of Particle Mineral Analysis (PMA). QEMSCAN starts by conducting energy dispersive X-ray spectroscopy to analyze the chemical composition and identify the minerals present. Then, using particle volume and density, it calculates the mineralogical composition (Mackay, 2016). Also, particle and pore size distributions can be generated.

3.3.4 Thermogravimetric analysis

Thermogravimetric analysis (TGA) was carried out to study the shale samples in terms of the mass loss upon decomposition, oxidation or loss of volatiles. It is a useful tool to examine the stability of a rock sample subjected to controlled thermal treatment. TGA is basically a thermobalance, operated at pre-determined environment conditions including heating rate and gas atmosphere, used to measure the weight loss or gain of a sample as a function of temperature. In this study, it was used to give an indication about the total organic carbon (TOC) and investigate any effect TOC has on physio-chemical properties of the shale samples. TGA can provide information about thermal stability, weight loss due to physical processes (vaporization,

sublimation and desorption), chemical processes (oxidation, reduction and dehydration reactions). In addition, this analysis was carried out to help in interpreting subsequent nuclear magnetic resonance (NMR) results for studying pore network characteristics. The TGA instrument (NETZSCH TG 209 F1 Iris), Figure 28, whose resolution is 0.1 µg, was utilized to conduct TGA using nitrogen gas flowing at 100 ml/min from room temperature until 800 °C with heating rate of 20 °C/min (Shabbar Syed, 2011).

3.4 Reactivity potential testing

3.4.1 Cation exchange capacity test

Cation exchange capacity test (CEC) was carried out to measure the exchangeable cations and have indication about shale reactivity and swelling tendency. To neutralize the negatively-charged clay sheet surfaces, cations such as sodium, potassium and calcium occupies the interlayer space. Shale samples with high CEC have the ability to exchange more cations and, as a result, are more reactive than those with low CEC.

In this test, 1 gram of the shale sample was prepared by grinding to a maximum particle size of 75 microns before being mixed in an Erlenmeyer flask with 10 ml of de-ionized water with 15 ml Hydrogen Peroxide and 1 ml sulfuric acid (5N). Then, the flask was placed on a hot plate to boil the contents gently for 10 minutes. After that, the sample was cooled down to room temperature and water was added to dilute the contents to 50 mL. Then, the sample was titrated by adding methylene blue solution in increments of 0.5 ml and using a magnetic stirrer with swirling to have a homogeneous solution. One drop of the solution was transferred each time using a stirring rod to a filter paper. The titration process finished when the dye appeared as a faint blue ring.

Figure 20: Mortar and Pestle for primary grinding

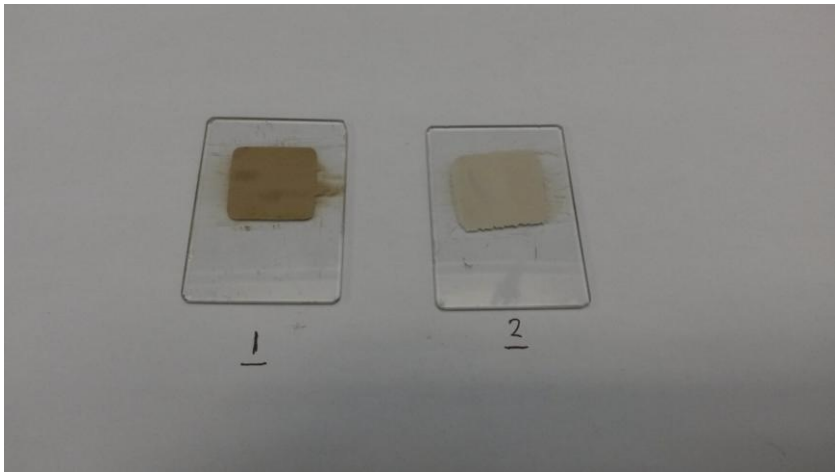

Figure 21: Samples for bulk XRD test

Figure 22: Centrifuge

Figure 23: The cell for McCrone micronizing mill

Figure 24: Sonifier

Figure 25: XRD Device connected to PC for analysis

Figure 26: QEMSCAN samples

Figure 27: QEMSCAN Device

Figure 28: TGA instrument

3.4.2 Capillary suction time test

Capillary suction test (CST) was conducted to study the shale tendency for dispersion and disintegration. Some factors that have impact on the dispersion process include: the stresses around the borehole, clay type, degree of hydration and brittleness degree of the shale rock. (Bol, 1986) The capillary suction time represents the time taken by water to be released from the slurry. The dispersion tendency is high when the value of CST is high because water release from the solution takes long time and shale particles tend to disperse into water.

The assembly of the CST test apparatus started with placing test blotter paper on the top of sensory trays. After that, the sensor plate was fixed on the test blotter paper while having the probe side down to touch the blotter paper. This was followed by inserting the stainless steel funnel into the sensor plates, Figure 29. The test was performed by mixing 3 grams of ground shale sample with 75 mL of de-ionized water in an Erlenmeyer flask for 5 minutes. Complete blending was ensured by having high mixing speed to produce a vortex to help in maintaining the shale particles suspended in the solution. After that, 5 mL of the solution was transferred into the stainless steel funnel where the filtrate of the solution started to spread and advance on the blotter paper. When the filtrate reached the first circle (probe), the timer was triggered and the actual test started. When the filtrate reached the second circle (probe), the timer stopped and the time taken by the filtrate to travel between the two circles was recorded.

3.4.3 Moisture content and adsorption isotherms

The procedure to determine moisture content started with weighing approximately 5 grams of each sample with particle size below 500 microns (W1). Then, the samples were dried in an oven for 24 hours at 200 °F and the weights were recorded (W2). This procedure was carried out for the four shale samples and three pure clays: sodium montmorillonite, illite and illite-smectite.

After that, the moisture content was calculated as the following:

$$MC\% = \frac{W_1 - W_2}{W_2} \times 100$$

Adsorption isotherms were generated using six different saturated salt solutions to have six different relative humidities and establish the curves with six data points: sodium hydroxide, calcium chloride, sodium bromide, sodium chloride, potassium chloride and potassium nitrate, Table 1. After finishing the moisture content determination, the same samples were kept inside desiccators containing the corresponding saturated salt solution for 10 days. Then, the weight was recorded and the weight percent of water was calculated. (Chenevert, 1970)

First, an attempt was carried out to fit the adsorption isotherms to Langmuir adsorption model to check if the adsorption is monolayer mode. Langmuir adsorption equation can be written as the following:

$$\frac{RH}{q_e} = \frac{1}{q_m K_l} + \frac{1}{q_m} RH$$

where: RH is the relative humidity (equivalent to vapor partial pressure in other forms of the equation), q_e is the amount sorbed of water at equilibrium, q_m is the maximum amount of water sorbed for one hydrate layer and K_l is the Langmuir constant. If the adsorption isotherm follows a mono-layer hydrate adsorption, a plot of $\frac{RH}{q_e}$ vs. RH should give a straight line with a slope of $\frac{1}{q_m}$ and y-intercept of $\frac{1}{q_m K_l}$

If the adsorption data could not be fit to Langmuir model, the adsorption might be of multi-layer mode. Therefore, Freundlich adsorption model can be utilized to fit the data as per the following equation:

$$\frac{x}{m} k P^{\frac{1}{n}}$$

where: x is the amount of vapor sorbed on mass m of adsorobent (clay). k and n are constants that depend on the adsorbent and temperature.

Linearization of Freundlich equation gives:

$$ln\left(\frac{x}{m}\right) = \ln k + \left(\frac{1}{n}\right) ln\left(\frac{P}{P_0}\right)$$

Here, $\left(\frac{P}{P_0}\right)$ is the vapor partial pressure and can be replaced by the relative humidity. Using Freundlich equation, a plot of $ln\left(\frac{x}{m}\right)$ vs. $ln\left(\frac{P}{P_0}\right)$ gives a straight line with a slope equal to $\left(\frac{1}{n}\right)$ and y-intercept equal to $\ln k$. If the adsorption data fits to this model, the adsorption is of multi-layer nature.

3.5 Fluid imbibition testing

3.5.1 NMR relaxation time (T_2) test

NMR has been used extensively to study fluid imbibition into shale and other types of rocks, Figure 30. However, there is no study in literature that uses this tool to investigate the imbibition of different shale inhibitive and non-inhibitive fluids into shale pore system from drilling point of view. Therefore, this piece of work tries to introduce NMR T_2 distribution as a tool to study the diffusion and propagation of water and shale inhibitors in an attempt to better explain clay-fluid interactions in the micro level. This part of the thesis was limited by the small number of core plugs available for this type of study. Hence, only two shale core plugs with two different fluids were tested. As it is a new and immature idea, further and repeated testing is necessary to prove the reproducibility of the results introduced in the current work.

Figure 29: Capillary Suction Time tester

Table 1: The saturated salt solutions used in this work and the corresponding relative humidities

Saturated Salt Solution	**Relative Humidity (%)**
Sodium hydroxide	7.5
Calcium chloride	29.5
Sodium bromide	50
Sodium chloride	75
Potassium chloride	85
Potassium nitrate	93

Two shale core plugs were acquired to conduct NMR T_2 experiment. For both samples, the initial T_2 distribution was generated before starting the saturation process with two different types of fluids: de-ionized water and 5% KCl solution. The sample, then, were saturated in the corresponding fluids for 24 and 72 hours and, after that, they were tested again for T_2 distribution. This was followed by extended core plug saturating at high pressure of 1500 psi for an additional one week, Figure 31. The initial T_2 distribution was compared to the consequent T_2 distributions taken at different times to reveal the diffusion of the corresponding fluids into shale pore network.

3.6 Shale inhibition testing

3.6.1 Dispersion test

This test was carried out using the following pieces of equipment, Figure 32:

1. 8 mm, 4mm and 500 micron sieve sizes, a blank (pan) and a sieve shaker to prepare shale cuttings for inhibition using an inhibitive mud system to represent an inhibited shale formation of a borehole environment.
2. A cylindrical cell with an inner volume of more than 400 cc to mimic a borehole annulus along with a leak proof lid, a sealing cap and a relieve valve to release internal pressure after a high temperature rolling test, Figure 1.
3. A controlled temperature rolling apparatus to conduct room temperature and/or high temperature rolling to create the hydrodynamic effect of a borehole annulus, Figure 2.
4. An oven or micro-oven for drying the cuttings after dispersion and re-dispersion tests for the designated period of time.

Figure 30: NMR Apparatus


Figure 31: Pressure cell to saturate the NMR samples at high pressure

The testing procedure is the following:

i) Prepare 350 ml inhibitive mud for each of the selected mud systems using standard test equipment and procedure.

ii) Prepare 4-8 mm shale cuttings using shale cores or outcrop shales. For this development outcrop shale was used.

iii) Add 10 g of shale cuttings and 350 cc inhibitive drilling fluid into the hot roll cell. Screw the cap tightly and then place the cell on the roller of the hot roll oven and roll at 35 rpm for 16 hours in the first stage of the test method.

iv) After 16 hours, remove the cell from the hot roll oven and then pour the cell content into a 500 micron sieve.

v) Wash the content of the sieve with mildly running water to remove all shale pieces smaller than 500 micron.

vi) Dry the cuttings in an oven at 105 °C for 24 hours

vii) Weigh the dried shale, record the dry weight.

3.6.2 Inhibition durability test

The inhibition durability assessment test was performed for evaluation of the longevity or durability of inhibition by conducting dispersion test again (Variable Time Re-dispersion Test) for different time intervals using the already inhibited shale cuttings that were recovered after the dispersion test. In this test, water was used as a representative of the most aggressive reactive fluid to assess the durability of inhibition of shale cuttings. Water was also used to represent the fresh water or sea water that is usually used to drill a severe loss zone below a reactive shale formation.

Figure 32: Equipment used to conduct shale dispersion test

i) Pour 350 cc fresh water into the hot roll cell again to represent a highly reactive fluid environment.

ii) Place 5 gm dried shale cuttings that were recovered after first stage dispersion test into the fresh water of the hot roll cell.

iii) Place the cell in the rolling oven and roll for 1 to 9 hours using several inhibited cuttings samples that were inhibited by the same inhibitive mud system.

iv) After rolling for the designated time period, pour the content into a 500 micron sieve and wash using mildly running water to remove all particles below 500 microns.

v) Measure the weight after drying at 105 °C for 24 hours and then plot the mass recovered as a function of rolling time.

3.6.3 Swelling test

The shale sample in this study was tested for shale swelling test to evaluate its reactivity in the presence of fresh water and the two inhibitive muds. This test also can assess the inhibition quality provided by the drilling fluid being tested. It helps in evaluating and ranking different inhibitive drilling fluids in order of their capability to inhibit clay-rich formations. In theory, as the percentage of smectite and mixed-layer clays increases, the swelling percentage should increase as well. Therefore, swelling test gives indication about the chemical interaction, i.e. hydration of clay particles when exposed to water. This test is carried out using the linear swell meter. The shale sample is crushed then a pellet of the crushed sample was reconstituted using special equipment. The apparatus to measure the linear swelling of the shale pellet is shown in Figure 33. Unlike some other types of apparatus that measure the diameter increase of uncontained shale sample, this apparatus measures the increase in length, i.e. thickness, of a

contained shale sample where the diameter is kept constant.

The sample to be tested was crushed to particle size below 150 microns. Then, the crushed sample was compacted in a hydraulic compactor for 2 hours under pressure of 8000 psi. After that, the compacted sample was tested in the linear swell meter using water, 5% potassium chloride and 5% polyamines solutions while the swelling percentage is being monitored. The test was run until there was no further volume expansion and the swelling curve stabilized.

3.7 Molecular modelling and simulation

3.7.1 Building basic molecular units of clay systems

Molecular modeling calculations were carried out on systems of one type of pure clay and one mixed clay layer: smectite (sodium montmorillonite), illite-smectite. Different types of dry and wet clays are used and MedeA-LAMMPS interface software is utilized to build the structures and run MD calculations. The energetics of the systems such as, swelling behavior, effect of temperature on swelling, interlayer structure and atom-atom interactions were analyzed. Pure layer of montmorillonite was built as a dry system then, after that, water was introduced by stacking water layers of different loadings between clay layers. Illite-smectite mixed layer was built based on the model of rectorite that takes muscovite and pyrophyllite as the end-members. The number of water molecules was varied to study the effect of water adsorption on the clay behavior.

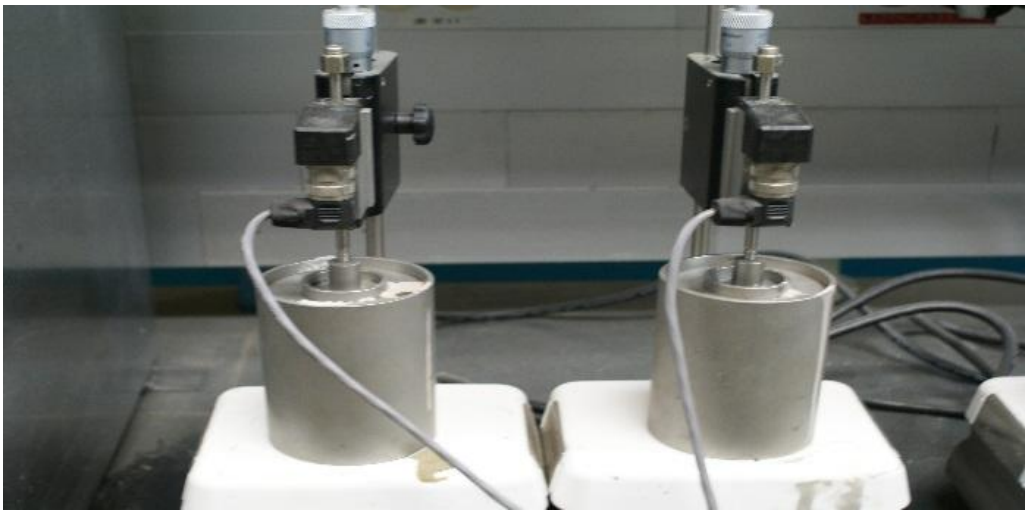

Figure 33: Linear swell meter

The original structure for montmorillonite was retrieved from MedeA structure library, InfoMatica. The structure was further modified to get the following stoichiometry: $Na_3(Si_{31}$ $Al)(Al_{14}$ $Mg_2)$ O_{80} $(OH)_{16}$. Modification included the addition of hydrogen atoms to get the required number of hydroxyl groups. In addition, amorphous substitution was done randomly with two magnesium atoms replacing two aluminum atoms in the octahedral sheet and 1 aluminum atom replacing 1 silicon atom in the tetrahedral sheet. This amorphous substitution resulted in the negative charge on clay surface that needed to be balanced by interlayer cations. The simulation cell was built of one montmorillonite layer containing eight unit cells, Figure 34. Dry montmorillonite layer was simulated then water layers were introduced in increment of 10 water molecules for each simulation run up to 100 molecules. The simulation cell was replicated in three dimensions with eight unit cells using periodic boundary conditions.

Two structures of 1:1 R1 illite-smectite mixed layers (I-S) were built based on two models for the mineral rectorite that were studied by Stixrude (2002) using first principle density functional theory calculations. Both models have the same formula: $K_{0.5}(Si_{3.5}Al_{0.5})(Al_2)O_{10}(OH)_2$. However, in model A, rectorite is built to be centered on the layers while, for model B, it is centered on the interlayers. For model A, the isomorphic substitution of tetrahedral silicon atoms with aluminum atoms occurs in both tetrahedral sheets of one layer while no substitution in the adjacent layer. As a result, each interlayer is adjacent to a high-charge and a low-charge sheet, Figure 35. On the other hand, for model B, the substitution occurs only in one tetrahedral sheet of every layer with up-down alternation. Therefore, one interlayer is adjacent to two low-charge sheets while the next interlayer is adjacent to two high-charge sheets, Figure 36.

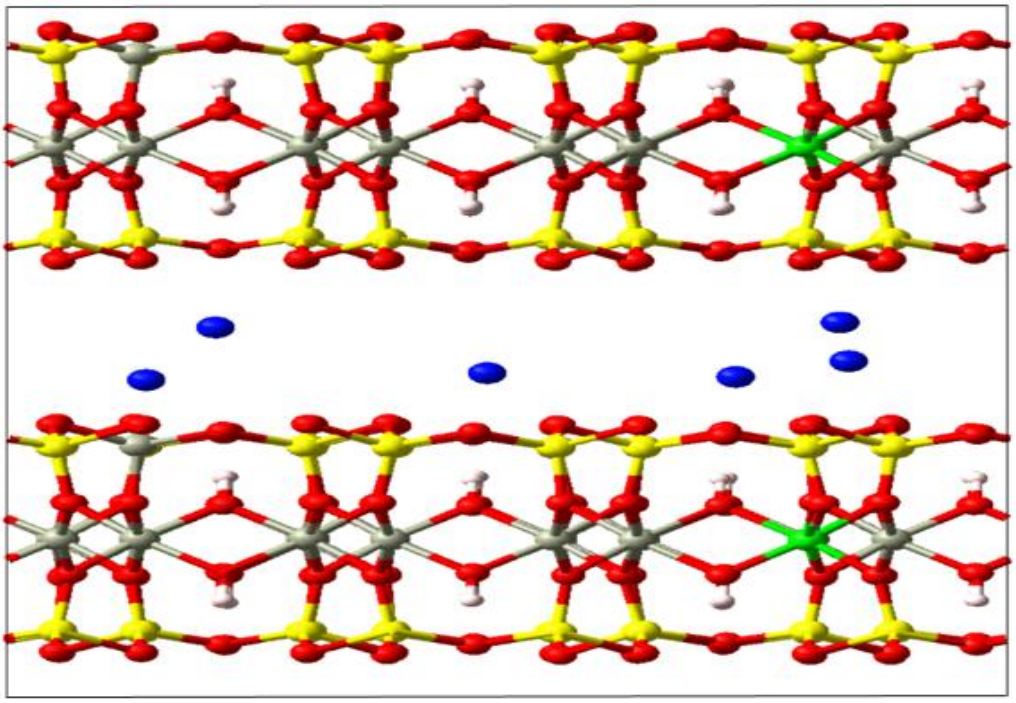

Figure 34: Sodium montmorillonite layer. red: O_2; white: H_2; yellow: Si; grey: Al; blue: Na; green: Mg.

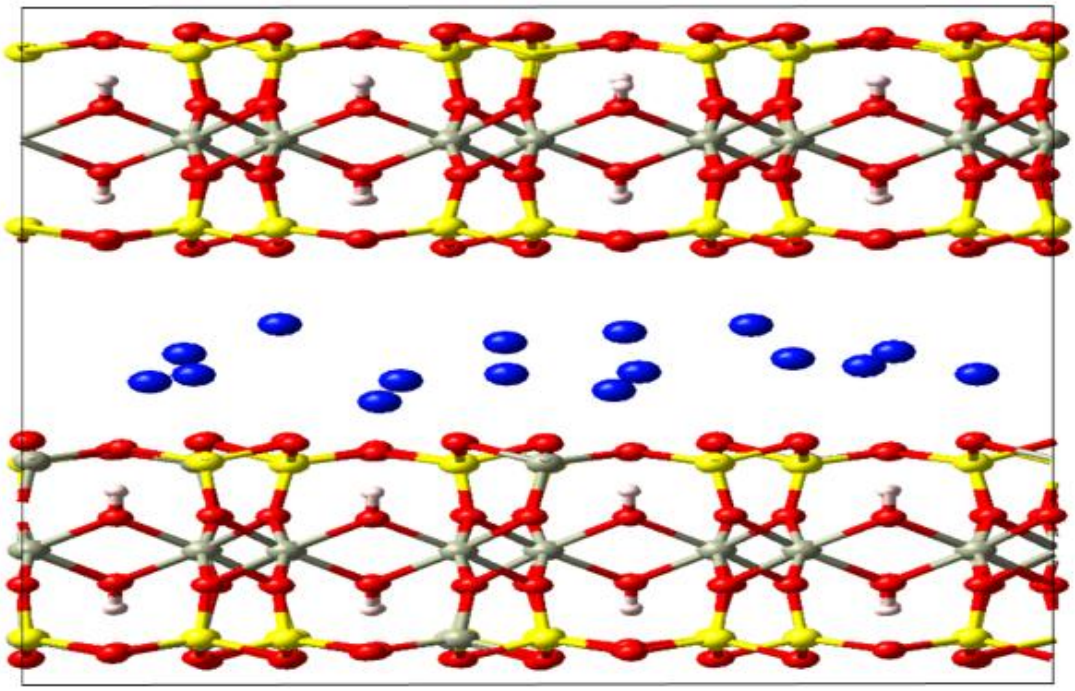

Figure 35: Illite-smectite model A. Red: O_2; white: H_2; yellow: Si; grey: Al; blue: Na

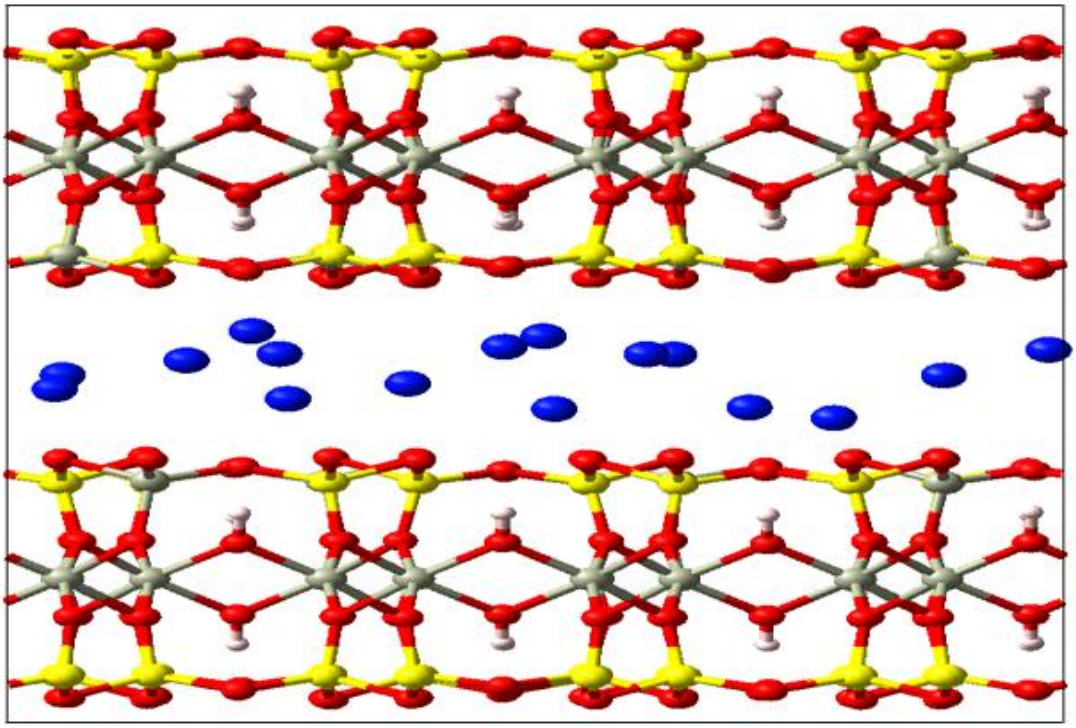

Figure 36: Illite-smectite model B. red: O_2; white: H_2; yellow: Si; grey: Al; blue: Na

3.7.2 Selection of the forcefield

In this study, we used ClayFF_dioctahedral forcefield to account for all atom interactions in the modelled system (Cygan, 2004). For 2:1 clays such as smectites (montmorillonite in our case), there are six sites in the octahedral sheet and eight sites in the tetrahedral sheet. Based on the number of occupied sites in the octahedral sheet, clays are classified into trioctahedral or dioctahedral. The 2:1 clay is classified as trioctahedral when all the six octahedral sites are occupied. However, when only four of the six octahedral sites are occupied, it is classified as dioctahedral and this is the case for montmorillonite (Brigatti, 2013).

The original ClayFF forcefield was developed by Cygan et. al (2004) as a new approach to handle the metal-oxygen interactions of hydrated phases in the modelled system as ionic (non-bonded). It used an atomistic approach and the non-bond terms are handled with a cutoff of 9.5 Å while the pppm (particle-particle/particle-mesh method) method is used to handle the long-range Coulomb interactions to a precision of 0.00001 and the long-range Van der Waals interactions are included via tail corrections. Atoms are considered as point charges and complete translational freedom is allowed. A simple Lennard-Jones (12-6) potential with electrostatics are used to control the metal-oxygen interactions. For water and hydroxyl molecules, flexible single point charge (SPC) model was used. Total energy is the sum of Coulombic and van der Waals energies with the energy contributions from bonded interactions.

$$E_{total} = E_{Coul} + E_{VDW} + E_{bond\ stretch} + E_{angle\ bend} \quad (5)$$

Coulombic energy is calculated using the distance between the two charges:

$$E_{Coul} = \frac{e^2}{4\pi\epsilon_0}\sum_{i\neq j}\frac{q_i q_j}{r_{ij}} \quad (6)$$

where: e is the charge of the electron and $\epsilon_0$is the dielectric permittivity of vacuum (8.85419 × 10-12 F/m).

Van der Waals energy is calculated based on the Lennard-Jones (12-6) function:

$$E_{VDW} = \sum_{i \neq j} D_{o,ij} \left[\left(\frac{R_{o,ij}}{r_{ij}} \right)^{12} - 2 \left(\frac{R_{o,ij}}{r_{ij}} \right)^{6} \right] \quad (7)$$

where: $D_{o,ij}$ and $R_{o,ij}$ are empirical parameters based on structural and physical property data.

The two bonded energy terms are calculated using:

$$E_{bond\ stretch\ ij} = k_1 (r_{ij} - r_0)^2 \quad (8)$$

$$E_{angle\ bend\ ijk} = k_2 (\theta_{ijk} - \theta_0)^2 \quad (9)$$

where: $k_1$and k_2 are force constants, r_0 is the bond length at equilibrium, θ_{ijk} is the bond angle for the metal-oxygen-hydrogen and θ_0 is the bond angle at equilibrium.

3.7.3 Simulation run workflow and conditions

The simulation run consisted of three LAMMPS stages. In the first stage, we initialize the system, minimize and optimize atom positions. After that, in the second stage short NVT and NPT runs were conducted on the system to relax. Finally, in the third stage, a longer NPT was run of up to 2000 ps for the equilibration of the system and calculation of the averages. This sequence was followed for different water loadings. Simulation runs were carried out at a temperature of 300 K and atmospheric pressure with a time step of 1 fs.

To study the effect of temperature changes on the swelling behavior of the clay models and carry out sensitivity analysis, the simulation runs were repeated at 300 K, 350 K and 400 K at a fixed pressure of 5 atm. The selection of this pressure was to keep water in the liquid phase at the highest temperature, 400 K. For the purpose of studying the effect of temperature on swelling, an unhydrated as well as a hydrated system of 100 water molecules were used.

CHAPTER 4

RESULTS AND DISCUSSIONS

4.1 Micro-level imaging

4.1.1 Micro-Computed Tomography

Micro-CT images for cross-sectional and side views are shown in Figure 37 through Figure 40. The density variation was utilized to identify the various solid phases based on the following: low-density minerals identified by while color while high-density minerals represented by brighter while color as the CT number increases, matrix represented by grey color, organic matter identified by black color and micro-fractures are clearly visible lines intersecting the matrix.

For sample A, heavy mineral grain patch is visible in the middle of the sample and flanges out to both sides. A clear microfracture or a lamina of high density minerals exist where it might be filled with materials such as pyrite and/or calcite. Grey color represents the matrix, white color represents the existing minerals and black color represents the organic matter. Clearly, this sample is not rich in organic matter and mainly consists of a matrix of grains with some infilled minerals.

Sample B is showing some sort of lamination with some laminas rich in heavy minerals as represented by the white color. It is built mainly of clay matrix with some patches of organic matter as the black color dictates. A micro-fracture with very small aperture is visible that might be due to the lamination and plate-like structure of this sample.

Sample C shows relatively more homogeneous characteristics with only few exceptions. The slice shows a matrix of grains with clays all over sample. However, there is on patch of low

density minerals present on the lower side. In addition, there are few black color patches that can be attributed to the existence of organic matter. White color grains are spread over the whole sample which might indicates the presence of mica.

For sample D, the slice is showing a structure dominated by clays and heavy materials with minor presence of grains. The white color patches are well spread over the whole sample and, also, the organic matter can be noticed in different parts.

4.1.2 Thin-section analysis

Thin section images are shown in Figure 41. Thin section for sample A revealed that it is composed mainly of very fine sand with bi-modal quartz grains and less than 10% clay minerals. This sample has an estimated porosity of 5%. In addition, minor rock fragments can be detected in the thin section. It was studied also under a reflected light microscope and minor pyrite content was detected.

Sample B is characterized with a massive background of clay-rich shale and very fine sand as minority. It is rich in organic matter (estimated as 6-7%) and also has scattered pyrite. It has microfractures shown in some planes.

Sample C is composed mainly of siltstone that is rich in silica and clay with moderate mica content. It also has significant content of organic matter and scattered pyrite and fossils. No carbonate (dolomite or calcite) was detected.

The quality of thin section of sample D was lower than the quality for the other samples due to the nature of the sample. Sample D has higher clay content that has high reactivity with water during the sample preparation process. Therefore, little amount of information can be withdrawn from this thin section. The sample is clearly clay-rich mudstone (brownish color) with high organic content (black color). The organic rich particles are scattered over the whole area.

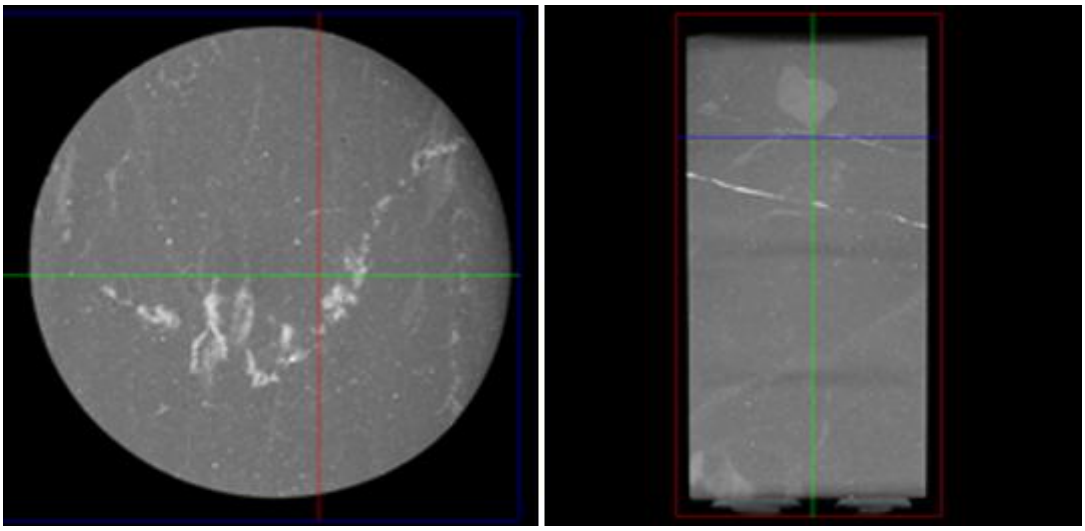

Figure 37: Micro-CT images for sample A

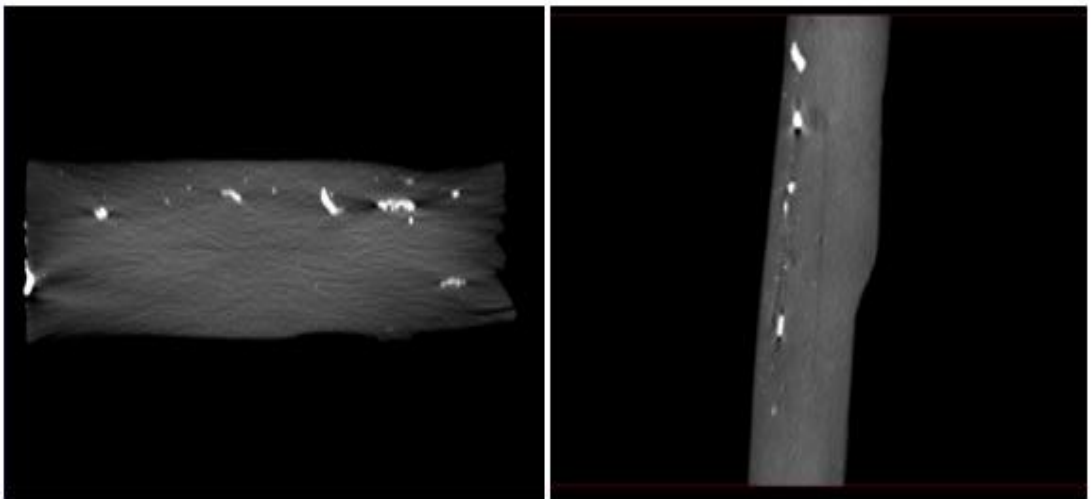

Figure 38: Micro-CT images for sample B

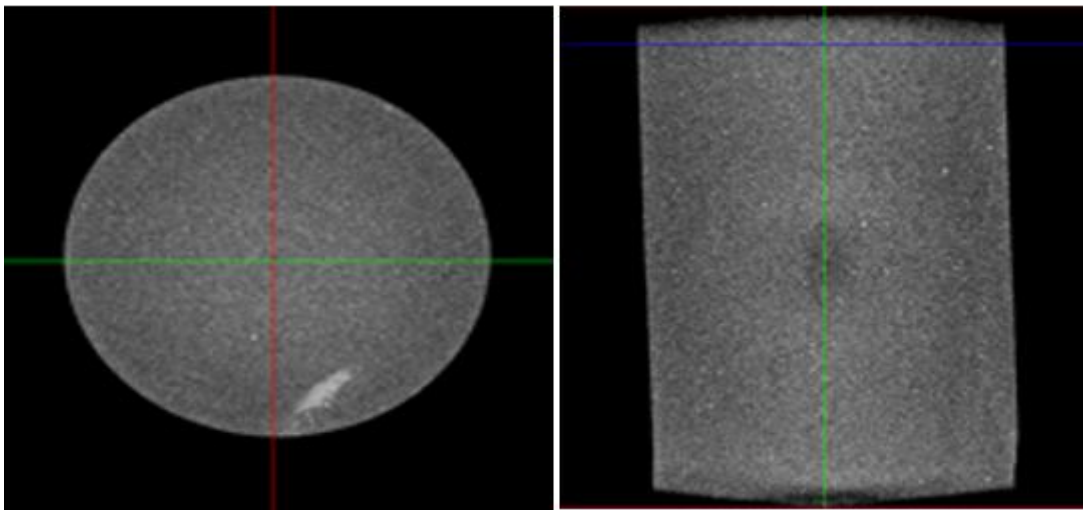

Figure 39: Micro-CT images for sample C

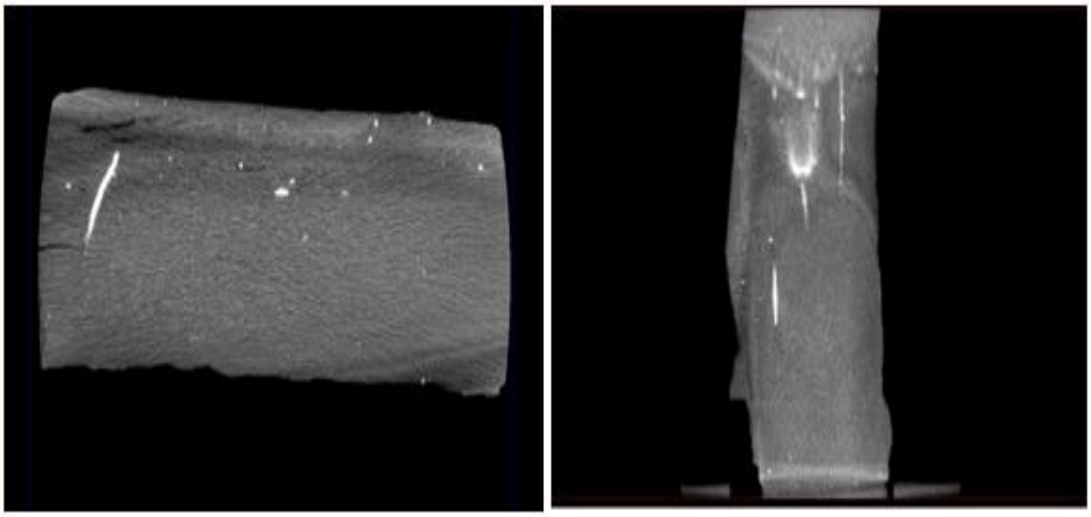

Figure 40: Micro-CT images for sample D

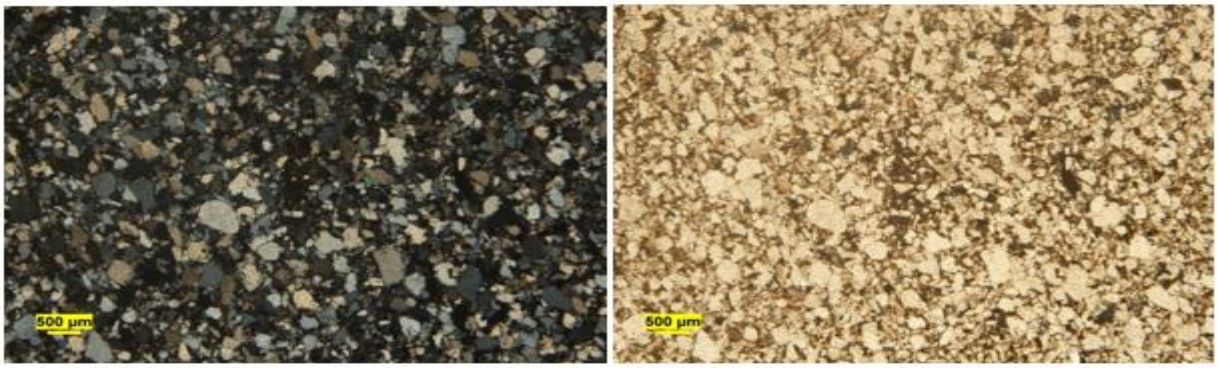

Sample A

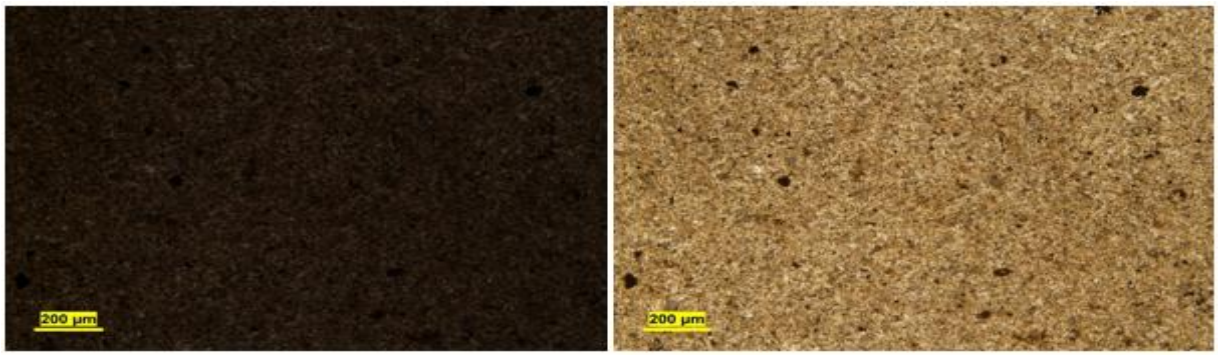

Sample B

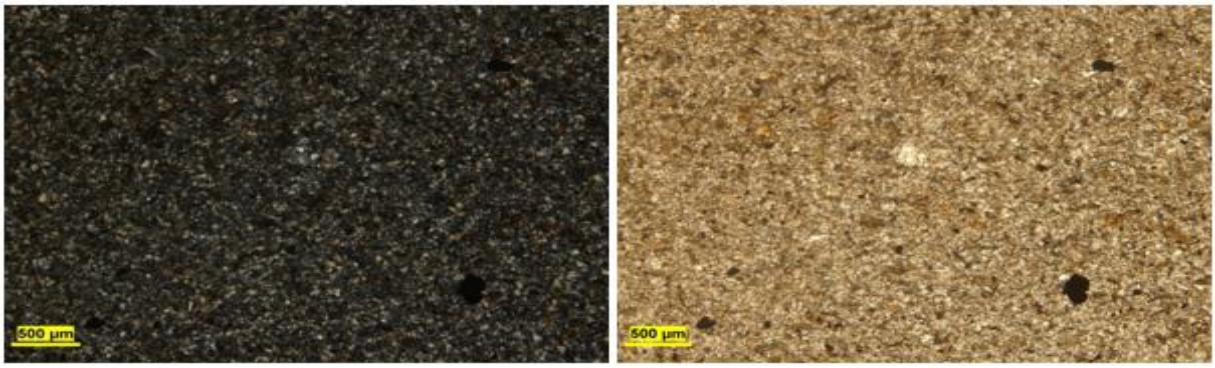

Sample C

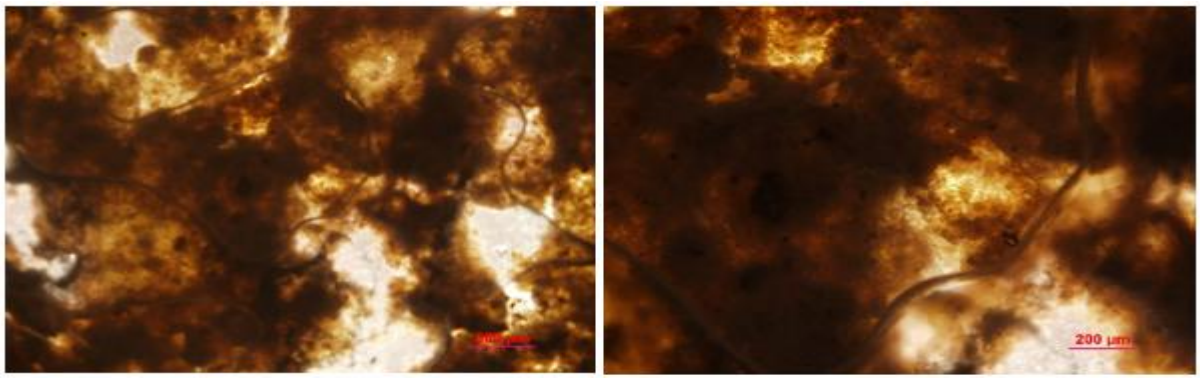

Sample D

Figure 41: Thin section images for sample A, B, C and D.

4.1.3 Scanning Electron Microscopy

Figure 42 through Figure 45 show the SEM images for the four samples at two different magnifications to study the submicron pore structures. Elements of higher atomic number appear brighter in SEM images due to stronger backscattering effect. The SEM images for sample A clearly show the presence of quartz in abundance while appreciable amount of clay plate-like particles can be seen in the image with higher resolution. The presence of potential micro-fracture is also evident from the high resolution image with aperture up to 1 μm. Also, a small amount of organic matter pores are present.

Sample B is dominated by clay particles that are clearly visible as sheets covering the whole area. Quartz grains can also be detected in small amounts. The image also shows the presence of interparticle pores as well as intraparticle pores to a lesser extent. Also, chlorite clay particles are visible in appreciable amounts that were confirmed using XRD analysis that estimated the chlorite to be 31 wt % of the sample.

Sample C is a mixture of sheet-like clay particles and quartz grain particles. No clear micro-fracture is evident from the image. Intraparticle pores can be detected in appreciable amounts over the whole sample. Also, organic matter pores exist with relatively large pore sizes.

Sample D has abundant amounts of clay minerals while quartz is present as well but in small amounts. Potential micro-fractures can be detected with aperture less than 0.5 μm. Organic matter pores are scattered over the whole sample in abundant amounts confirming the results of thin section as well as the high weight loss in thermogravimetric analysis (TGA). Interparticle pores can be observed in appreciable amounts while intraparticle pores are not detected. This is due to the low porosity found in clay-rich samples.

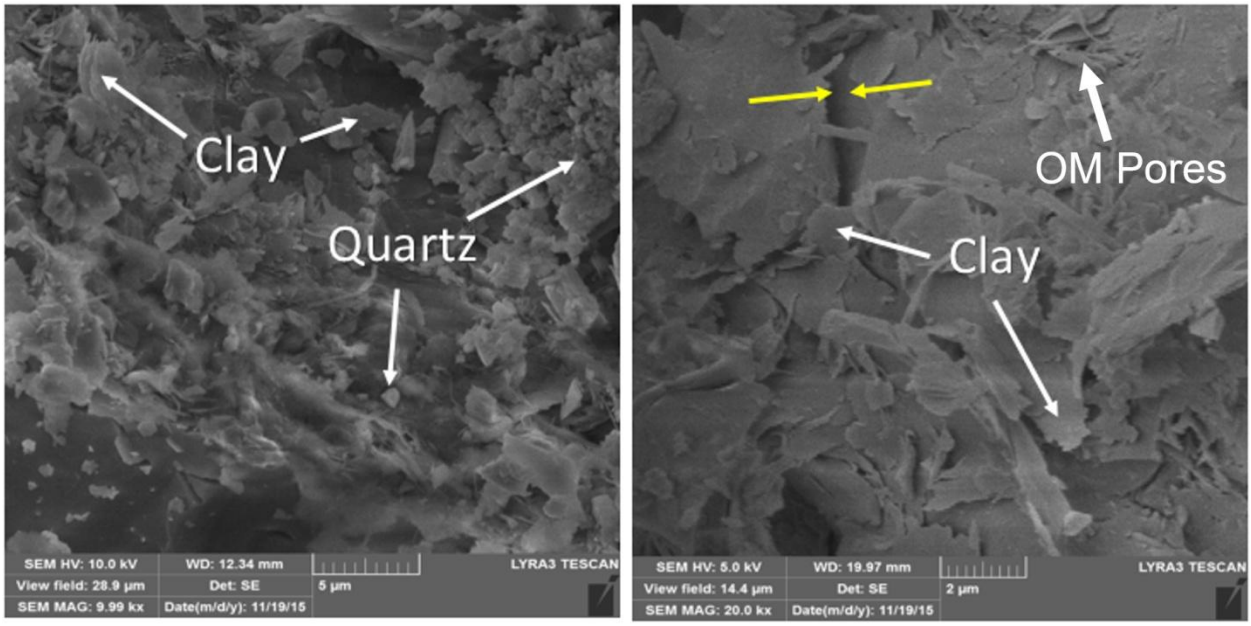

Figure 42: SEM images for sample A; yellow arrows point towards micro-fractures.

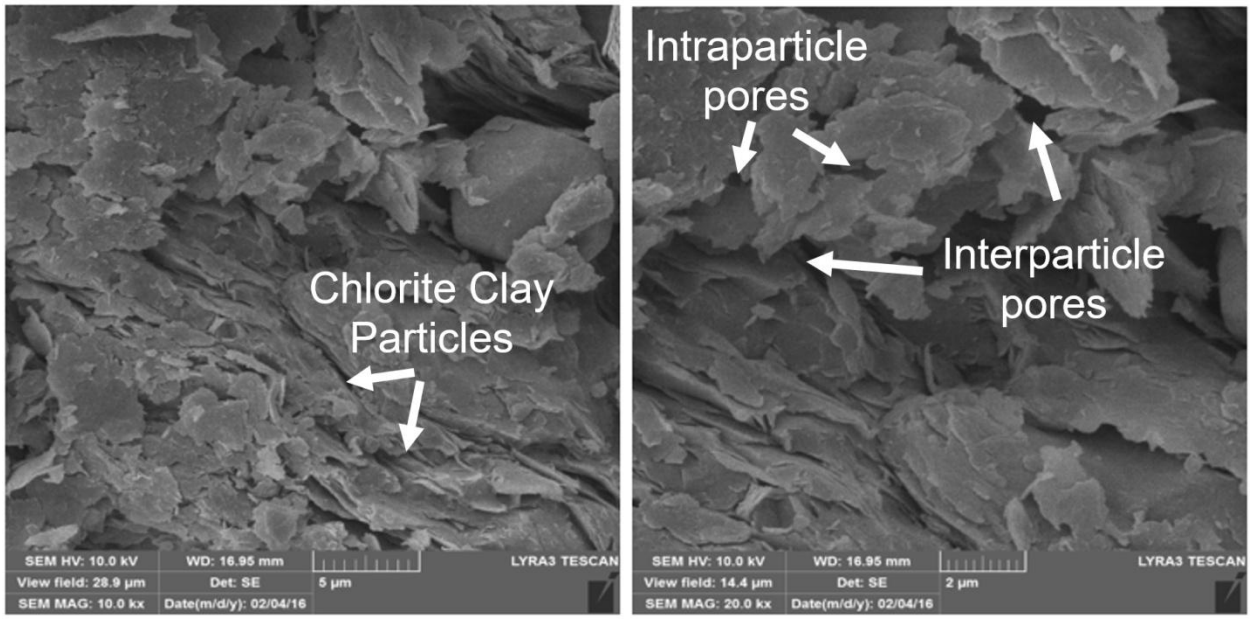

Figure 43: SEM images for sample B. Clay sheets dominate the whole surface. No clear micro-fractures exist.

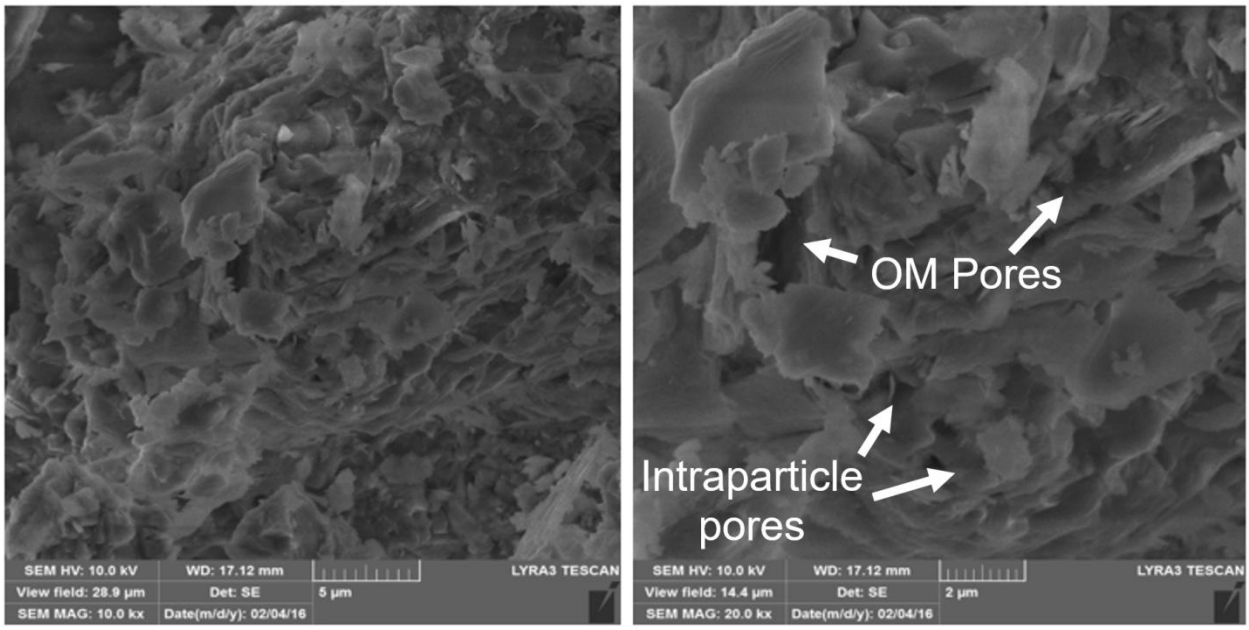

Figure 44: SEM images for sample C. Clay sheet-like particles are clearly visible. No clear micro-fractures exist.

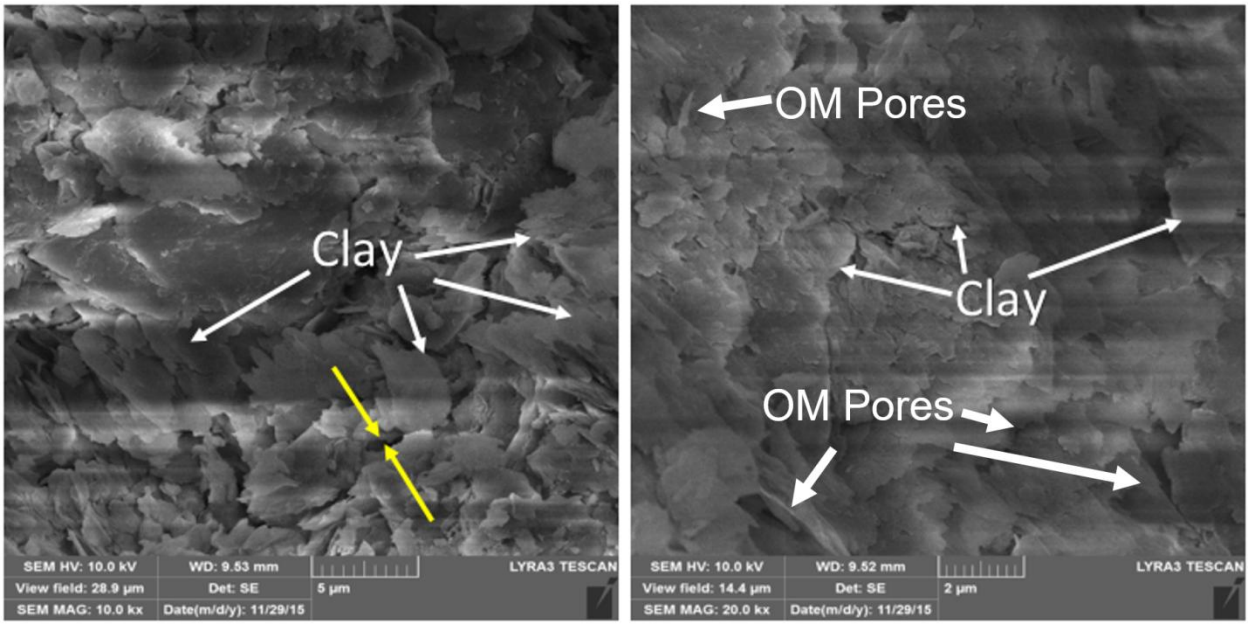

Figure 45: SEM images for sample D; yellow arrows point towards micro-fractures.

4.2 Mineralogical composition and organic matter content

4.2.1 X-ray fluorescence

Elemental composition was determined using X-ray fluorescence and results are summarized in Table 2. Silicon and aluminum are the two most abundant elements in all the samples as it is expected since clays are classified as aluminosilicates minerals. Moreover, the four samples show minor presence of other cations such as calcium and magnesium in general. Only sample D showed appreciable amount of sulfur present.

Samples with high clay content, B and D, contain significant amounts of iron and potassium compared to the other two samples with low clay content. Iron and potassium are common elements in illite and chlorite as well as smectites to a lesser extent. These two ions can be an original constituent of the clay minerals or substituents to other ions that already exist. Isomorphic substitution, or cation exchange, is common in different types of clays especially smectite and this process gives rise to the negative charge on the clay surface. Some types of clays are more readily available for cation exchange than others and, therefore, cation exchange capacity test is conducted to quantify this behavior.

4.2.2 X-ray diffraction

X-ray diffraction results for the four samples are summarized in Table 2 for both the bulk shale samples and the clay fraction composition. Samples B and D have the highest clay content and they are composed mainly of illite, chlorite and kaolinite while the analysis of the clay size fraction shows the presence of illite-smectite mixed layer. On the other hand, sample A has high quartz content with minor presence of illite and chlorite clays. Sample C is intermediate between

Table 2: Summary of quantitative Analysis

Analysis	Mineral/Element	Unit	Sample A	Sample B	Sample C	Sample D
XRD Bulk Mineralogy	Quartz	wt%	80.4	27.5	63	23
	Muscovite	wt%	1.1	4.7	4.6	8.9
	Albite	wt%	9.5	1.4	14.3	0
	Siderite	wt%	1.8	0.8	1.8	0
	Illite & Mixed	wt%	3.4	17.2	3.5	5.4
	Chlorite	wt%	3.8	31.2	11.3	6.8
	Kaolinite	wt%	Trace	17.2	Trace	51
	Total Clay	wt%	7.2	65.6	14.8	63.2
XRD Clay Size Fraction Analysis	Illite	wt%	0	22	0	6
	I-S Random	wt%	84	0	68	15
	I-S Ordered	wt%	0	26	0	0
	% S in I-S	wt%	5-10	0	1-5	5-10
	Chlorite	wt%	16	27	32	19
	Kaolinite	wt%	0	25	0	60
	Clay Size Fraction	wt%	4	12	7	16
XRF Elemental Composition	Si	wt%	76.4	41.5	65.4	40
	Al	wt%	7.9	23.8	11.9	21.6
	Fe	wt%	7.8	21.1	10.8	20.4
	K	wt%	3	7.6	3.9	7.3
	Ca	wt%	2.1	0.7	4	0
	Mg	wt%	0.6	1.7	1.3	3.4
	Cl	wt%	0.1	0	0	0.7
	S	wt%	0	0.6	0	3.4
TGA Weight Loss		wt%	2.22	9.55	4.75	17.61
Cation Exchange Capacity (CEC)		meq/100 g	2.5	13.5	5.5	15
Capillary Suction Time (CST)		Sec	42.1	77.7	42.6	38.5

the two extremes and contains mainly quartz, chlorite and illite. Figure 50 shows the ternary classification plot that was utilized to have a sense of comparison to other shale plays such as Barnett and Eagleford. Based on mineralogy-based classification ternary plots, sample A can be classified as mixed siliceous mudstone, sample B as silica-rich argillaceous mudstone, sample C as mixed siliceous mudstone and sample D as mixed argillaceous mudstone.

Non-clay minerals found in the four shale samples include muscovite, albite and siderite. Muscovite, belongs to the mica group, is present in all the four samples with a range starting from 1.1% up to 8.9%. It is a sheet-like material and classified as a phyllosilicate, similar to clays, but composed mainly of aluminum and potassium. Albite, that is a feldspar mineral rich in sodium, is also present in samples A and C, and to a lesser extent, in sample B. Siderite is a diagenetic mineral found in shales with small amounts. This mineral is rich in iron that can be substituted with zinc, magnesium or manganese.

The XRD patterns of both bulk and clay size fraction samples of the four types of clays are shown in Figure 51 through Figure 54. For sodium montmorillonite, the sample was almost pure indicated by the strong peak between 2-theta values of 8 º and 9º. Upon glycolation, this peak shifted to the left which is a characteristic of the swelling clays. Illite sample showed a peak at 9.5º which is the standard value for illite clays. However, it contained impurities such as quartz indicated by the strong peak at 26.6º as well as minor amounts of kaolinite and microcline. Similarly, Illite smectite mixed layer was found to be a major clay mineral but there exist high amounts of quartz and kaolinite as well as traces of illite. Kaolinite sample was almost pure with trace amounts of quartz.

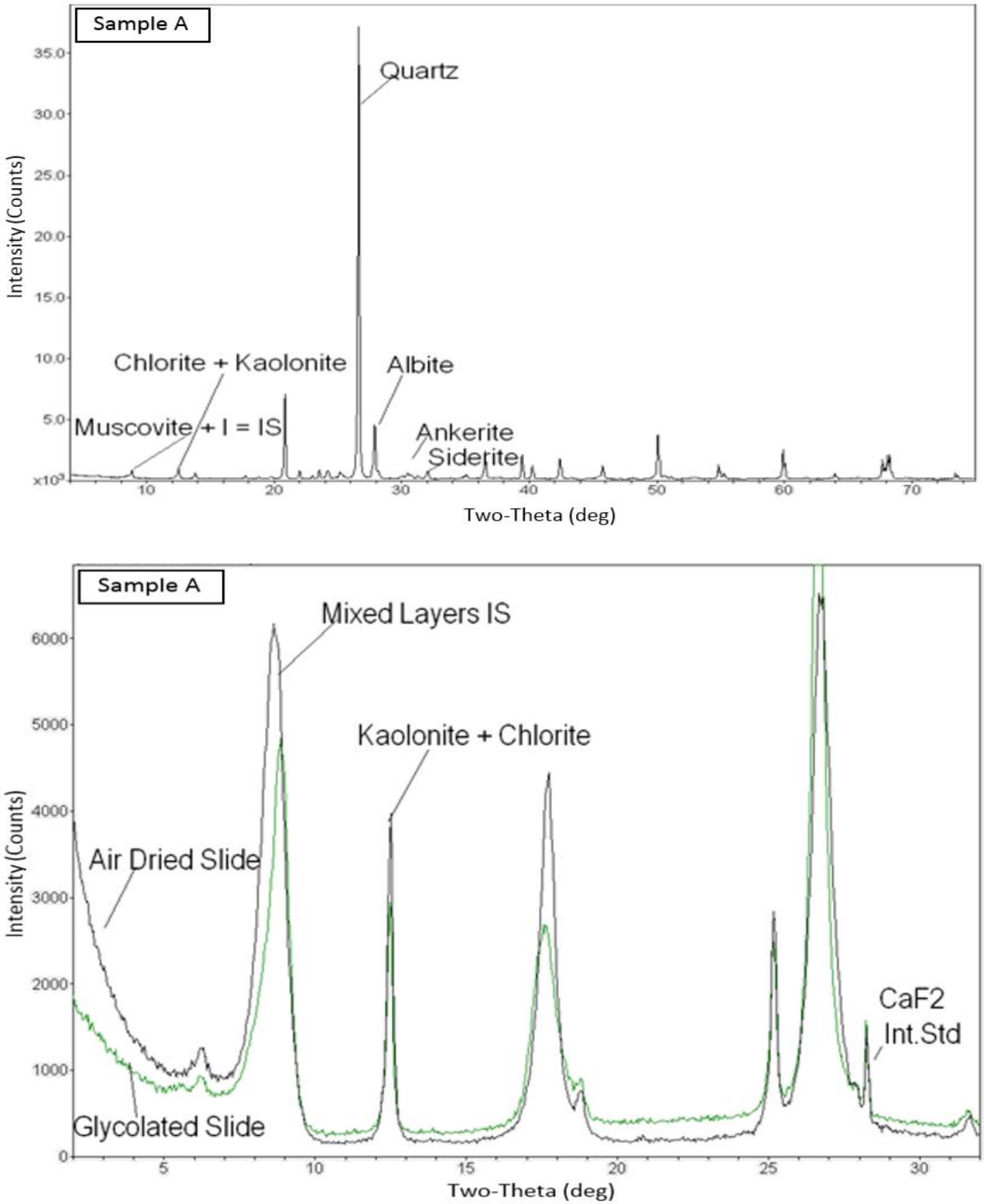

Figure 46: XRD Patterns for sample A (Bulk and Clay size fraction)

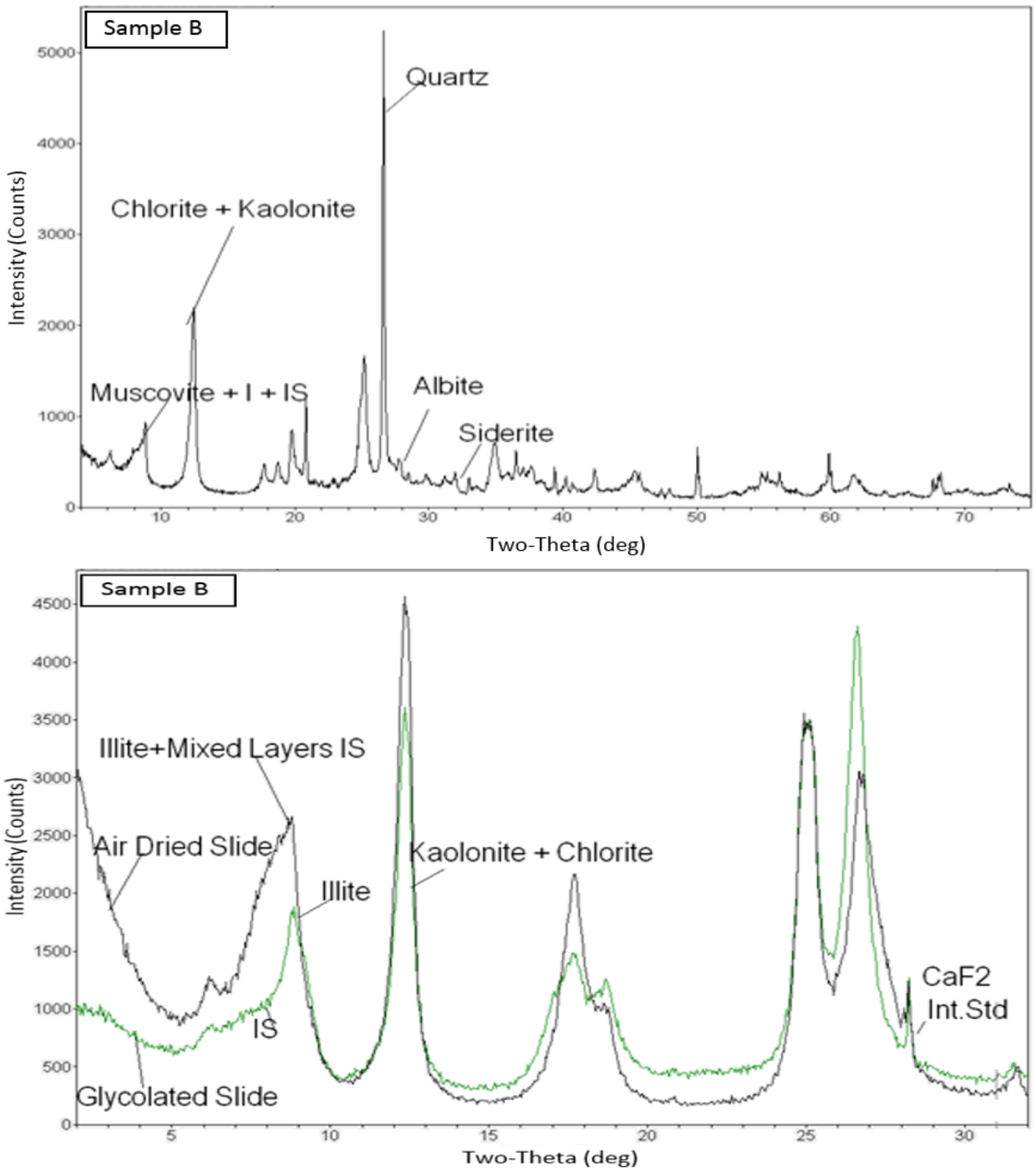

Figure 47: XRD Patterns for sample B (Bulk and Clay size fraction)

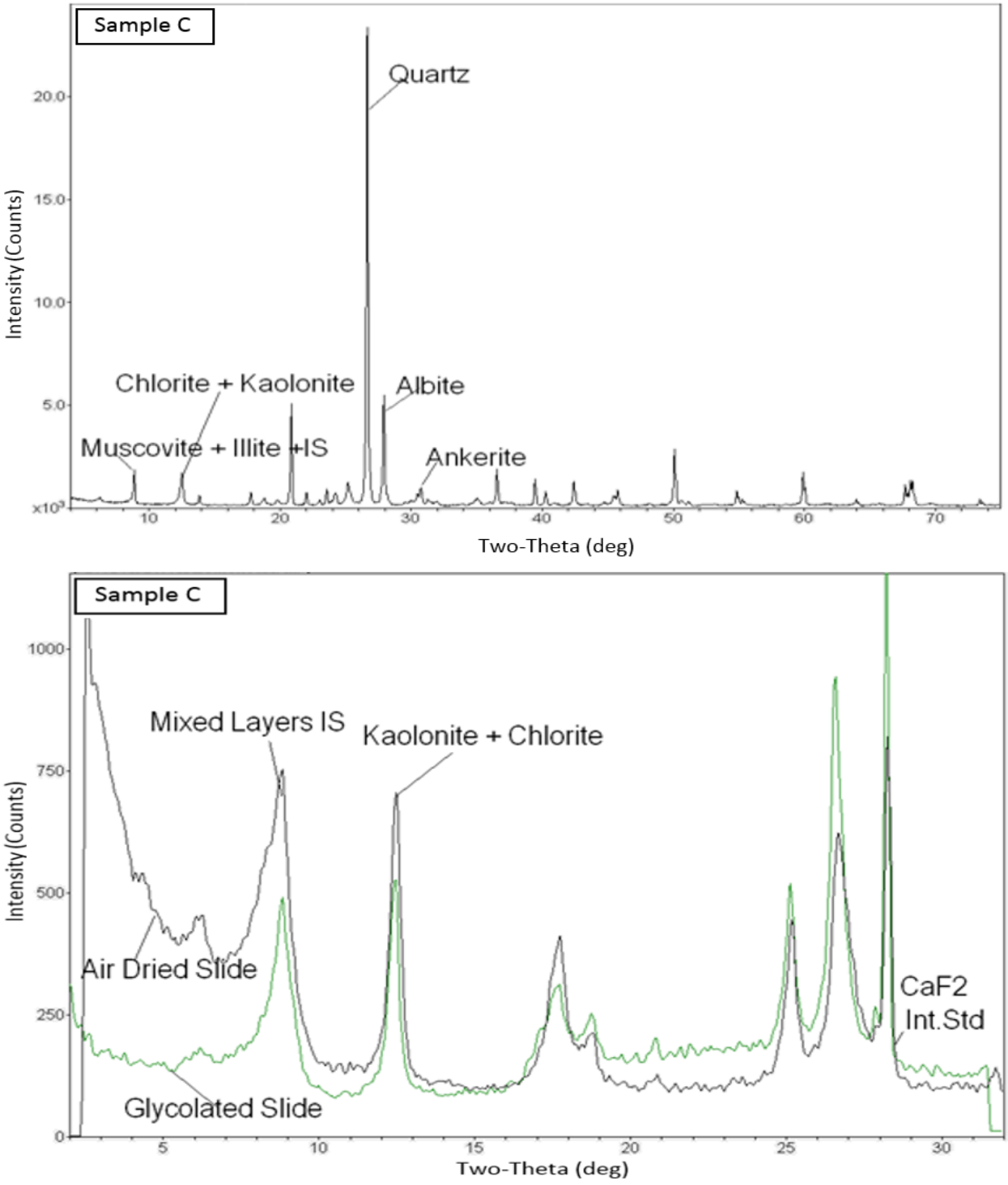

Figure 48: XRD Patterns for sample C (Bulk and Clay size fraction)

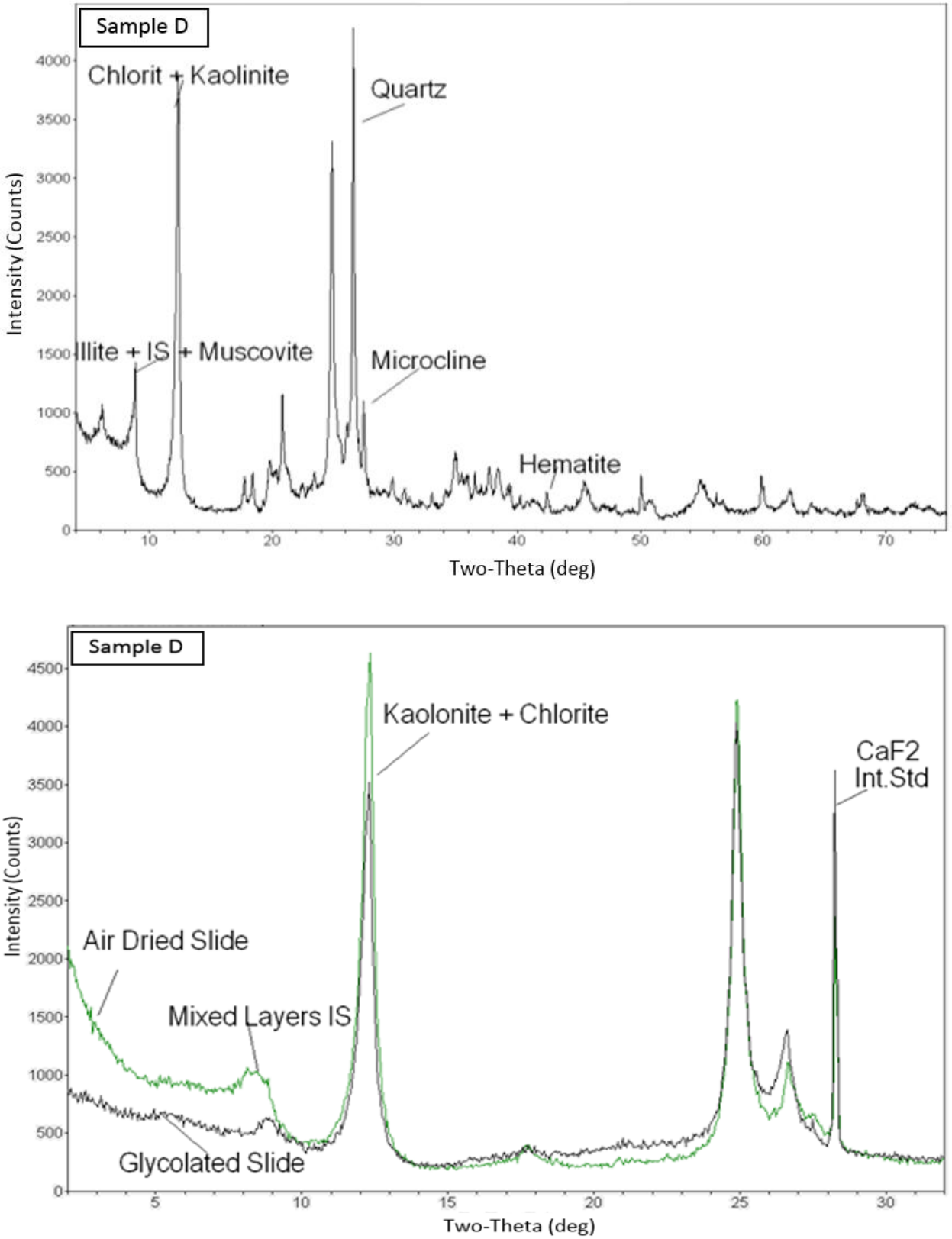

Figure 49: XRD Patterns for sample D (Bulk and Clay size fraction)

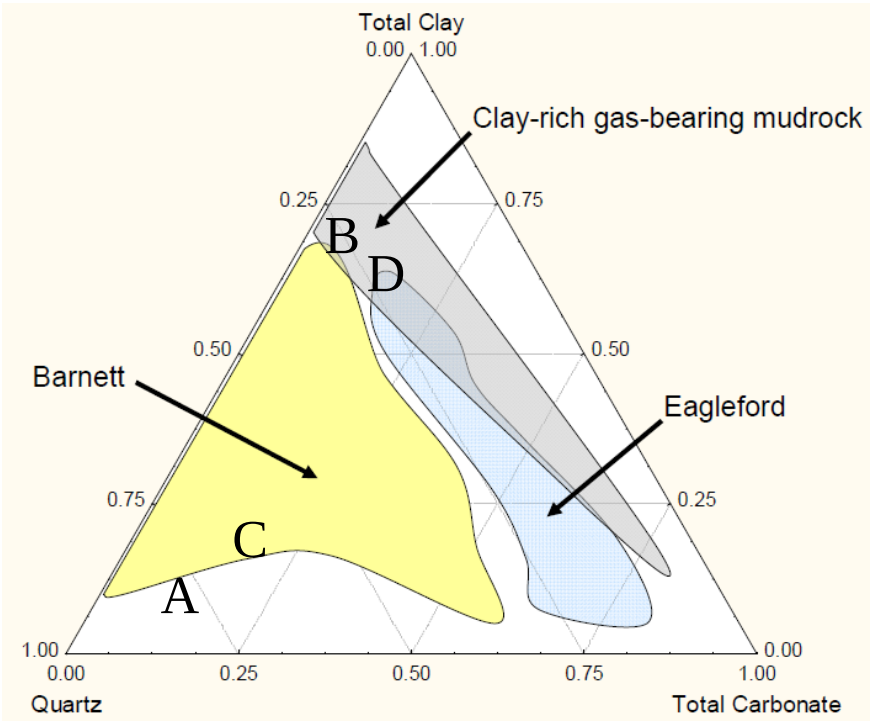

Figure 50: Mineralogy-based ternary diagram showing the four samples (Modified after Passey et. al. 2010)

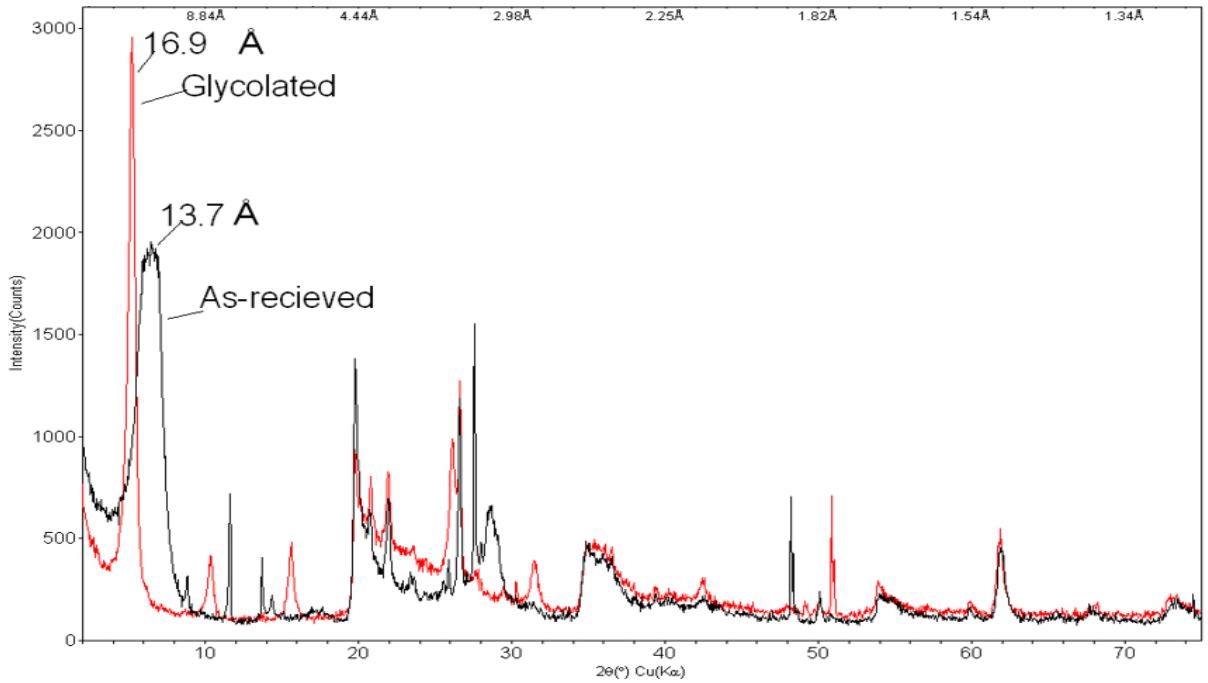

Figure 51: XRD Patterns for sodium montmorillonite

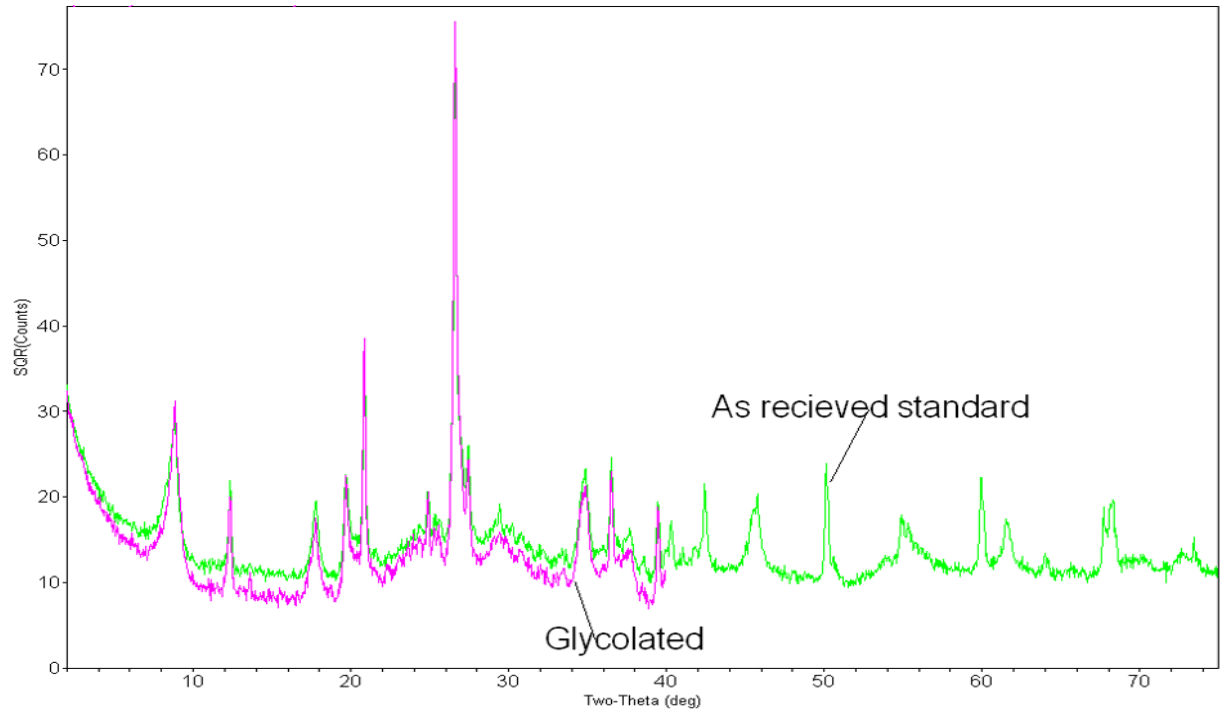

Figure 52: XRD Patterns for illite

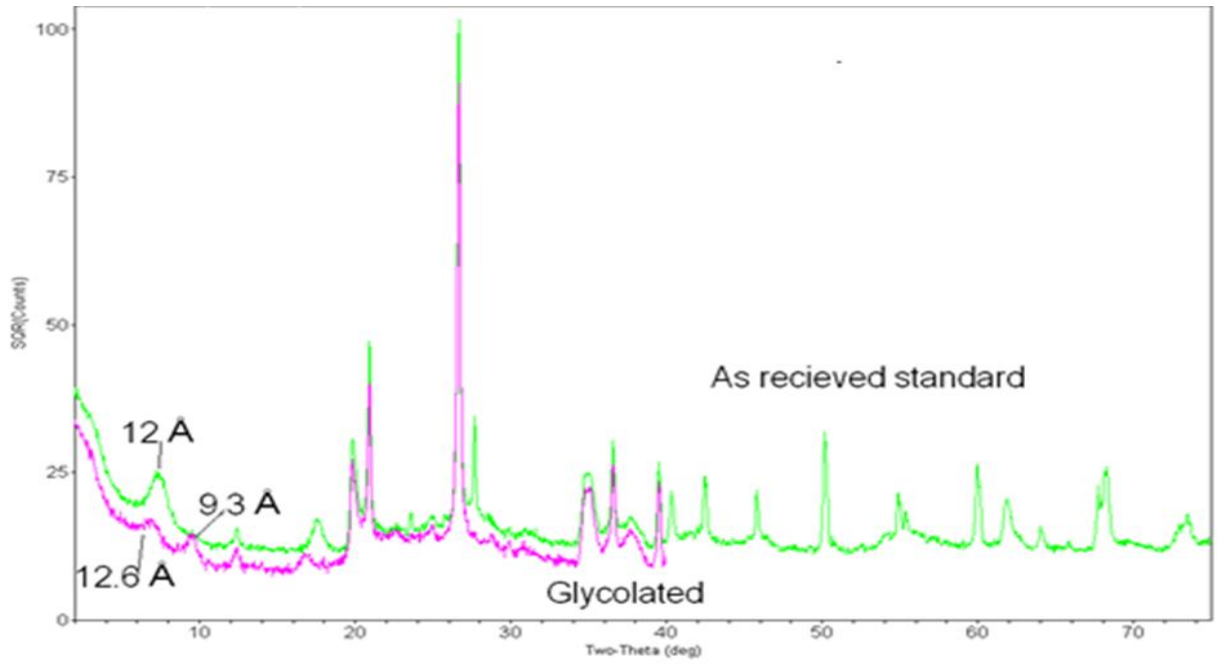

Figure 53: XRD Patterns for illite-smectite

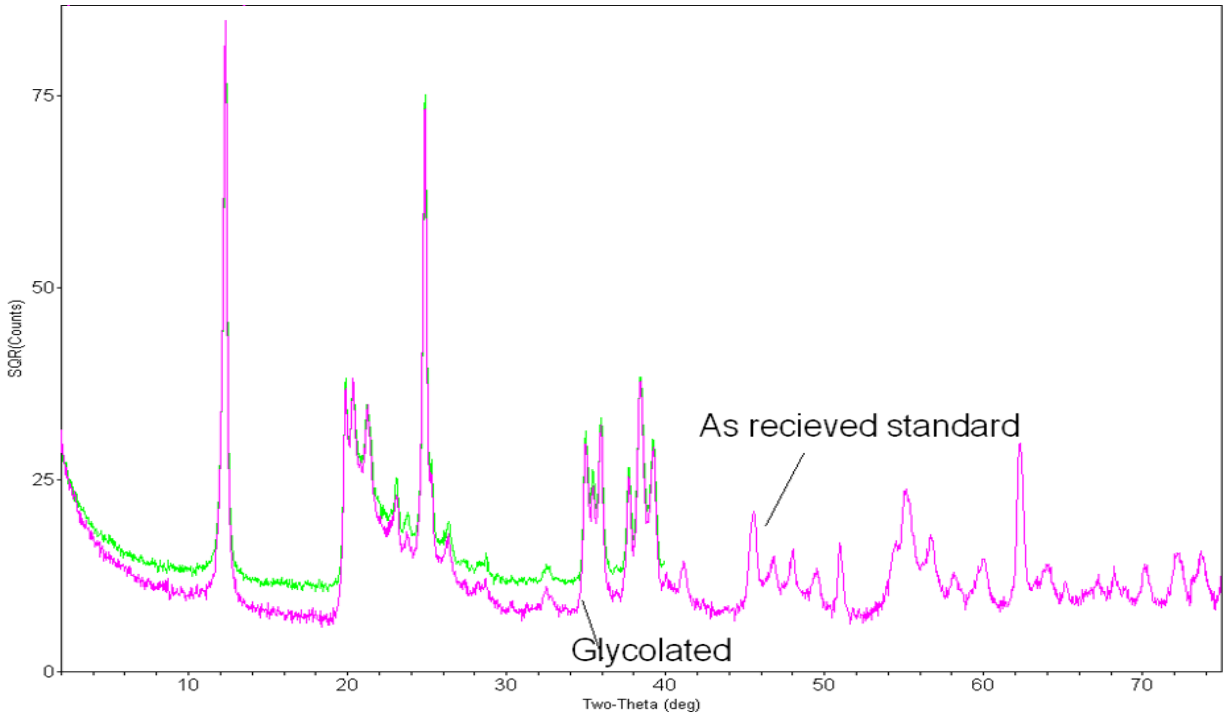

Figure 54: XRD Patterns for kaolinite

4.2.3 QEMSCAN

Figure 55 through Figure 58 show QEMSCAN images for the four shale samples. Samples A and C are dominated by quartz with small concentrations of kaolinite, illite and semctite. On the other hand, samples B and D are dominated by clays such as kaolinite, illite and semctite with small amounts of quartz, muscovite and feldspars. These results are in good agreement with XRD results.

QEMSCAN gives detailed view of the samples with much higher resolution compared to thin section analysis. A detailed study of the images can estimate the porosity, pore size distribution, organic matter, particle count, particle size distribution, matrix density and elemental analysis.

Porosity maps are shown in Figure 59 through Figure 62 that give indication of the porosity in every sample. Clearly, sample A followed by sample C have the highest porosities as indicated by the blue color. This is due the abundant amounts of quartz over other minerals. Porosity and permeability is greater for quartz than other minerals, especially clays because of their high level of sphericity and larger grain size. Unlike quartz, clay particles are sheet-like with have poor sphericity and much smaller in particle size. Therefore, samples B and D have low porosity. The mapping feature of QEMSCAN allows the analysis of the distribution and locations of pores. As evident from the images, pores are more concentrated where there is high concentration of quartz grain. However, the areas that are rich in clay particles, significantly a lower number of pores are present. Moreover, the pore sizes can be inferred from the QEMSCAN maps. Where the majority of pore sizes are close to 14.7 μm in sample B and D, the pore sizes are much larger in samples A and C where a good number of the pores are in the range of 63 μm.

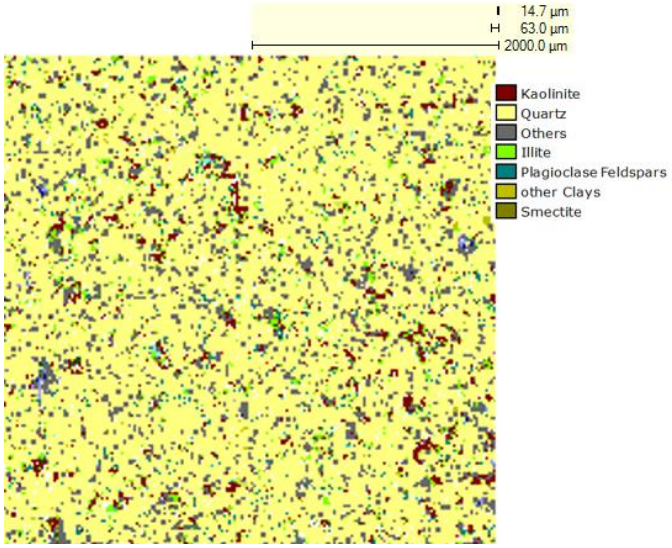

Figure 55: QEMSCAN Image showing the mineralogical content of Sample A

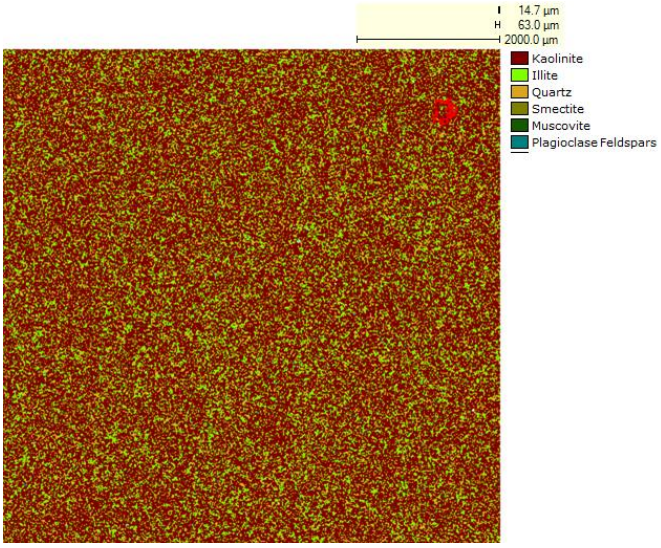

Figure 56: QEMSCAN Image showing the mineralogical content of Sample B

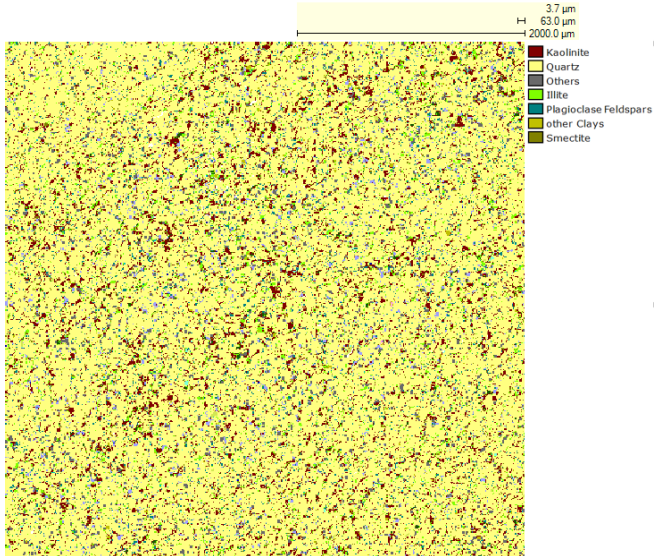

Figure 57: QEMSCAN Image showing the mineralogical content of Sample C

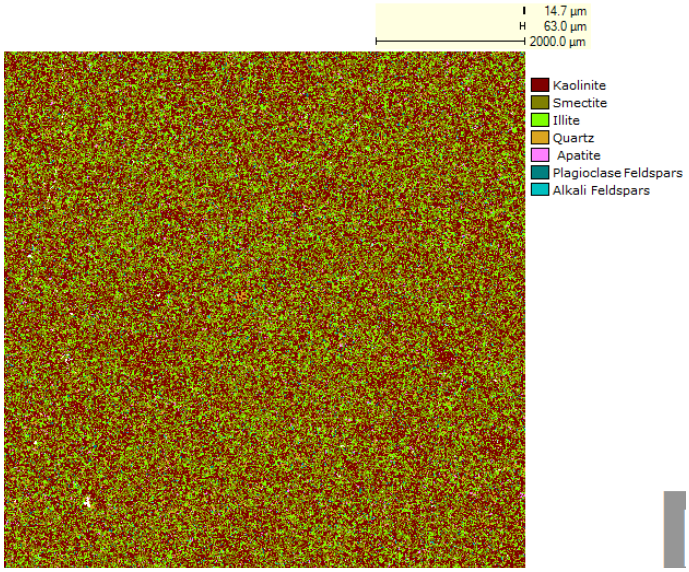

Figure 58: QEMSCAN Image showing the mineralogical content of Sample D

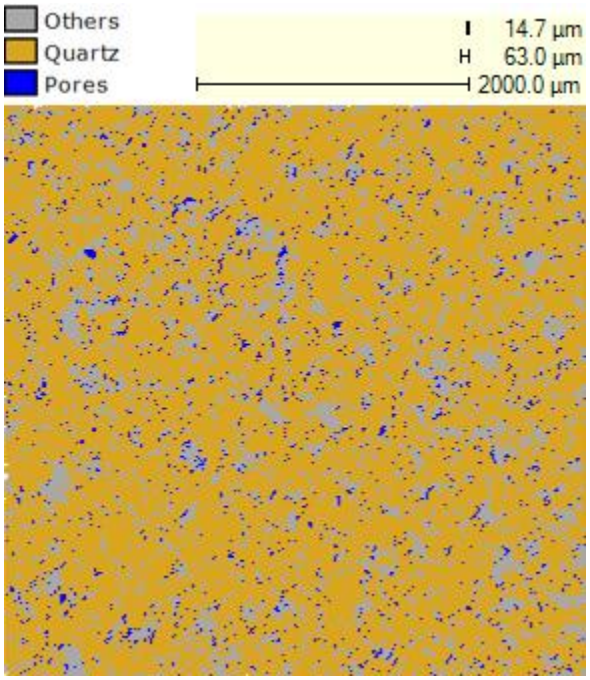

Figure 59: QEMSCAN image showing porosity in Sample A

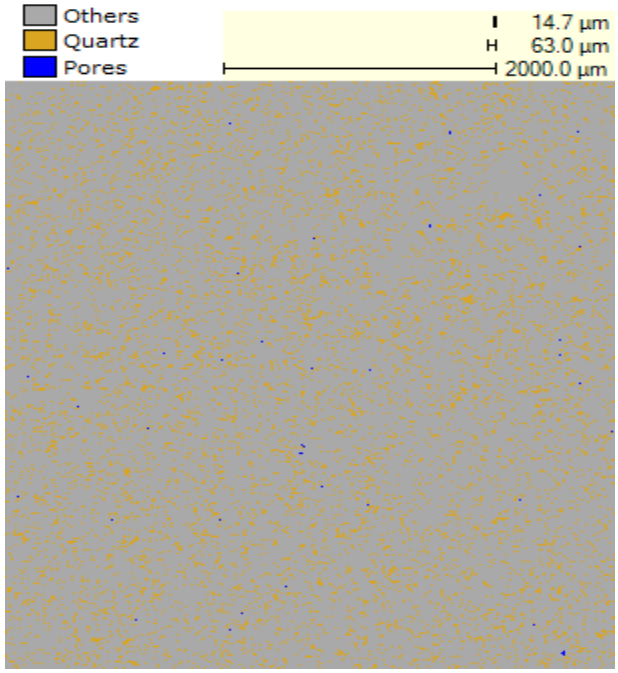

Figure 60: QEMSCAN image showing porosity in sample B

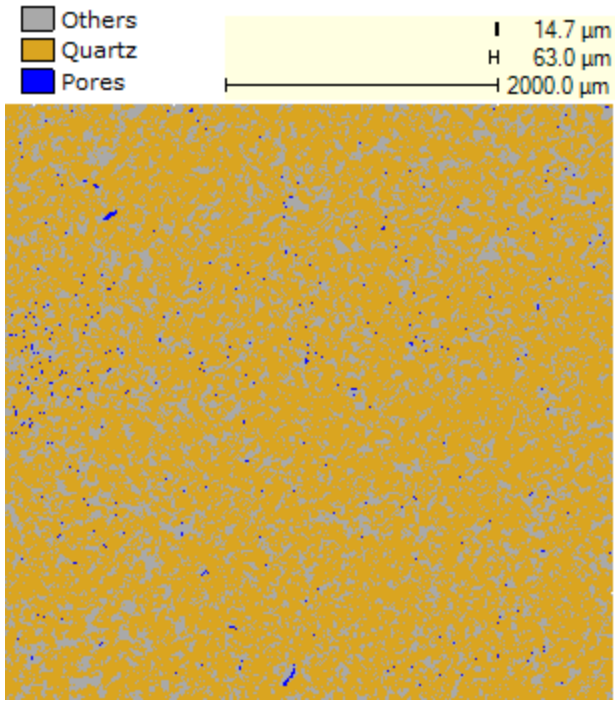

Figure 61: QEMSCAN image showing porosity in sample C

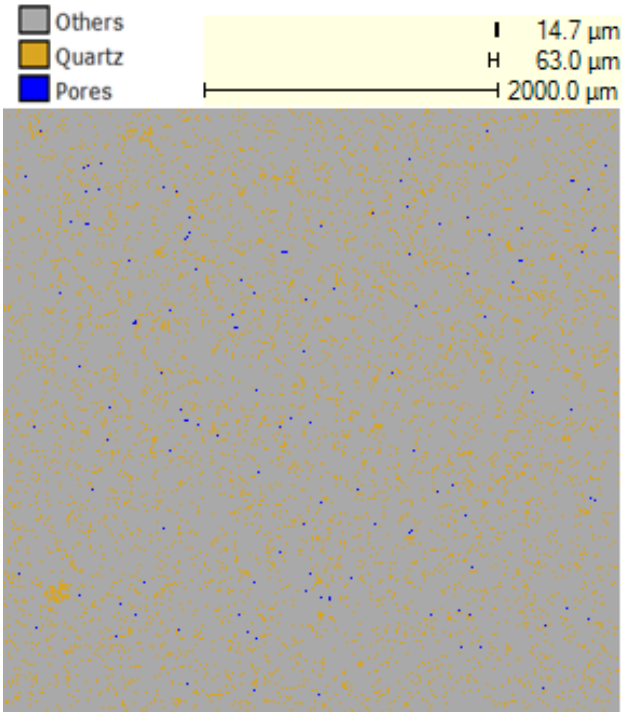

Figure 62: QEMSCAN image showing porosity in sample D

4.2.4 Thermogravimetric analysis

TGA results are shown in Figure 63. Curves of weight loss using thermogravimetric procedure and also the differential thermogravimetric curve to show the rate of change of mass are presented. Three distinct regions can be clearly noticed in these curves. The weight loss in the first region can be attributed to the vaporization of water (lattice water and coordinated water) and light hydrocarbons. This region is covering the temperature range up to 290 °C. Then comes the second region starting from 290 °C up to 550 °C where heavier hydrocarbons decompose and cause the weight loss. The third region is after 550 °C when inorganic content starts to decompose.

Sample A has the lowest weight loss among the four samples, 2.22%. This can be attributed to the low organic content and high quartz composition. Similar TGA results can be noticed for sample C where less than 5% of sample weight was lost. These two samples had comparable weight loss in the first and second regions but, however, sample C showed much more weight loss in the third region where the inorganic content decomposes. Therefore, no major difference in the organic matter is expected between sample A and C. After that comes Sample B with about 10% weight loss out of which only 4% weight loss in the light and heavy hydrocarbons regions. Thus, an intermediate content of organic matter is expected in this sample. Sample D had the highest weight loss with 18%. The weight loss values over the three regions were close enough. This predicts the high organic matter present in this sample that is indicated by the significant weight loss in the second region, 6.8%. Even for the first region where water and light hydrocarbons evaporate, 4.99% of the weight was lost which is indicative again of the relatively high percentage of light organic matter.

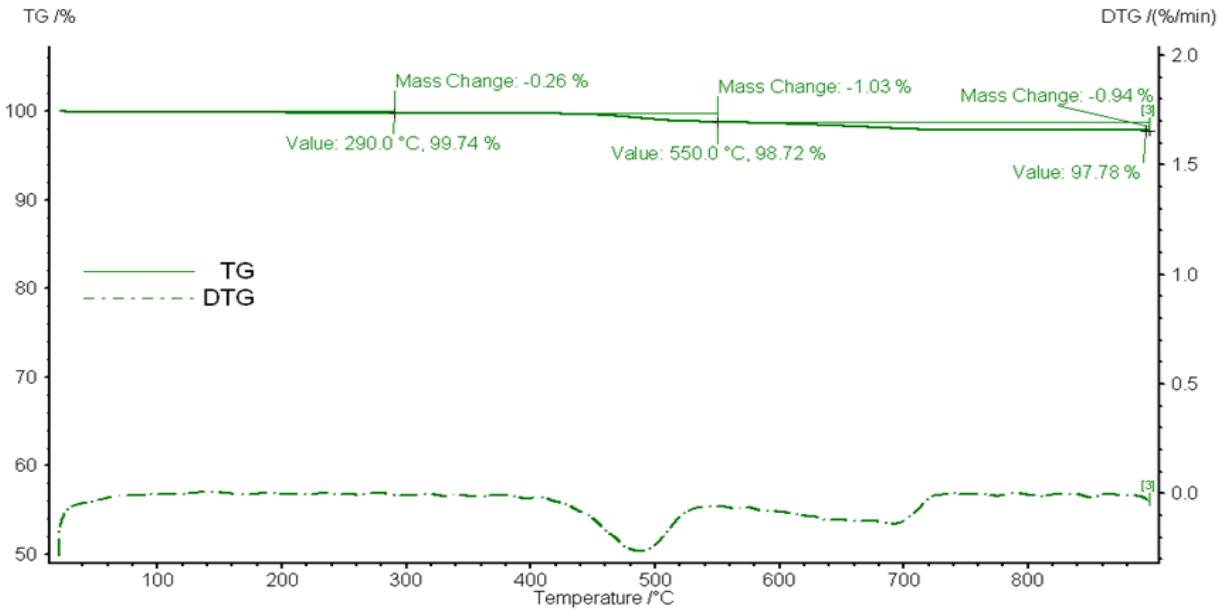

Sample A

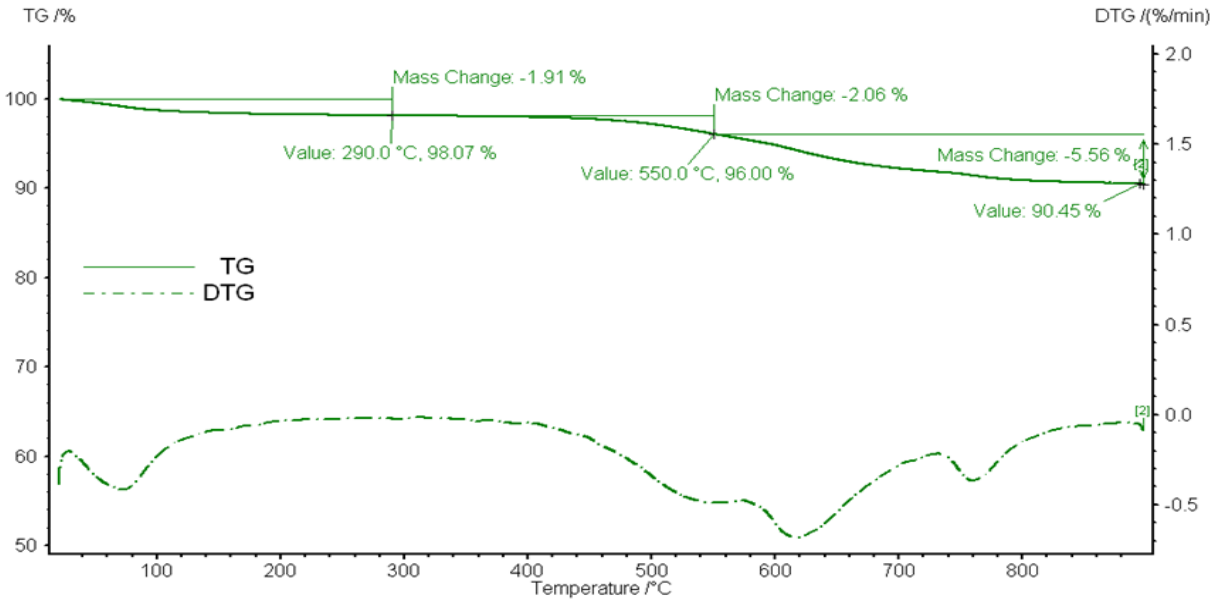

Sample B

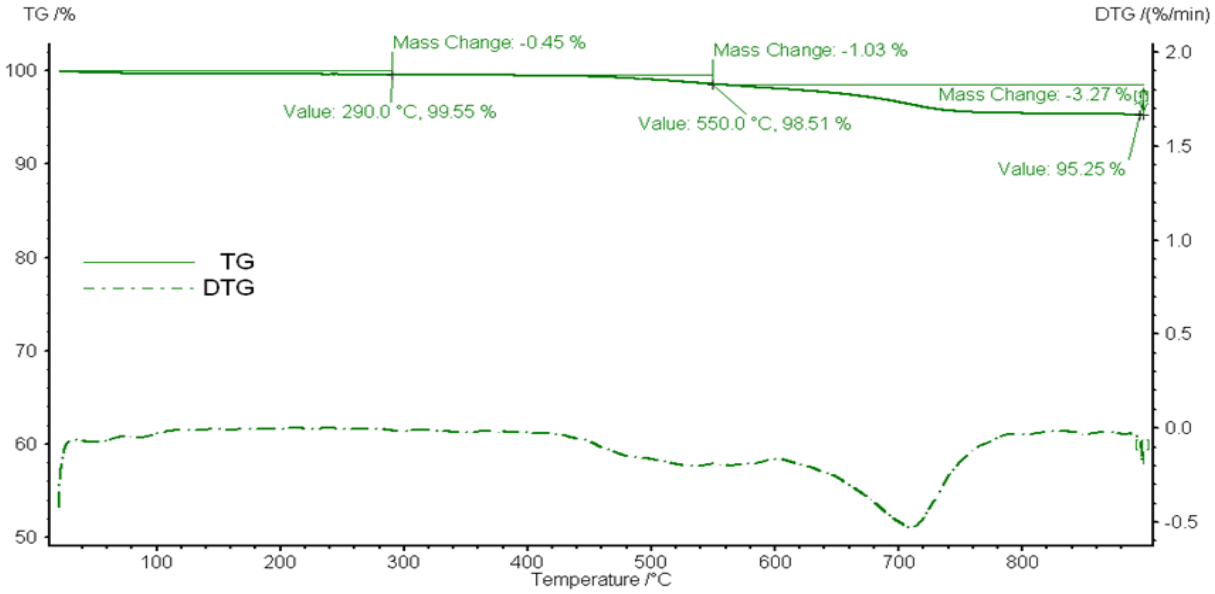

Sample C

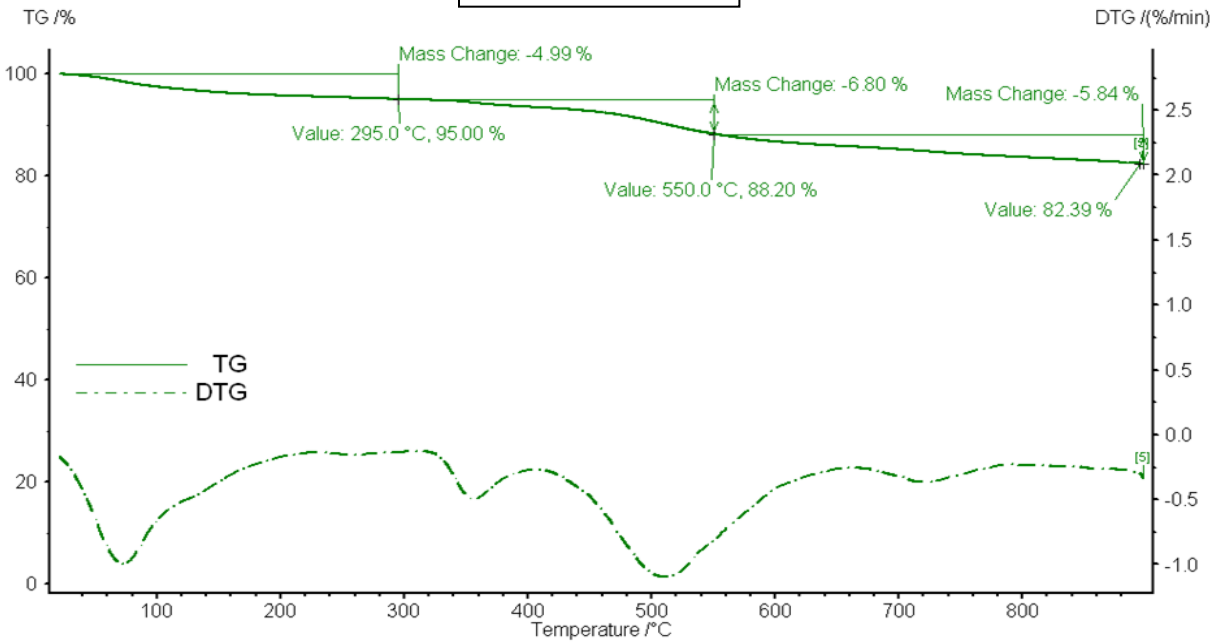

Sample D

Figure 63: TGA Results for the four samples

4.3 Reactivity potential testing

4.3.1 Cation exchange capacity test

CEC results, Table 1, show the holding capacity of the shale sample for cations. It also gives indication about the surface area. Because clay particles are in the micron size range and, thus, have large surface area, they can hold and exchange a large number of cations. The results can be directly correlated with the XRD and SEM results where the mineralogical composition of high clay content showed clearly higher values of CEC, starting with the silica rich sample, sample A, and ending with the two clay-rich samples, samples B and D while sample C of intermediate clay content has intermediate CEC value. The CEC results reveal the high reactivity level for samples B and D which can be attributed to the high clay content and, especially, the high content of illite and smectite either in pure forms or in mixed layers as shown by XRD results.

Shale reactivity can be further investigated by conducting inhibition tests: swelling and dispersion. Shales with high CEC values, in general, show more tendency to swelling due to the large surface area that is available for contact with fluids and also because of readiness of the cations to exchange.

4.3.2 Capillary suction time test

Capillary Suction Time test results are summarized in

Table 3. Once the slurry is injected into the funnel of the CST apparatus, filter cake forms due to the presence of suspended clay particles. The liquid part of the slurry, filtrate, starts to imbibe into the filter paper as a result of capillary force. The movement of this filtrate can be fast or slow depending on the shale sample. The relative flow capacity is measured as CST value in

seconds. High CST values indicate the high tendency to form colloidal suspension and, therefore, high swelling/dispersion. Three main parameters control the CST values: shale particle size, solids content and settling rates of slurry.

For subsurface samples, A and C showed the lowest CST values while sample B showed the highest. This can be related directly to the mineralogy and clay content revealed from X-ray diffraction analysis since as clay content increases, the CST value increases as well due to the smaller particle size and lower pseudo permeability. The CST values of sample A and C are close to each other although the clay content is higher for sample C. This can be attributed to the types of clays present in each sample where sample A has higher illite-smectite content than sample C.

The outcrop sample D showed inconsistent results with mineralogy and this might be attributed to the nature of the sample where it is not packed to same degree as it is the case for subsurface samples. This increases the pseudo permeability and lowers the value of CST.

4.3.3 Moisture content and Adsorption isotherms

Initial moisture content results are summarized in Table 4. For shale sample, moisture content correlates with the amount of clay present. As the particle sizes of clays are in the micron range, they have large surface area to interact with and adsorb water. Therefore, as the clay content increase, there is an increase in the moisture content. The moisture content also depends on the type of the clay. Smectites, in general, have more tendency to adsorb water and expand while illite does not show high level of adsorption and swelling.

Based on the results from both tests: swelling and moisture content, the ultimate swelling percentages of the shale and clay samples were plotted against moisture content, Figure 64. In agreement with the experimental results of Gomez et. al. (2011), the results showed a linear

correlation where the swelling percentage increases as moisture content increases as well. This correlation can be explained by the adsorption potential of the shale/clay sample. As the surface area available for interaction increases and, also, as the percentage of expansive type of clays increases, there will be an increase in the moisture content. The adsorbed moisture/water diffuse into the interlayer space and start hydrating the cations and, as a result, the average distance of cations to the clay surface increases. Therefore, the interlayer spacing increases and the clay particle expands.

Adsorption isotherms were established using six different saturated salt solutions to cover the relative humidity range from 7.5 to 93%, Figure 65 through Figure 72. Attempts have been carried out to fit the adsorption data to the Langmuir, Freundlich and BET adsorption models to describe the adsorption process and determine the mode of adsorption: mono-layer or multilayer. The first attempt was to fit the adsorption data to Langmuir to check if it follows a mono-layer mode of adsorption. All the shale and pure clay samples did not match to the Langmuir adsorption model and showed strong deviation when water sorbed values were plotted against the RH. This can be attributed to the amount of clay present in all shale samples. Due to their small particle size, clays have large surface areas, and therefore, multiple sites for adsorption. On the other hand, some shale and clay samples had good fits to the Freundlich model and some others had good fits to the BET model with high correlation coefficients, Table 5. To improve the correlation fitting of illite and kaolinite, the method described by Hatch et al. (2012) was followed. This method suggested dividing the RH axis to two regions: The first region is at low RH values and the second one is at high RH values to better fit the data.

Table 3: Capillary Suction Time results

Sample	CST (Seconds)			
	Test 1	Test 2	Test 3	Average
A	40.2	45.0	41.0	42.1
B	71.4	82.4	79.4	77.7
C	43.0	40.4	44.5	42.6
D	39.0	37.7	38.7	38.5

Table 4: Moisture content results

Initial Moisture Content	
Material	**MC (%)**
Sample A	0.21
Sample B	1.6
Sample C	0.29
Sample D	2.76
Na-Montmorillonite	10.99
Illite	1.57
Illite-smectite	4.21

Sodium montmorillonite and kaolinite results were in agreement with the work carried out by Johansen and Dunning (1957) while illite showed a small degree of deviation. Sodium montmorillonite fit to the Fruendlich adsorption model and had a stepwise multilayer adsorption behavior. Every step is indicative of the formation of one hydrate layer. The illite-smectite data fits accurately to the BET model. Illite and kaolinite showed a linear increase in the amount of adsorbed water until reaching 80% RH, then a sharp water content increase was observed with slight increases in the RH. This was attributed to the nature of the clay type where swelling clays has more tendency to swelling and hydration than the other clay types. Kaolinite and illite data did not fit the Freundlich model with a high correlation factor. Therefore, for kaolinite, two regions were established: the first one from 0% to 75% RH and the second one from 75% to 100% RH. The first region shows a behavior similar to the mono-layer adsorption where the affinity is high between the vapor and clay surface. The second region clearly shows the multilayer adsorption with the sharp increase in water uptake. Illite data fits to a reasonable correlation coefficient from 0% up to 60% RH. After that, a large deviation can be observed although the large increase in water uptake at values above 80% RH, which might indicate the multilayer adsorption mode.

The adsorption process can be divided into three stages. The first stage starts at low RH percentages with water molecules adsorbing on the outer surfaces of clay particles. As the RH increases, water molecules in the second stage start to invade the interlayer spacing and solvate the cations present in between the clay sheets. This results in expansion in clay particle's volume for swelling types of clays. As the lamellar space gets saturated with water, the water molecules in the third stage starts to occupy the mesopores and macropores and it can be in the form of bulk

fluid. It is in the third stage where sharp increases in water sorption can be observed as in the cases of illite and kaolinite.

Sample A followed the BET model with reasonable accuracy and some degree of deviation at very low RH. Sample B showed an excellent fit to the BET model with a multilayer mode of adsorption. The intermediate flat region indicates monolayer adsorption while at high RH, as other hydrate layers form. At the end of the isotherm, it showed a significant increase in the water content suggesting the starting of multilayer adsorption. This behavior is expected due to the high kaolinite, illite and chlorite content in the absence of swelling clays such as smectite and an illite-smectite mixed layer. Sample C followed the BET model to high correlation coefficient, although at high RH values, minor deviation can be observed. Sample D clearly showed the multilayer adsorption type and the Freundlich model behavior where it starts with a monolayer behavior but quickly goes into the multilayer mode. This is due to the high clay content in which appreciable amounts of swelling clays are present.

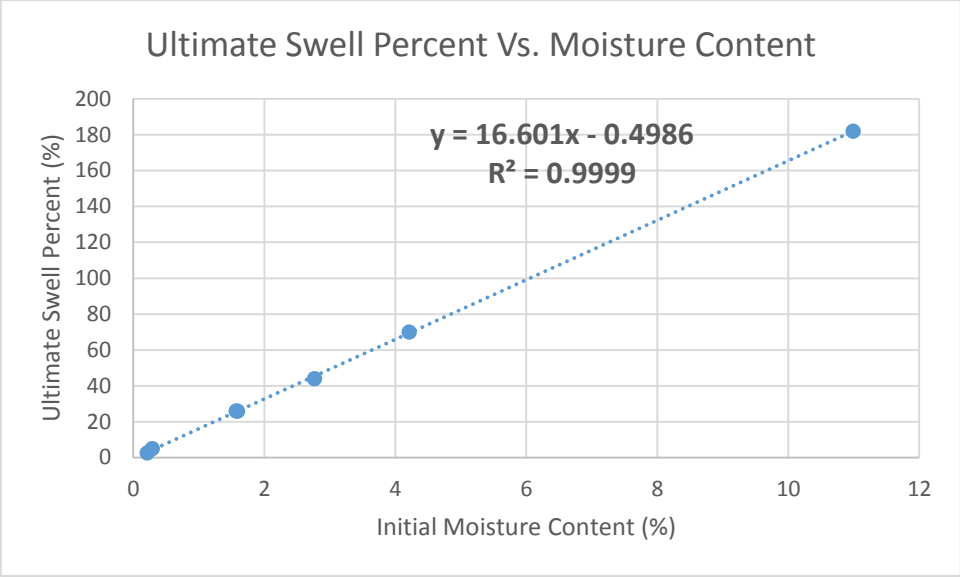

Figure 64: Ultimate swelling percentages as functions of initial moisture content

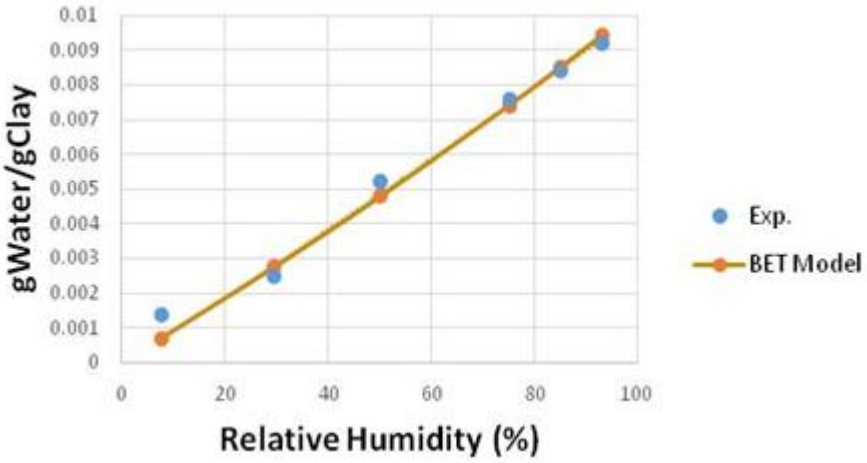

Figure 65: Adsorption isotherm for sample A

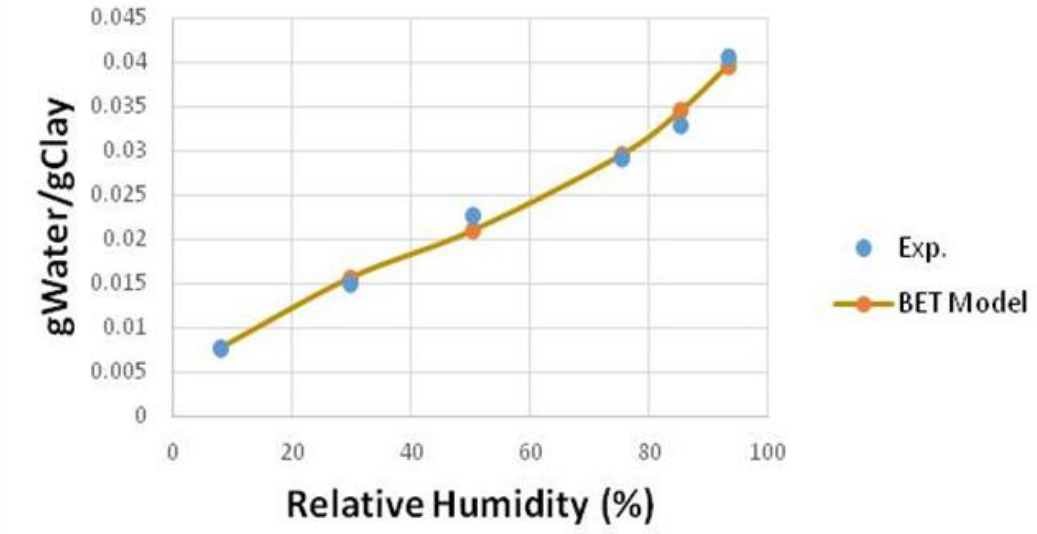

Figure 66: Adsorption isotherm for sample B

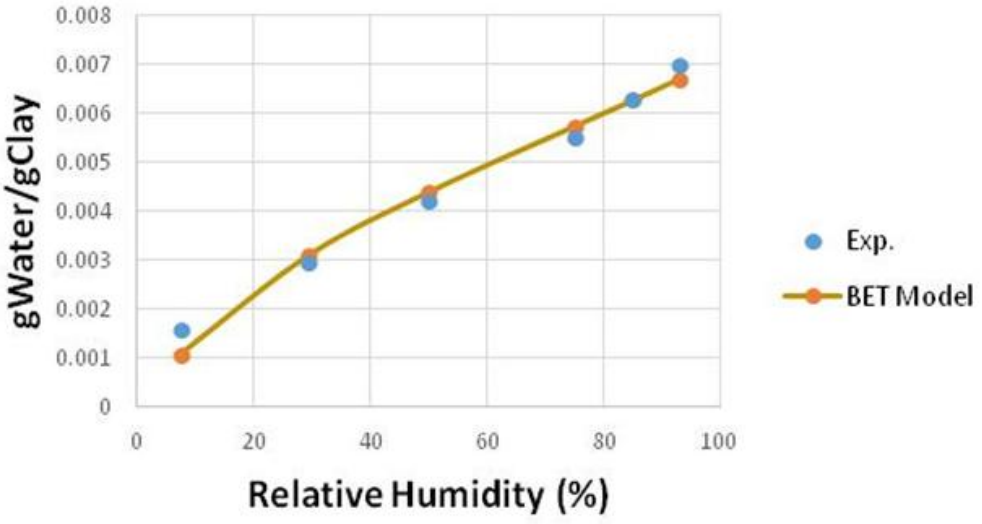

Figure 67: Adsorption isotherm for sample C

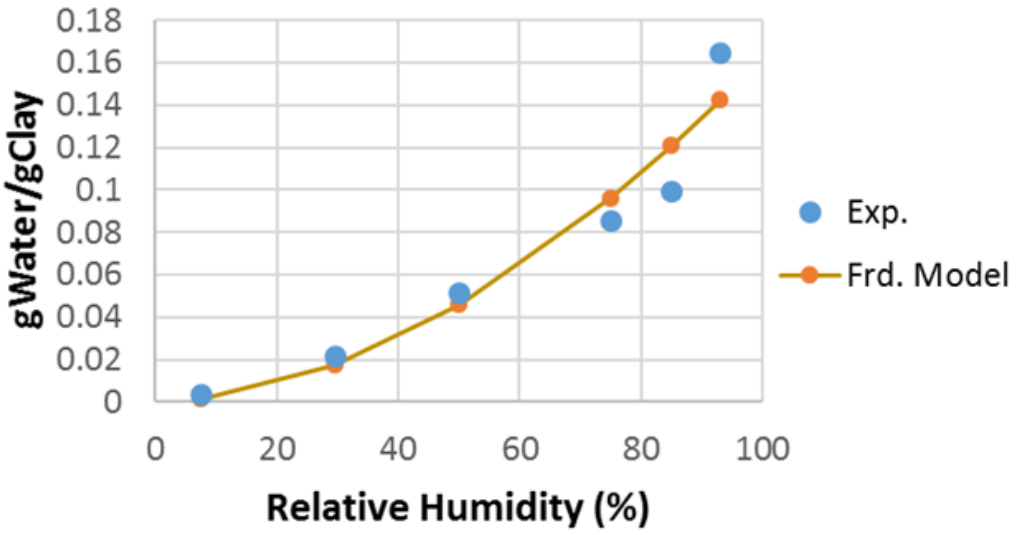

Figure 68: Adsorption isotherm for sample D

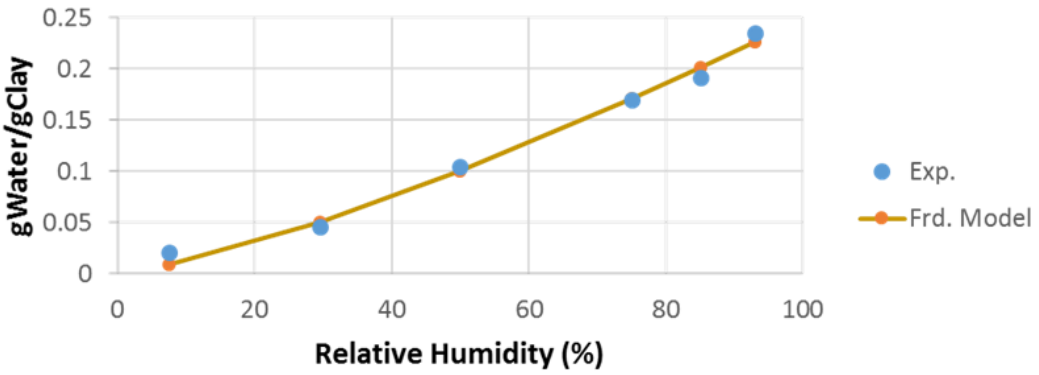

Figure 69: Adsorption isotherm for sodium montmorillonite

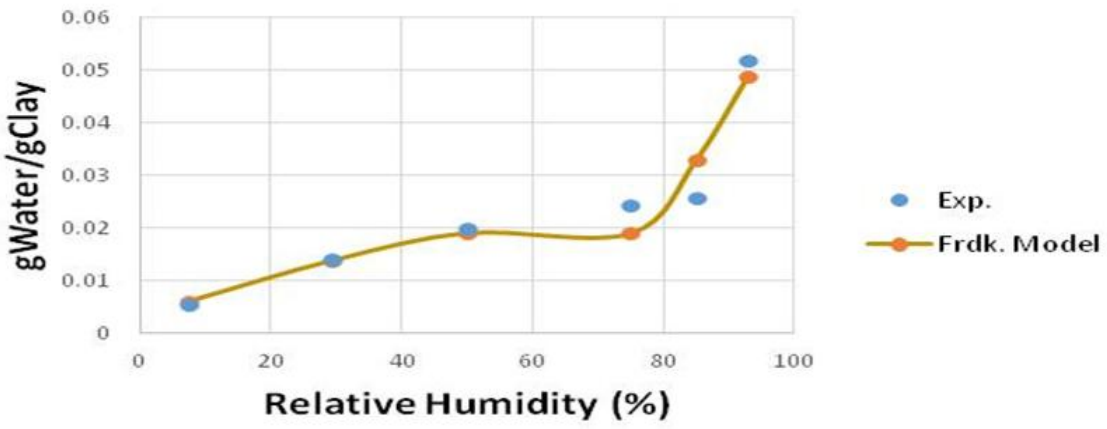

Figure 70: Adsorption isotherm for illite

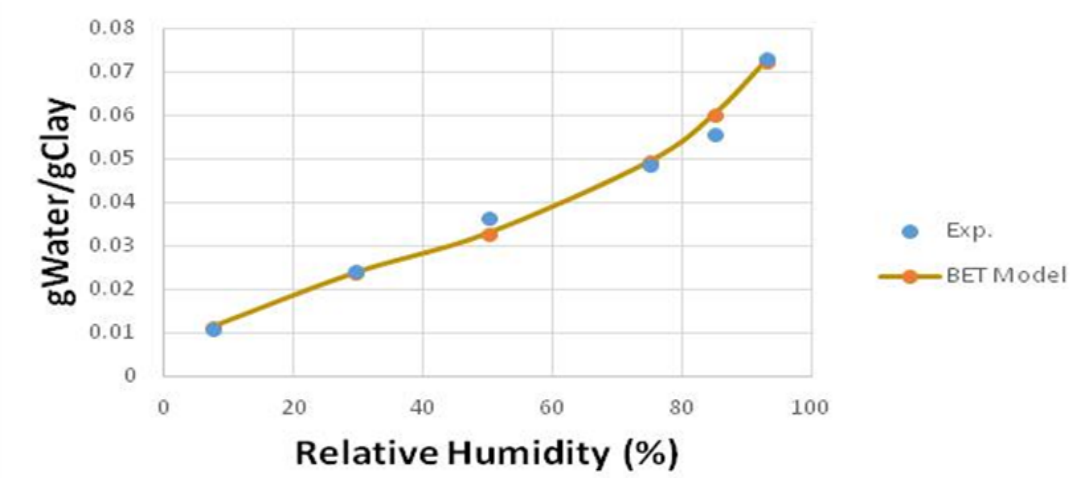

Figure 71: Adsorption isotherm for illite-smectite

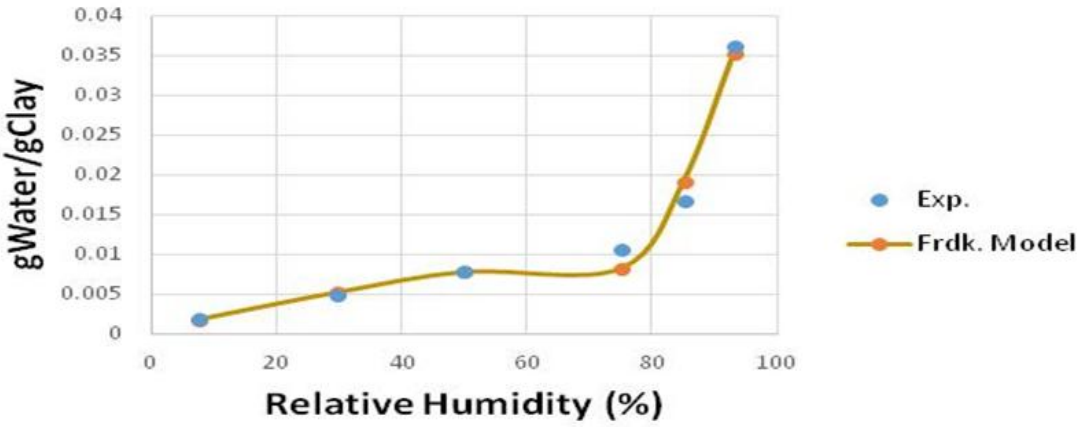

Figure 72: Adsorption isotherm for kaolinite

4.4 Fluid imbibition testing

4.4.1 NMR relaxation time (T_2) test

By applying magnetic field gradient, the positions in space for one nucleus over a short period of time can be estimated. Based on the molecular positions at two different points in time can detect the displacement and, therefore, diffusion. In this study T_2 curves are used to study the diffusion of water and KCl brine into one shale sample.

Results of NMR T_2 distribution curves, Figure 73 and Figure 74 , were analyzed in terms of cumulative porosity and incremental porosity. The ultimate values of cumulative porosity were compared to determine how much water imbibed into the shale pore network at different time intervals, Table 5 and Table 6 and Figure 75. On the other hand, the incremental porosity values were compared to investigate the preferential imbibition; i.e. whether fluids imbibe first in micro or large pores.

The two shale core plug samples were acquired from the same well of sample C but at different depths of the same formation. The first plug sample was tested as a dry sample and the first T_2 distribution was plotted. The cumulative porosity curve showed a porosity value of 0.7 p.u. After saturating the sample in deionized water for 24 hours, there was a sharp increase in the cumulative porosity to 0.95 p.u. Upon further exposing to water for 72 hours and 1 week, the cumulative porosity continued to increase to 1.08 and 1.13 p.u. respectively. Assuming this increase is directly related to the amount of water imbibed into shale pore network, the amounts of water imbibed were determined for every step. The results showed that the water amount increased by 61.3% at the end of the 11^{th} day. On the other hand, the second sample was tested as a dry sample showing cumulative porosity of 1 p.u. Although it had higher porosity initially, the amount of water imbibed after 24 hours was lower than that for the first plug sample. The

same trend was observed after saturating the sample for extended periods of time: 72 hours and 1 week. This decrease in water imbibition might be attributed to the inhibition performance of KCl which results in smaller amount of water invading the shale pore network.

The other parameter analyzed is the incremental porosity. As it is clear from the T_2 distributions for both samples, the difference in the signal amplitude is much larger at smaller relaxation times where the micro-pores exist. This indicates the preferential imbibition to the micro-pores rather than macro-pores and micro-fractures. One explanation for this behavior is that the micro-pores are well inter-connected compared to the macro-pores. Therefore, the micro-pores are filled with water before the macro-pores.

This finding should be considered when developing new types of shale inhibitors. Shale inhibitors comprising nano-scale particles can plug those micro-pores and prevent further advancement of water. Also, amines and polyamines with their small particle sizes can result in high quality shale inhibition. It can also be observed that for the KCl brine case, higher amounts of water diffuse into the macro pores especially at high injection pressure. The peaks continue to rise as the saturation increases while it stopped increasing for micro pores. The observation suggests that adding another shale inhibitor that can plug the macro pores, such as silicates, can result in redeuced amounts of water to invade the shale pore network.

A new generation of shale inhibitor may comprise both nano-particles to reduce the permeability by plugging micro-pores and, at the same time, functional groups such as polyamines and asphaltenes that showed good performance in terms of shale inhibition capability. The synergy of both mechanisms can provide shale inhibition with higher stability.

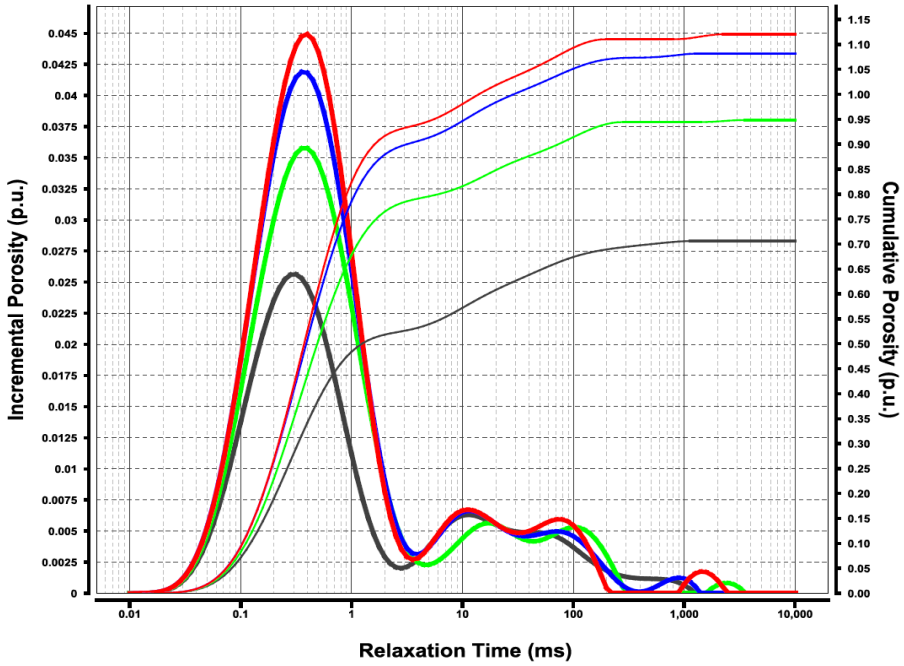

Figure 73: NMR T2 signal for shale saturated with water. Grey: dry sample. Yellow: after 24 hours of immersion. Blue: after additional 72 hours. Red: after additional 7 days at pressure of 1500 psi

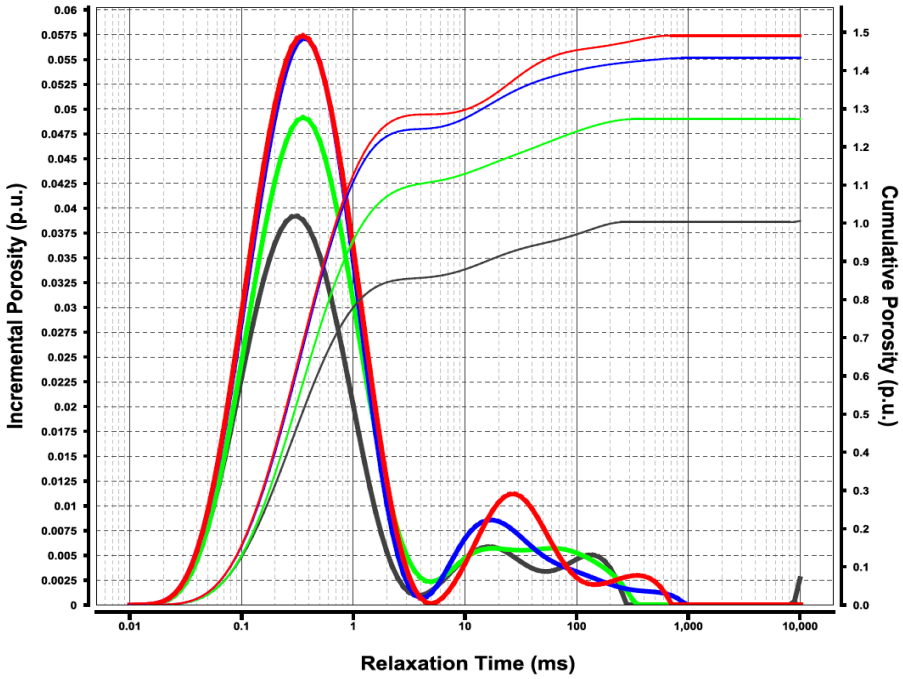

Figure 74: NMR T2 signal for shale saturated with KCl. Grey: dry sample. Yellow: after 24 hours of immersion. Blue: after additional 72 hours. Red: after additional 7 days at pressure of 1500 psi

Table 5: Results of NMR T2 cumulative porosities of shale core plug saturated with deionized water

Saturation time (days)	Cumulative Porosity (p.u.)	Apparent water imbibed (%)
0	0.7	0
1	0.95	35.71
4	1.08	54.29
11	1.13	61.43

Table 6: Results of NMR T2 cumulative porosities of shale core plug saturated with 5% KCl solution

Saturation time (days)	Cumulative Porosity (p.u.)	Apparent water imbibed (%)
0	1	0
1	1.28	28
4	1.42	42
11	1.5	50

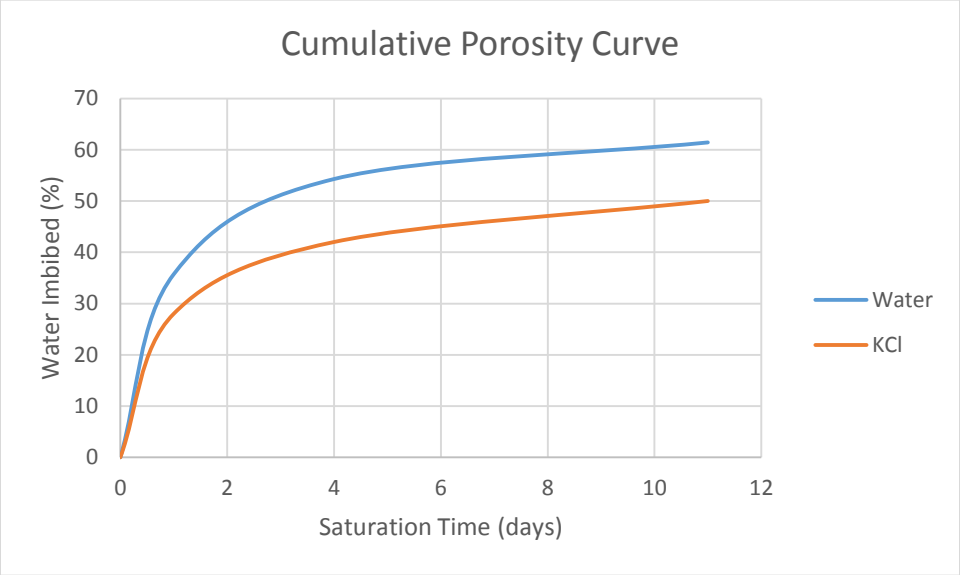

Figure 75: Comparison of percentage of water imbibed at the same conditions

4.5 Shale inhibition testing

4.5.1 Dispersion test

Dispersion test was carried out to investigate the effect of two types of shale inhibitors on the shale integrity and also, in the next step, to analyze the long-term shale inhibition performance. The dispersion results are shown in Figure 76 through Figure 79. Samples A and C did not show high tendency to dispersion due to the low clay content and the three fluids had almost equivalent performance. Therefore, no shale inhibitor is required to stabilize the shale. Similarly, sample B results showed high shale recovery and low dispersion tendency in spite of the high clay content it has. However, its clay content is mainly dominated by chlorite and illite with relatively small percentage of the dispersive type of clay: kaolinite. On the other hand, sample D with its high kaolinite content showed high level of dispersion and the effect of using appropriate shale inhibitors was evident. Polyamines showed significantly better performance than potassium chloride.

4.5.2 Inhibition durability test

Dispersion results do not provide any indication of the duration of the inhibition i.e. the longevity of inhibition life to protect the shale from any internal and external detrimental action. Hence, the conventional inhibition evaluation method is unable to predict the long term stability of the inhibited shale if the fluid environment changes or need to change due to some technical reason. As it provides no clues about the durability or permanency of the inhibition to protect the shale from any detrimental effect after drilling the shale section, the industry needs a predicting tool and index parameter to overcome the limitation of conventional shale inhibition tests.

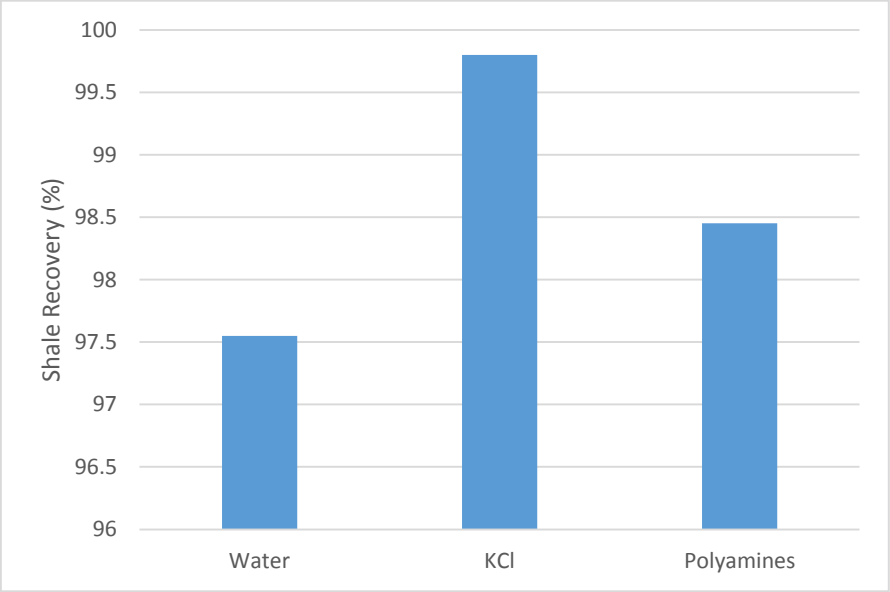

Figure 76: Dispersion results for sample A

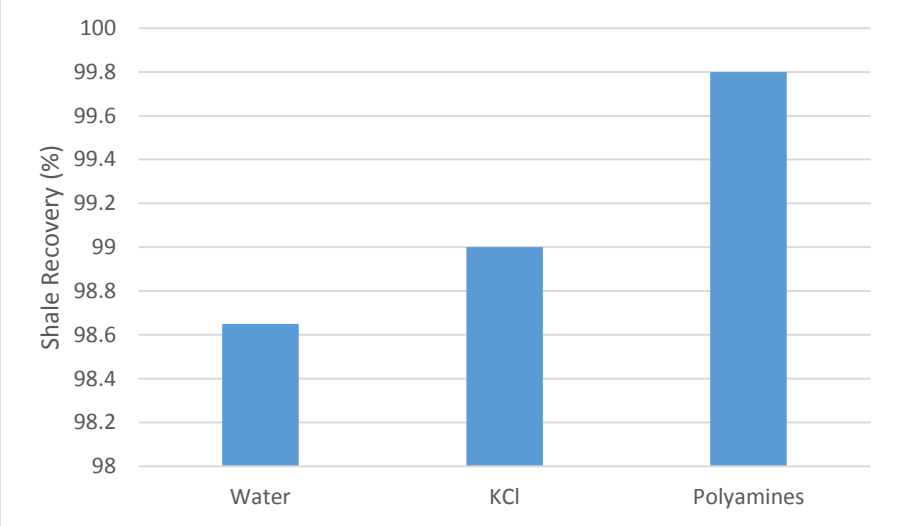

Figure 77: Dispersion results for sample B

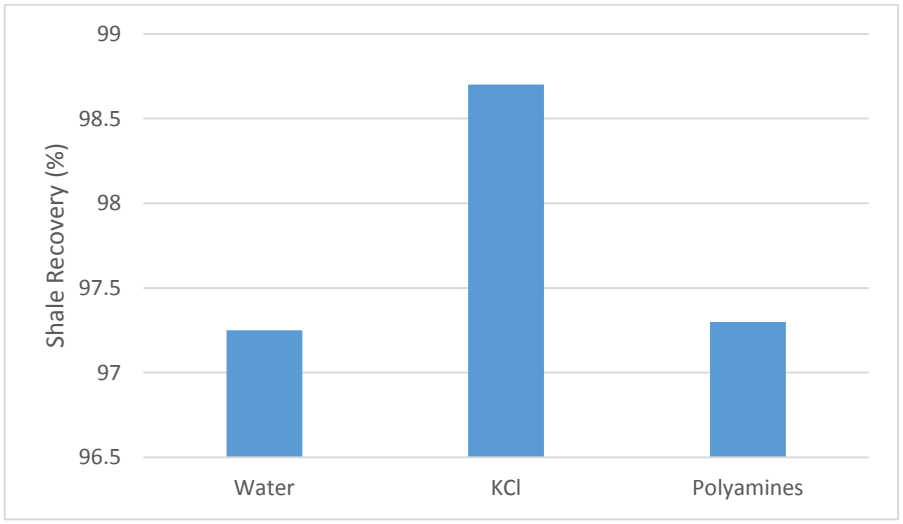

Figure 78: Dispersion results for sample C

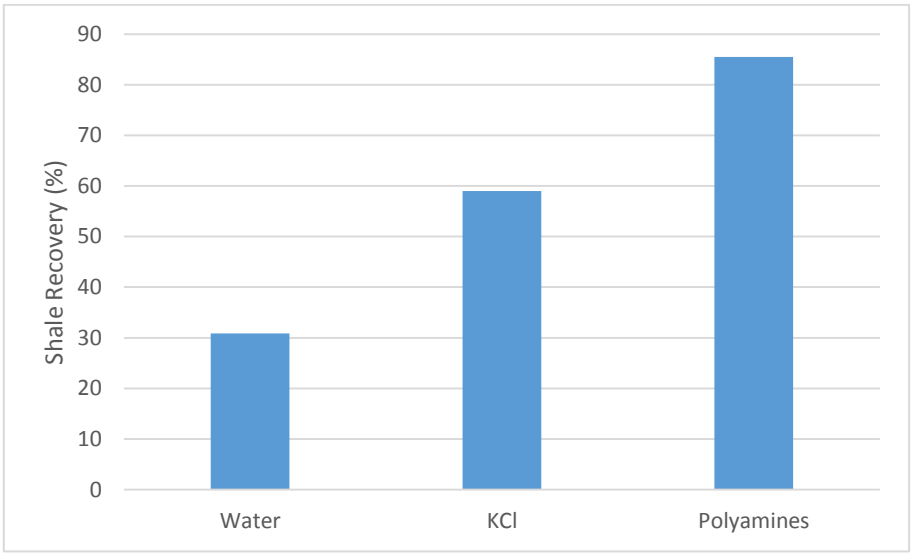

Figure 79: Dispersion results for sample D

The technical significance of the inhibition durability test is that if the results shows non-permanent inhibition with a short durability, then the inhibited shale mass will create time dependent borehole instability problems in spite of good inhibition of reactive shale while drilling the shale section.

To test the inhibition durability, the shale cuttings recovered in the dispersion test are hot-rolled again in presence of water, which is non-inhibitive fluid. The hot-rolling is conducted for different periods of time to assess the longevity of the inhibition, i.e. after how many hours the shale inhibition breaks down. In this study, the complete inhibition durability test was carried out only for sample D. This is because it showed the highest tendency for dispersion and, therefore, there is clear effect on the shale inhibition performance. For other samples, the results for only one data point are shown here.

A permanent inhibition will indicate no loss of materials due to the reappearance of a reactive fluid environment in contact with the inhibited shale cuttings. Permanent shale inhibitors can easily overcome the detrimental attack of reactive water molecules and thus can prevent the disintegration and dispersion of the inhibited shale cuttings. If the inhibition is not permanent but has a life span, the defense provided by the inhibitors will break down at some stage leading to the disintegration and dispersion of the inhibited shale cuttings with a drastic reduction in inhibited cutting mass.

Table 7 and Table 8 show the results for sample D after being recovered from dispersion test with 5% KCl in one case and 5% polyamines solution in the other one. The shale inhibition provided by KCl started to break down after 6 hours of hot-rolling in a non-inhibitive environment. After 18 hours, the shale sample was almost completely dispersed in water. On the other hand, results of the shale cuttings inhibited with the polyamines solution showed clearly

significantly higher inhibition permanency and, therefore, the testing was continued for long intervals of time to determine the point where the inhibition breaks down. However, after 12 days, the inhibition still show high resistance to water and almost 85% of the shale sample was recovered.

At the initial stage of the test, the defensive barrier or mechanism created by the inhibitors of the inhibitive mud was able to provide sufficient protection to the reactive clays of the cutting matrix. Hence, the inhibited cuttings were able to repel the detrimental and damaging action of water molecules. This is reflected by little changes in the mass of the cuttings at the early stage of the inhibited cuttings mass versus rolling time curves. Over the time, the invading water molecules progressively overcome the resistance offered by the defensive barriers created by the inhibitors of the inhibitive muds. Hence, there is a serious damage to the cuttings matrix due to softening and weakening of the fabric and structures of the cuttings. This is reflected by a massive loss of material from the bulk cuttings mass in the case of shale cuttings inhibited with KCl. The loss of materials after the inhibition break down time occurs in a short time. As the defensive mechanism created by the inhibitors of the inhibitive muds become weak and fragile, inhibited cuttings can no longer provide enough resistance to the aggressive and damaging action of reactive water. Hence, there is a quick loss of materials from the cuttings matrix with sudden drop in the curves.

Shale cuttings inhibited with polyamines showed longer resistance to water to prevent damage, degradation, weakening, softening and thus the ultimate loss of the materials. Hence, a shale formation drilled using shale inhibitor provide long-term protection of reactive shale if exposed to fresh water or a non-inhibitive mud.

Table 7: Results of inhibition durability test for sample D with 5% KCl solution

Time (hr)	Original Weight	Recovered cuttings weight (g)	Shale Recovery %
0	5	5	100
2	5	4.01	80.2
6	5	3.2	64
10	5	1.3	26
14	5	0.82	16.4
18	5	0.6	12

Table 8: Results of inhibition durability test for sample D with 5% Polyamines solution

Time (hr)	Original Weight	Recovered Cuttings Weight (g)	Shale Recovery %
0	5	5	100
6	5	4.72	94.4
10	5	4.7	94
28	5	4.7	94
120	5	4.65	93
288	5	4.24	84.8

The above mentioned method to test the shale inhibition durability does not represent the field and downhole conditions accurately. Therefore, this work suggests an enhancement to that method to get results with higher accuracy. The original inhibition durability method (Amanullah, 2015) is conducted in three stages. First, dispersion test of a pre-determined amount of shale cuttings is conducted for 16 hours at 150 °F. Second, the amount of shale cuttings recovered is dried for 24 hours. Then, a pre-determined amount of the recovered cuttings, is reacted with water for different periods of time. In the enhanced method, the second stage of drying is eliminated. Advantages of this elimination include: better simulating the real situation since the borehole is always full of fluid, shortening the time of the test without compromising the accuracy of the results and eliminating the effect of drying temperature on the shale properties.

Shale sample D whose clay content is greater than 60% was selected to do the shale inhibition durability tests. The original and enhanced methods were carried out with a solution of 5% potassium chloride.

The original method starts with 20 g of shale cuttings for conducting the first stage (dispersion test) then the amount of recovered shale cuttings is recorded. After the dispersion test, the recovered shale cuttings are dried. Then, 5 grams are taken from the dried shale cuttings and re-dispersed with water and the recovered shale cuttings is recorded. In the original method, there are two shale recovery percentages while for the enhanced method, there is only one shale recovery percentage at the end of the whole testing. Therefore, if we need to compare the results from the two methods, we need to have one shale recovery percentage for the original method and here it is called "Equivalent". This Equivalent is compared to the shale recovery percentage of the enhanced method. Equivalent is determined in a way as if we take the whole shale

recovered from the first stage (11.2 g out of 20 g in this case) and do the re-dispersion, Table 9 through Table 11.

Comparing the “Equivalent Original Method%” and “From enhanced Method%” values reveals that at short periods of time, i.e. 2-6 hours, the original method gave higher shale recovery than the enhanced method. This might be due to the drying effect on the shale cuttings properties where the shale inhibitors molecules were able to coat the shale cuttings surfaces, increase their strength and stabilize them. However, in the real case, the borehole is always full of drilling fluid and, therefore, this method is not accurately representing the downhole conditions. For extended periods of time, i.e. 10 hours, the apparent shale inhibition effect breaks down significantly giving very low shale recovery, Figure 80 and Figure 81.

The enhanced durability method, on the other hand, gave more realistic results with more uniform behavior. It is better representing the downhole conditions, shortening the testing time by 24 hours and producing more accurate results.

4.5.3 Swelling test

Linear swell meter was utilized in this work to study the swelling behavior of the shale and pure clay samples when exposed to water, 5% potassium chloride and 5% polyamines solutions. The test was run until no further volume increase is observed and the swelling curve stabilized. The results were interpreted based on two parameters: the ultimate swelling percentage and the slope of the swelling curve especially at the beginning of the test, Figure 82 through Figure 88.

Table 9: Results of original inhibition durability method

Shale recovered from first stage of original method (out of 20 g)	11.2	g	
Time (hr)	**Original Weight (g)**	**Recovered cuttings weight (g)**	**Recovery %**
0	5	5	100
2	5	4.01	80.2
6	5	3.2	64
10	5	1.3	26

Table 10: Results of modified inhibition durability method

Time (hr)	**Original Weight (g)**	**Recovered cuttings weight (g)**	**Recovery %**
0	10	10	100
2	10	4.17	41.7
6	10	3.05	30.5
10	10	2.3	23

Table 11: Comparison of shale recovery from the two inhibition durability methods

Time (hr)	**From Original Method %**	**Equivalent Original Method %**	**From enhanced Method %**
0	100	100	100
2	80.2	44.912	41.7
6	64	35.84	30.5
10	26	14.56	23

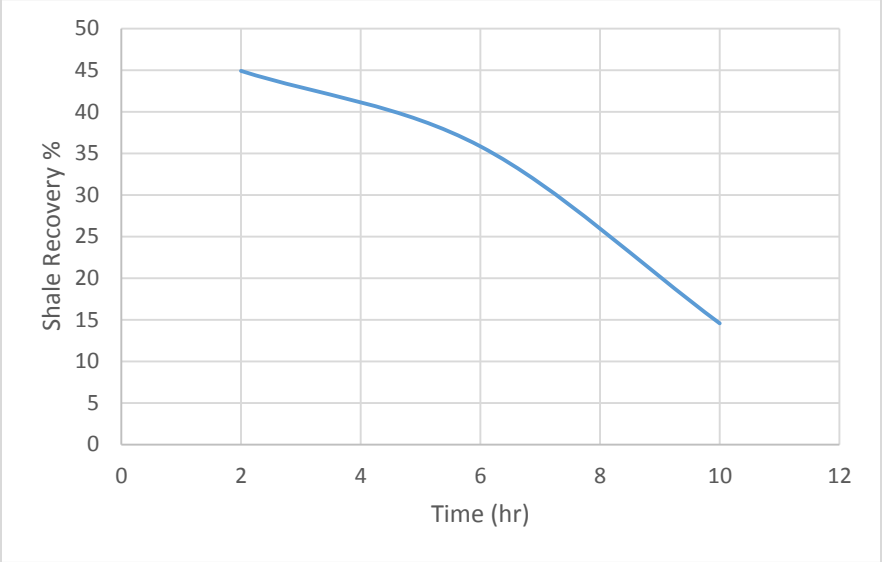

Figure 80: Results of sample D using Original inhibition durability method

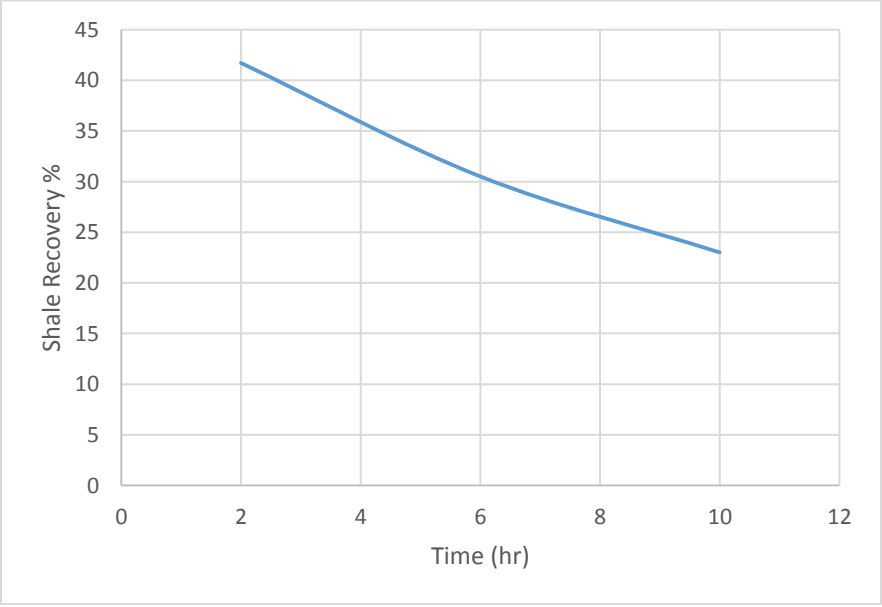

Figure 81: Results of sample D using enhanced inhibition durability method

Comparing the swelling curves of sodium montmorillonite and illite, the slope of swelling curve of the latter is very steep and the curve stabilizes earlier than montmorillonite. On the other hand, montmorillonite has lower slope and takes more time but it reaches to higher swelling percentages. This is a direct result of how both types of clays are structured. Illite has more cations than montmorillonite but, however, they are not willing to exchange and, therefore, it has low CEC. The reason behind this behavior is the location of the negative charge in illite compared to montmorillonite. The negative charge in illite is concentrated in the tetrahedral sheet and, hence, it is closer to the interlayer cations. The small distance between the interlayer cations to the negatively charged surface results in higher attraction and lower tendency of the cations to be exchanged, i.e. the number of cations willing to exchange is small. Thus, the fluid requires significantly shorter time to complete the cation exchange process and stabilizes the clay. For the case of montmorillonite, the isomorphic substitution takes place mainly in the octahedral sheet which is a little bit away from the interlayer cations. Therefore, the cations have more freedom to move away from clay surfaces. As the number of water molecules increases, there will be more solvation effect where the water forms shells of hydration around the cations. As a result, montmorillonite expands in volume and have significantly higher swelling percentages.

Illite-smectite mixed layer showed swelling behavior that is intermediate between the two extremes: sodium montmorillonite and illite. The mixed layer is composed of sheet-like particles of thickness of 10 Å approximately that can expand by adsorbing water on both surfaces. The ultimate swelling percentage with water was 70% with the swelling curve slope being, again, intermediate between the two end members.

Sample A and C did not show significant swelling as the clay content is low. However, the

KCl and polyamines solutions could reduce the ultimate swelling percentage even further from 2.6% to 0.8%. Both solutions achieved eventually the same swell percentage. Also, it is clear that the swelling curve of KCl solution was not uniform. It the curve had multiple platues before it reaches the ultimate swelling percentage. However, polyamines solution was able to stabilize this shale sample in uniform manner and reached the ultimate swelling percentage in shorter time.

Sample B showed swelling behavior very close to that of pure illite. This is in strong agreement with the XRD results that showed that sample B has 17.2% of illite, with no mixed layer. The other clay types present in this sample are chlorite and kaolinite that are known to be of non-expandable nature. KCl did not show significant swelling inhibition and it could reduce the swelling percent by only 1%. On the other hand, polyamines showed excellent performance by reducing the ultimate swell percentage from 25.9% to 12.4%.

Sample D showed the highest swelling percentage among the shale samples. This was attributed to the high clay content and the presence of appreciable amounts of swelling clays as was revealed by XRD analysis. The use of KCl and polyamines as swelling inhibitors did not help significantly to reduce the ultimate swelling percentage. KCl showed slight inhibition performance by stabilizing the shale sample earlier, as indicated by the high slope of the curve in the first five hours of the test, while polyamines showed a better performance by reducing the swelling percentage from 42% to 38%. However, it took longer time to stabilize the shale, 30 hours approximately.

From the discussion above, it can be concluded that KCl has the advantage of stabilizing the shale in short time with good performance in in the presence of smectites and illite-smectites mixed layer. On the other hand, polyamines has good performance in the presence of illite and provide better performance for longer periods of time.

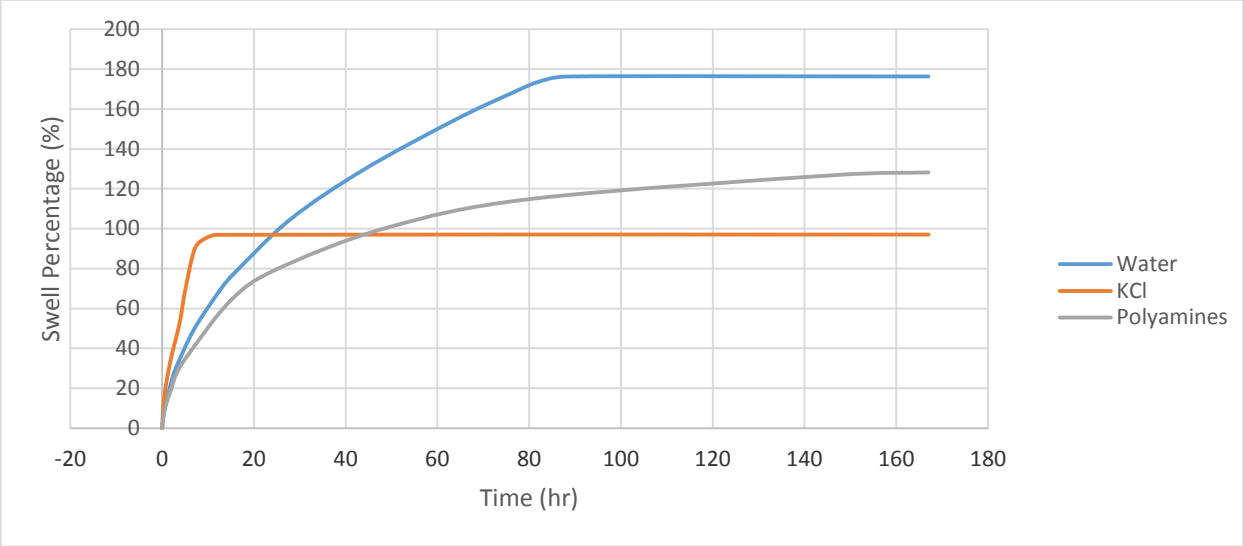

Figure 82: Swelling curves for sodium montmorillonite

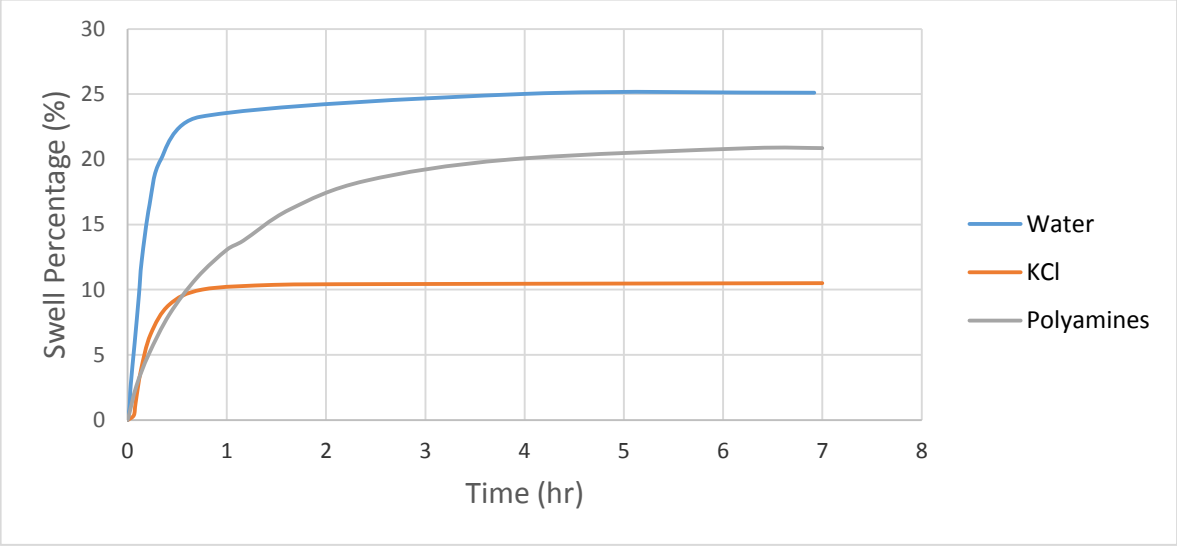

Figure 83: Swelling curves for illite

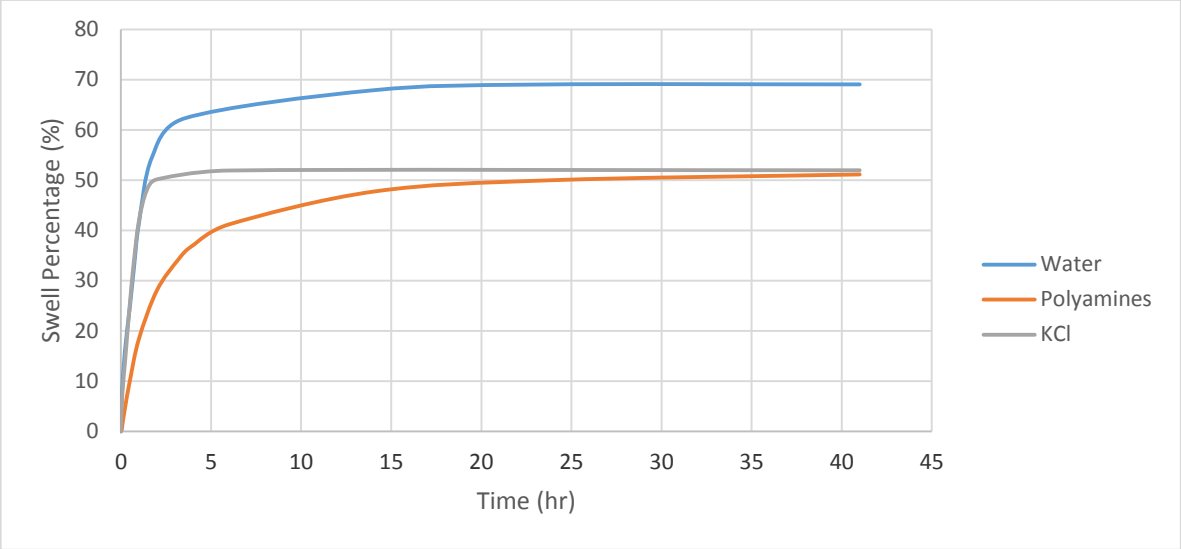

Figure 84: Swelling curves for illite-smectite

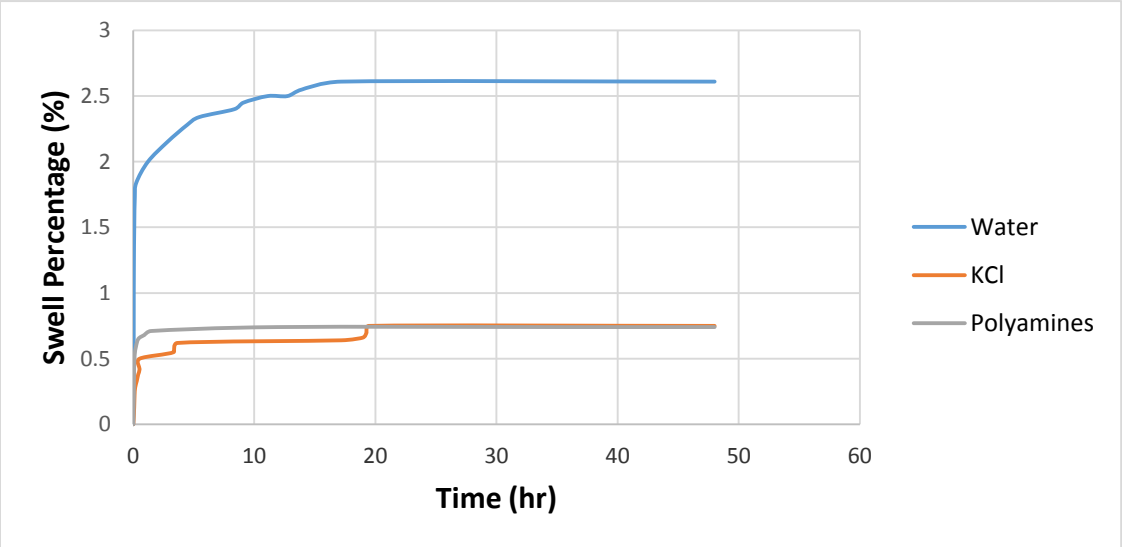

Figure 85: Swelling curves for sample A

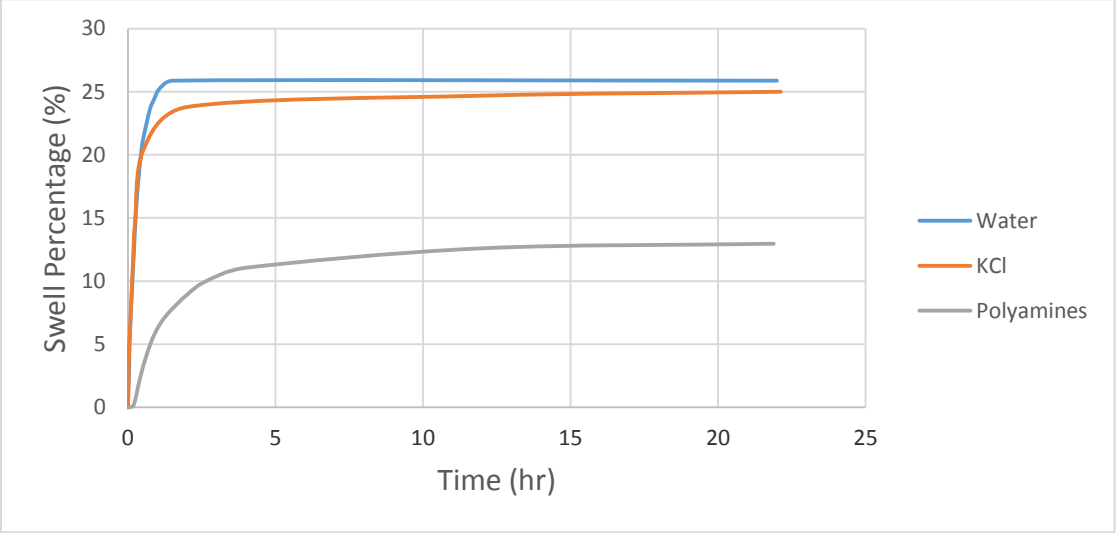

Figure 86: Swelling curves for sample B

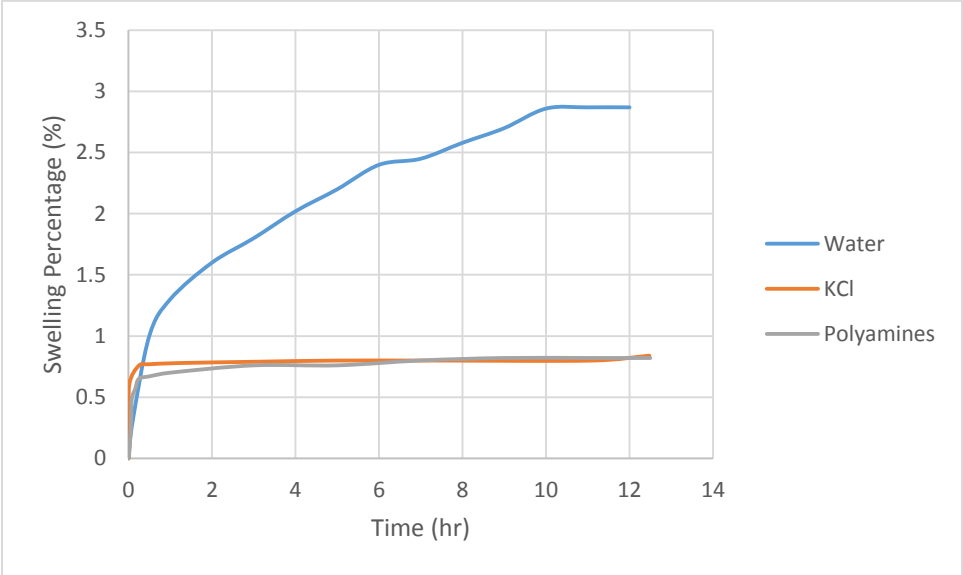

Figure 87: Swelling curves for sample C

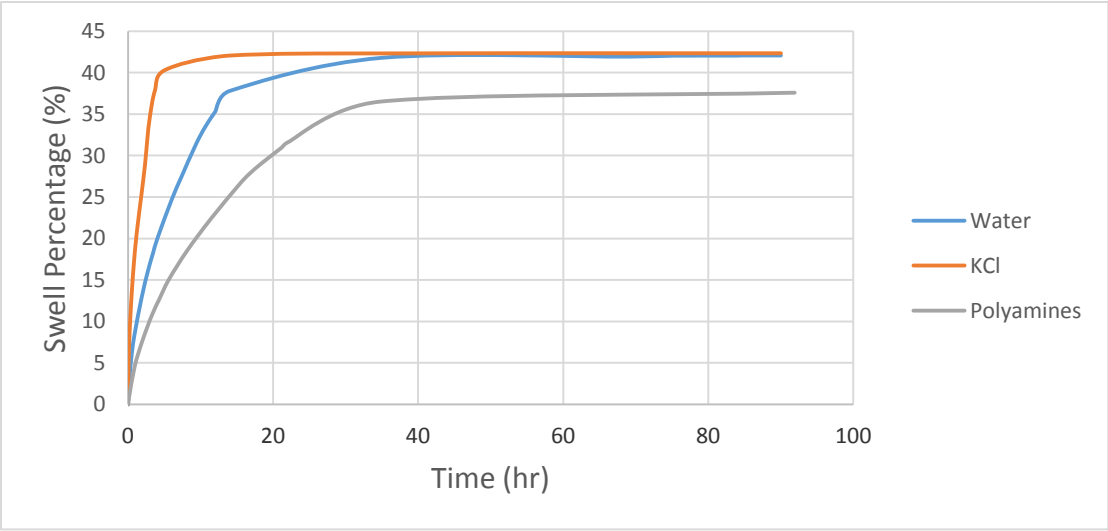

Figure 88: Swelling curves for sample D

4.6 Molecular modelling and simulation

4.6.1 Simulation Runs Output (to be deleted)

4.6.2 Total energy

Total energies of the systems were calculated using equations 5 through 9. Figure 89 shows the total energy in kJ mol^{-1} $atom^{-1}$ for pure montmorillonite and illite and also the two models of illite-smectite mixed layer. Total energy includes both bonded and non-bonded energies. The difference between the total energies of the two models of the illite-smectite mixed layer was compared to the difference calculated by Stixrude and Peacor (2002) using first-principles density-functional theory. They found that due to structural distortions in model A, its total energy was 2.3 kJ mol^{-1} $atom^{-1}$ higher than that of model B.

Using MD calculations, in this study, the energy difference was calculated to be 2.4 kJ mol^{-1} $atom^{-1}$ for the unhydrated system. As it is evident from Figure 6, almost the same energy difference was maintained with increasing level of hydration. The energy difference is in the range of 2.25 up to 2.67 kJ mol^{-1} $atom^{-1}$. Model B was built on the basis that each potassium ion lies between two layers with equal charge deficiency. Potassium ions were located around the center of the interlayer spacing. For model A, because the layers do not have equal charge deficiency, potassium ions moved closer to the layer with higher charge deficiency. This finding can provide validation for the two illite-smectite models built for MD simulations.

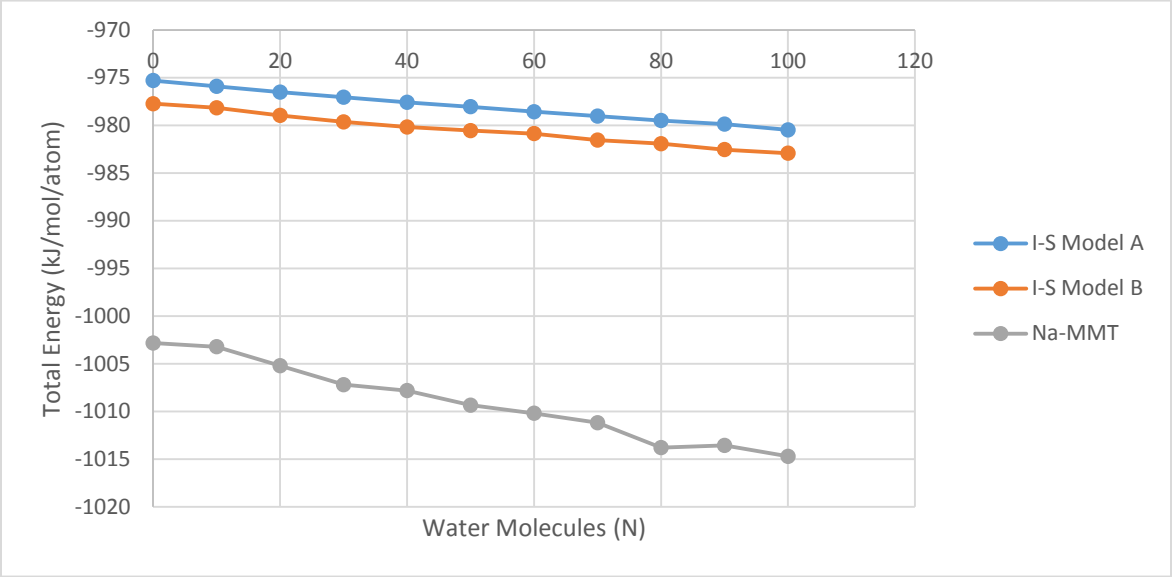

Figure 89: Total energy curves for pure and mixed-layer clays

4.6.3 Clay swelling behaviour

Interaction of different clay surfaces with water molecules was investigated through evaluating the d001 spacing for unhydrated and hydrated clay models. Figure 90 shows the swelling behavior results for sodium montmorillonite and Figure 91 shows the results for both models of illite-smectite mixed layers. Swelling curves showed several plateaus as water content is increased. This can be attributed to the formation of hydrate layers in the interlayer spacing and, thus, at every plateau, one layer of hydrate forms. For sodium montmorillonite, two plateaus occur around 30 and 80 water molecules corresponding to d-spacing of 12.1 and 15.6 Å, respectively. This suggests the formation of a mono-layer hydrate at 12.1 Å and a bi-layer hydrate at 15.6 Å. This is in agreement with the experimental and modeling work carried out by previous investigators (Fu, 1990; Cygan, 2004; Boek, 1995). For illite smectite models, the first plateau appears close to a hydration level of 35 water molecules with d-spacing values of 21.6 Å and 22.1 Å for models A and B, respectively. These results are in agreement with experimental work conducted by Kawano (1992) on the one-layer hydrate for potassium illite-smectite (potassium rectorite) where a d-spacing value of 22.1 Å was reported. The second plateau appears around 70 water molecules at a d-spacing values of 24 Å and 24.3 Å for models A and B, respectively.

For the case of illite-smectite mixed layer, the starting d-spacing for the unhydrated system is different for both models. Therefore, the swelling percentage can be calculated and compared as a function of the number of water molecules as shown in Figure 92. Here, the initial d-spacing of the unhydrated system was taken into account to concentrate only on the effect of increasing water content while keeping all other parameters fixed. Based on the swelling percentage results, illite-smectite model A showed higher swelling percentages compared to model B for most

levels of hydration.

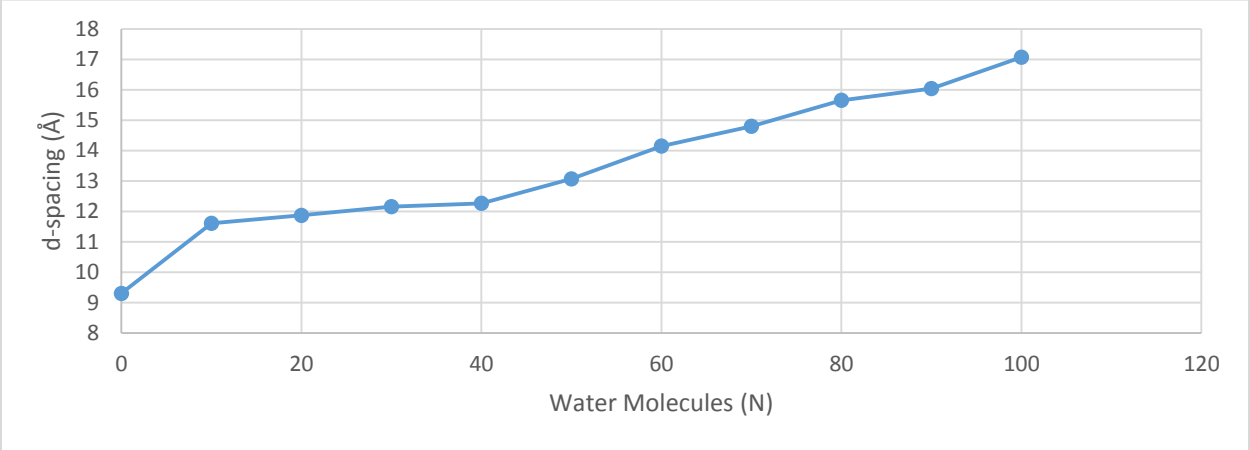

Figure 90: Swelling curves for sodium montmorillonite

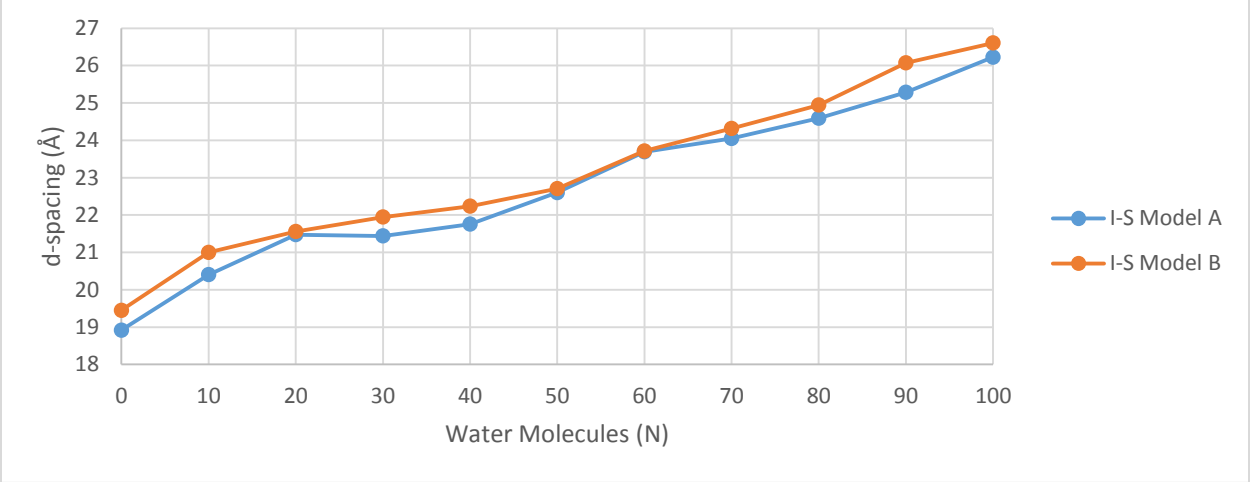

Figure 91: Swelling curves for illite-smectite mixed layers

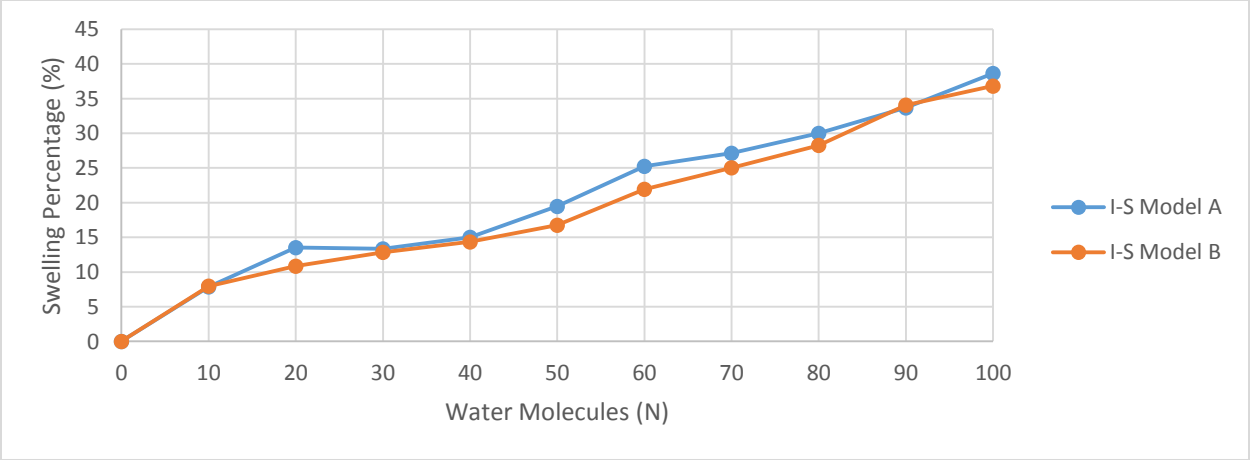

Figure 92: Swelling percentage profiles for illite-smectite mixed layers

Another experimental method that help to integrate with modeling results is the adsorption testing. As discussed in section 4.3.3, sodium montmorillonite and illite-smectite showed strong multi-layer adsorption behavior. Their adsorption isotherms were fitted to Fredluich adsorption model. Examining the swelling curves obtained with molecular dynamics calculations shows that both sodium montmorillonite and illite-smectite have several layers of hydrate. Every plateaue of the curves indicates the formation of a single hydrate layer. For sodium montorillonite, the first hydate layer occurs around 12 Å, the second around 15 Å and the third layer starts to form after 17 Å as in the literature. For illite-smectite, the first hydrate layer forms around 21.6 Å and 22.1 Å for models A and B, respectively while the second hydrate layer forms between 24 and 25 Å for both models.

4.6.4 Effect of temperature on swelling behaviour

The simulation runs were conducted at 300 K, 350 K and 400 K at a fixed pressure of 5 atm to investigate the effect of temperature on the d-spacing. Table 12 shows the results of sodium montmorillonite and both models of Illite-smectite mixed layer as a function of temperature. The increase in swelling is calculated as d-spacing and tabulated. The hydrated system used in these calculations has 100 water molecules.

In general, as the temperature increases, d-spacing values increase for the three clay models. This is attributed to the increased thermal energy of the system. For sodium montmorillonite, the results showed higher d-spacing increase for the hydrated model in agreement with previous modeling work carried out by Sun (2015). Similarly, illite-smectite model B showed higher d-spacing values for the hydrated system. However, for illite-smectite model A, there was not a major change in the d-spacing values for both the unhydrated and hydrated models.

4.6.5 Interlayer structure and clay-water cations interactions

Interactions between different atoms in a system can be analyzed using similar statistical techniques. These techniques include: distance analysis, pair correlation functions and radial distribution functions. In this paper, distance analysis tables and profiles were utilized to reveal information about the interlayer structure and atom-atom interactions. Table 13 and Table 14 summarize the distance analysis results and show the smallest and the mean distances between each two components. This type of analysis was carried out for sodium montmorillonite and only model B of the mixed layer since it was found to be the mixed layer of lower total energy and higher stability. The distance analysis data was performed starting with the unhydrated systems then for increasing amount of water content: 20, 60 and 100 water molecules.

Table 12: d-spacing values (Å) at specified Temp (K)

System	Water (N)	Temperature (K)		
		300	350	400
Na-MMT	0	9.37	9.37	9.43
	100	16.84	17.39	17.90
I-S Model A	0	19.39	19.32	19.42
	100	26.30	26.64	26.42
I-S Model B	0	19.22	19.30	19.29
	100	26.58	26.71	27.16

Table 13: Distance analysis for sodium montmorillonite

Distance Analysis				
Smallest	**Clay O - Na**	**Clay O – Water OH**	**HO - Na**	**$H_2O – OH_2$**
Dry	2.131			
20	2.187	2.424	2.089	2.46
60	2.193	2.423	2.105	2.412
100	2.198	2.456	2.102	2.402
Mean	**Clay O - K**	**Clay O – Water OH**	**HO - K**	**$H_2O – OH_2$**
Dry	9.371			
20	10.1	10.07	10.27	10.65
60	10.95	10.92	11.42	11.58
100	12	11.94	12.42	12.55

Table 14: Distance analysis for illite-smectite model B

Distance Analysis				
Smallest	**Clay O - K**	**Clay O – Water OH**	**HO - K**	**$H_2O – OH_2$**
Dry	2.53			
20	2.487	2.479	2.461	2.459
60	2.613	2.471	2.465	2.448
100	2.513	2.448	2.516	2.423
Mean	**Clay O - K**	**Clay O – Water OH**	**HO - K**	**$H_2O – OH_2$**
Dry	11.76			
20	10.81	10.9	7.938	7.635
60	11.5	12.36	9.754	7.804
100	11.65	12.99	10.05	8.182

4.6.5.1 Clay-cations and clay-water interactions

We investigated the interaction between clay surfaces and interlayer cations using distance analysis of clay surface oxygen in the tetrahedral sheet and the interlayer cations. We also performed this analysis to the clay-water interactions using the tetrahedral clay oxygen and water oxygen.

Sodium montmorillonite results showed that the smallest distance between the tetrahedral clay oxygen and sodium cations increases as water content increases. This behavior is due to the increasing amount of water that form hydration shells around the sodium cations. This solvation process gives the cations more freedom to diffuse within the interlayer spacing and, therefore, results in decreasing the number of clay oxygen and cations coordination at small distances. Also, the high degree of swelling for montmorillonites in general compared to other types of clay and the significant increase in d-spacing with higher number of water molecules give the molecules larger space to move and diffuse.

For the results of the distance analysis of tetrahedral clay oxygen with water oxygen, the smallest distance tends to, generally, decrease as water content increases because of the higher number of water molecules occupying the interlayer spacing. This effect, however, is counter-balanced by the interlayer spacing expansion as water loading increases and causes the clay to swell. Water molecules diffuse and travel to achieve the most stable configuration that has the lowest energy. The first peak appears around 3.2 Å for the three hydration levels although the peak is less pronounced at higher levels of hydration. At the same time and due to the increasing amount of water molecules, the intensity increases significantly as water content increases.

For illite-smectite model B results there appears no clear trend for the profiles of tetrahedral clay oxygen with potassium cations. Looking at the smallest and the mean distances

as well, suggests that either there is no consistent trend or the distances tend to be almost constant and in the same range regardless of the level of hydration.

The distance analysis of clay oxygen with water oxygen, shows that the smallest distance decreases as water content increases. As increasing number of water molecules fill up the interlayer space, there is high probability for coordination to the clay surface. Higher coordination of water molecules with oxygen atoms in the clay surfaces result in more adsorption of water to the surface and, hence, higher degree of swelling.

4.6.5.2 Water-cations interactions

The interaction between water molecules and cations was evaluated for the case of montmorillonite and illite-smectite model B using distance analysis of water oxygen and the cations. Sodium montmorillonite results show the smallest distance near 2.472 and 2.481 Å with a small increase due to the swelling effect. The results for Illite-smectite model B showed similar results as those of sodium montmorillonite with the smallest distance between 2.461 and 2.516 Å.

4.6.5.3 Interlayer water structure

Interlayer water structure was studied using distance analysis for water oxygen to water oxygen interactions. The general trend for both systems shows a decrease in the smallest distance with the increase in water content as can be noticed in Tables 1 and 2 above. This is due to the increase in the number of water molecules that need to position themselves in the confined interlayer spacing. On the other hand, the mean values of distance increase as the water loading increases. This is attributed to the enlarged interlayer spacing where more water molecules can travel to.

CHAPTER 5

CONCLUSIONS AND RECOMMENDATIONS

This study investigates shale-fluid interactions at different levels to help in mitigating problems while drilling through shale. It consists of three phases. The first phase was devoted to shale characterization where different tests were carried out to reveal the mineralogy, structure, reactivity and adsorption potential of the shale samples under study. The second phase tested the behavior of the shale samples under simulated downhole conditions. Finally, the third stage looked into the molecular level interactions using molecular dynamics simulation to better understand the adsorption at the micro-scale.

5.1 Conclusions

The conclusions and findings of this study are either new contributions to the research in this area or confirmation to the existing literature using different techniques. The main outcomes and conclusions of this research are highlighted below.

i) Shale characterization was conducted using a wide range of testing procedures that have not been utilized in the past on the same Qusaiba shale samples. Different studies in the past had used few characterization methods that gave partial information about the samples. However, in this study, a large number of testing techniques were employed and integrated to have deep insights into the nature of the tested shale formation. These included: Micro-CT, Thin section, SEM, XRF, XRD, QEMSCAN, TGA, CEC, CST, moisture content and adsorption potential. Out of this

characterization phase, the following protocal is recommended to test Qusaiba shale samples:

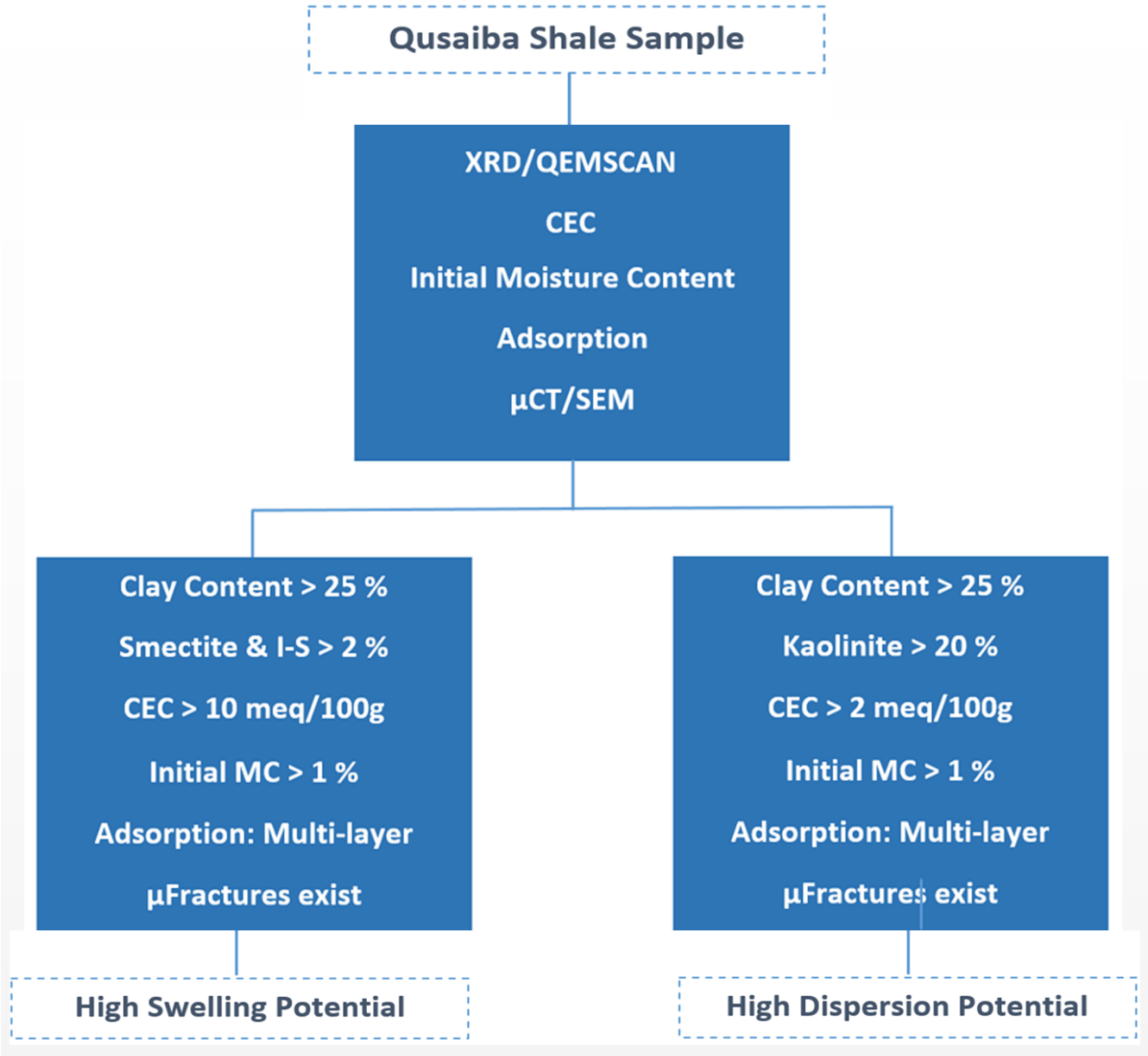

i) Results of this study showed the significant heterogeneity of Silurian shale in Saudi Arabia. Ranging from silica-rich shale to extremely clay-rich shales, water-based drilling fluids and best practices required to drill different locations within this

formation can vary significantly. After conducting shale characterization tests, swelling and dispersion inhibition tests need to be carried out to study the performance of different drilling fluids with different shale samples. Gaining the required knowledge about every type of shale samples can have a positive impact on the economics of shale drilling operations. Due to the heterogeneous nature of shale samples in terms of clay content and reactivity, different shale inhibitors and shale inhibition mechanisms are to be used to address specific shale drilling problems as explained in this investigation. After conducting such comprehensive study, wellbore instability problems can be mitigated with the use of appropriately designed drilling fluids.

ii) Integrating more than one method to study the mineralogical and organic matter content of the shale samples helps in understanding the shale-fluid interactions and the response of the shale when exposed to fluids.

iii) The use of different levels of shale characterization methods to confirm the existence of some features gives absolutely enhanced understanding of the tested shale formations. This was done in the current study utilizing three different levels of imaging techniques: Micro-CT, thin section analysis and SEM.

iv) The use of nuclear magnetic resonance, NMR, to study the imbibition of different shale inhibitors for drilling applications has not be done in the past. This work utilizes this powerful technique to understand the theory behind shale inhibition mechanisms using different fluids.

v) Adsorption is a phenomenon that requires extensive amount of work at the micro-scale and macro-scale to be understood. In this study, it was tackled on different

levels of investigation ranging from molecular dynamics simulation to examining the behavior of the clay samples as relative humidity increases as well as establishing swelling curves using macro-level swelling test method.

vi) Integrating data from adsorption potential and reactivity potential tests such as cation exchange capacity and capillary suction time is the key to comprehend the response of different types of shale samples when exposed to aqueous fluids. This is an important step that should be kept in mind while introducing high performance water-based drilling fluids with shale inhibition capability. Every clay type has its own structure and behaves differently when exposed to water. Hence, comprehensive characterization and testing for the shale should be conducted to develop an inhibitive drilling fluid with the desired properties.

vii) This is one of the first studies to introduce the concept of long-term shale inhibition. The next generation of inhibitive drilling fluids should have this feature to be able to reduce the cost and avoid operational problems. When an inhibitive mud comes in contact with clay-rich formations, it forms a high resistance barrier around the formation particles. This reduces the contact area available for water molecules to enter and hydrate the clay-rich particles, though limited degree of contact might exist. However, with time, this barrier degrades and loses the required strength to prevent water molecules from attacking the clay-rich particles and causing the recurrence of dispersion and disintegration. Developing drilling fluids with long-life inhibition capability can reduce the cost of well construction by minimizing the number of required casing strings.

viii) Different types of shale inhibitors have different mechanisms to inhibit and

stabilize the shale. A combination of several inhibition mechanisms can provide effective control on reactive shale-related drilling problems.

ix) The current testing procedure to test the shale inhibition durability has some deficiencies in representing the real field conditions. Therefore, an enhanced method was proposed in this study and carried out to compare the results of both methods.

x) Based on the shale characterization scheme, it was found that the main clay type in downhole samples is illite and illite-smectite mixed layer. While illite does not have strong tendency to swelling, illite-smectite showed high level of swelling when tested experimentally. Therefore, the molecular dynamics simulation was conducted to study the behavior of this mixed layer that exists in abundance in the tested shale formation.

xi) Integrating the performance testing using swelling and dispersion procedures with shale characterization is important to explain the behavior more accurately.

xii) Molecular dynamics simulation of the illite-smectite has not received significant attention although it exists in abundant amounts in different shale formations. To the best of the authors' knowledge, this study is the first study that simulates the swelling behavior of potassium illite-smectite.

xiii) Few studies discussed the effect of temperature on the swelling behavior of clays, montmorillonite in particular. This study covers the sensitivity analysis for the temperature effect on potassium illite-smectite.

xiv) Previous literature in molecular dynamics frequently used the radial distribution function and density profiles to study the interlayer structure of clays. This study utilized distance analysis tool to perform the same task using different tools.

xv) The molecular dynamics part of this study calculated the total energy of two models for illite-smectite in order to compare the results with the values reported in the literature using first principles. Confirming the results at two different scales of calculations is a powerful tool to understand and comprehend the behavior of modeled systems.

xvi) Carrying out linear swell meter testing for pure clays (sodium montmorillonite, illite and illite-smectite) to integrate with modeling results validates the results at two different levels of investigation. In the literature, there are several micro-level studies that monitor the expansion of clays in terms of basal spacing as a function of relative humidity. Integrating that with the macro-level studies using linear swell meter can give useful data to help in explaining the swelling behavior of those types of clays.

5.2 Recommendations

The following are some ideas to be considered in subsequent research to be carried out in this area:

i) Molecular dynamics simulation carried out in this study concentrated on the hydration of swelling clays with water. It is recommended to build on the already developed modeled systems to carry out simulations of clays with shale inhibitors such as KCl, polyamines, silicates and glycol.

ii) To further experimentally validate the molecular dynamics calculations of the swelling behavior of montmorillonite and illite-smectite, it is recommended to conduct linear swell meter tests for the same clay type for different periods of time. This is to calculate the water to clay ratio and establish an experimental plot of

swelling percentage as a function of water loading. Then, it can be easily compared to molecular dynamics results.

iii) It is recommended to use humidity regulated cells to monitor the basal spacing using XRD to establish better understanding of the swelling of the shale samples and, then, integrate that with linear swell meter data

iv) Mechanical aspects of shale-drilling fluid interactions play a major role in the wellbore stability of shales. It is recommended to study mechanical factors using both experimental and molecular dynamics simulation methods.

v) Micro-CT can give detailed description of the tested core plug such as quantification or porosity and characterization of fractured formations. It could also be used for the quantification of fluid uptake to test how water advances through shale pore system in the presence/absence of shale inhibitors.

vi) Testing and evaluation of several conventional mud inhibitors indicate that these shale inhibitors though provide sufficient inhibition to reactive shale formation to avoid borehole problems while drilling, they are unable to create a long lasting inhibition barrier to protect the inhibited shale mass from the recurrent attack of aggressive water molecules. Hence, the industry needs to develop a new generation of shale inhibitors with superior inhibition properties for long term stabilization of reactive shale. The current ability of nanotechnology to manufacture tailored made nanomaterials, dendrimers and dendritic polymers with specific characteristic properties can play a leading role in the development of superior shale inhibitors with long lasting inhibition potential to avoid time-dependent borehole instability problems

REFERENCES

Adams, A., MacKenzie, W., Guilford, C.; Atlas of Sedimentary Rocks under the Microscope, Longman Scientific & Technical, 1984.

Akbarabadi, M., Piri, M.; Nanotomography of the Spontaneous Imbibition in Shale, paper URTeC 1922555 prepared for presentation at the Unconventional Resources Conference held in Colorado, USA, 25-27 August 2014

Al-Arfaj, M., and Amanullah, M.; An Innovative Experimental Method to Evaluate the Inhibition Durability of Drilling Fluids, paper SPE 171428 prepared for presentation at the SPE Asia Pacific Oil & Gas Conference and Exhibition held in Adelaide, Australia, 14–16 October, 2014.

Allen, M. and Tildesley, D., "Computer Simulation of Liquids", Oxford University Press, 1987.

Amanullah, Md. (1993), Shale-drilling Mud Interactions. Ph.D. Thesis, University of London, 275pp.

Amanullah, Md.; Screening and Evaluation of some Environment Friendly Mud Additives to Use in Water-based Drilling Muds. Paper SPE 98054 prepared for presentation at the SPE E&P Environmental & Safety Conf., Gelveston, Texas, 5-7 March.

Amanullah, Md.; Dendrimers and Dendritic Polymers - Application for Superior and Intelligent Fluid Development for Oil and Gas Field Applications, Paper SPE 164162 prepared for presentation at the SPE Middle East Oil and Gas Show and Exhibition held in Manama, Bahrain, 10–13 March.

Amanullah, Md., Al-Arfaj, M., An-Ansari, A.; Method for prediction of inhibition durability index of shale inhibitors and inhibitive drilling mud systems, US Patent 9164018 B2, 2014.

Amanullah, Md., and Al-Tahini, Ashraf; Nano-Technology- Its Significance in Smart Fluid Development for Oil and Gas Field Application, paper SPE 126102 prepared for presentation at the SPE Saudi Arabia Section Technical Symposium and Exhibition, AlKhobar, Saudi Arabia, 09–11 May 2009.

Anderson, R., Ratcliffe, I., Greenwell, H, Williams, P, Cliffe, S, Coveney, P, Clay Swelling – A Challenge in the Oilfield, Earth-Science Reviews 98 (2010) 201-216.

Appel, M.; Nuclear Magnetic Resonance and Formation Porosity, Petrophsyics, 45 (03), 2004

Awaja, F., Bhargava, S.; The prediction of clay contents in oil shale using DRIFTS and TGA data facilitated by multivariate calibration, Fuel 85 (2006) 1396–1402.

Bailey, L., Sawdon, C., Brady, M., and Cliffe, S.; New Insight into the Mechanisms of Shale Inhibition Using Water Based Silicate Drilling Fluids, paper SPE 39401 prepared for presentation at the 1998 IADC/SPE Drilling Conference held in Dallas, Texas, 3-6 March.

Ballard, T.J., Beare, S.P. and Lawless, T.A. (1992) Fundamental of shale stabilization: water transport through shales, Eur. Petro. Conf., Cannes, France, 16-18 Nov. 115-126pp.

Bergaya, F., Lagaly, G., Developments in Clay Science, Vol 5, 2013
Brigatti, M., Galan, E., Theng, B., "Handbook of Clay Science", Developments in Clay Science, Volume 5, 2013.

Boek, E., Coveney, P., Skipper, N., Monte Carlo Molecular Modeling Studies of Hydrated Li-, Na-, and K-Smectites: Understanding the Role of Potassium as a Clay Swelling Inhibitor, J. Am. Chem. Soc., 1995, 117, 12608-12617.

Bol, G.; The Effect of Various Polymers and Salts on Borehole and Cutting Stability in Water-Base Shale Drilling Fluids, paper SPE 14802 prepared for presentation at the 1986 IADC/SPE Drilling Conference held in Dallas, Texas, February 10-12.

Boruah, A., Ganapathi, S.; Microstructure and pore system analysis of Barren Measures Shale of Raniganj field, India, Journal of Natural Gas Science and Engineering, 26 (2015) 427-437.

Bourgoune, A., Millheim, K., Chenevert, M., and Young, F.; Applied Drilling Engineering, Society of Petroleum Engineers, Richardson, Texas, USA, 1986. ISBN 1-55563-001-4

Chakraborty, N., Karpyn, Z., Liu, S., Yoon, H.; Permeability Evolution of Shale during Spontaneous Imbibition, Journal of Natural Gas Science and Engineering, 38 (2017) 590-596

Chalmers, G.; Characterization of gas shale pore systems by porosimetry, pycnometry, surface area, and field emission scanning electron microscopy/transmission electron microscopy image analyses: Examples from the Barnett, Woodford, Haynesville, Marcellus, and Doig units, University of British Columbia, Vancouver, Canada, 2012.

Chatterjee, A., Mizukami, F., Miyamoto, A., Effect of Exchangeable Cation and Hydration Layer on the Swelling Property of 2:1 Dioctahedral Smectite Clay- A Periodic Density Functional Study, Studies in surface Science and Catalysis, 156, 2015.

Chenevert, M.; Shale Control with Balanced-Activity Oil-Continuous Muds, paper SPE 2559 presented at the SPE 44th Annual Fall Meeting held in Denver, Colorado, 28 October, 1969.

Chenevert, M.E. (1970), Shale alteration by water adsorption. J. of Petrol. Technology, Sept. 1141-1148pp.

Chenevert, M.; Shale Control with Balance-Activity Oil-Continuous Muds, Journal of Petroleum Technology, October, 1970.

Chen, T., Feng, X., Pan, Z.; Experimental study of swelling of organic rich shale in methane, International Journal of Coal Geology 150–151 (2015) 64–73.

C.P. Tan, Md. Amanullah, Fersheed K. Mody, and Uday M. Tare; Novel High Membrane Efficiency Water-Based Drilling Fluids for Alleviating Problems in Troublesome Shale Formations; Paper SPE 77192 prepared for presentation at the IADC/SPE Asia Pacific Drilling Technology (APDT), 9-11 September, Jakarta, Indonesia.

Cygan, R., Liang, J., Kalinichev, A., Molecular Models of Hydroxide, Oxyhydroxide, and Clay Phases and the Development of a General Force Field, Journal of Phys. Chem. (2004) 108, 1255-1266.

Cygan, R., Greathouse, J., Heinz, H., Kalinichev, A., Molecular models and simulations of layered materials, Journal of Materials Chemistry, 2009.

Darley, H.; A Laboratory Investigation of Borehole Stability, Journal of Petroleum Technology, July,

1969.

Deville, J., Fritz, B., and Jarrett, M.; Development of Water-Based Drilling Fluids Customized for Shale Reservoirs, SPE Drilling & Completion, December, 2011.

Ding, M. Kantzas, A.; "Estimation of Residual Gas Saturation from Different Reservoirs", paper PETSOC 2004-061, to be presented at the Petroleum Society's 5th Canadian International Petroleum Conference (55th Annual Technical Meeting), Calgary, Alberta, Canada, June 8 – 10, 2004.

Frenkel, H., Fey, M.; Clay Dispersion and Hydraulic Conductivity of Clay-Sand Mixtures as Affected by the Addition of Various Anions, Clay and Clay Minerals, Vol. 40, No. 5, pp 515-521, 1992.

Friedheim, J., and Sartor, G.; WBM with Triple- Inhibition Mechanism Demonstrates Near-OBM Performance in Deepwater Gulf of Mexico, paper presented at the Offshore Miditerranean Conference and Exhibition held in Ravenna, Italy, 26-28 Mrach, 2003.

Fu, M., Zhang, Z., Low, P.; Clays Clay Miner. 38 (1990) 485.

Ge, H., Yang, L., Shen, Y., Ren, K., Meng, F., Ji, W., Wu, S.; Experimental Investigation of Shale Imbibition Capacity and the Factors Influencing Loss of Hydraulic Fracturing Fluids, Journal of Petroleum Science (2015) 12:636-650

Gomaa, A., Zhang, B., Qu, Q., Nelson, S., Chen, J.; Using NMR Technology to Study the Flow of Fracture Fluids Inside Shale Formations, Paper SPE 168174 prepared for presentation at the SPE International Symposium and Exhibition on Formation Damage Control held in Lafayette, USA, 26-28 February 2014

Gomez, Sandra, and Patel, Arvind; Shale Inhibition: What Works?, paper SPE 164108 prepared for presentation at the SPE International Symposium on Oilfield Chemistry held in The Woodlands, Texas, USA, 8-10 April, 2013.

Gomez, I., Bryson, L., Hopkins, T.; Correlations between Geotechnical Properties and the Swell Behavior of Compacted Shales, ASCE, 2011.

Goodall, W,; Characterisation of mineralogy and gold deportment for complex tailings deposits using QEMSCAN, Minerals Engineering 21 (2008) 518–523.

Halawani, M., Duaiji, A., Bahabri, B., Basyoni, M., Dabbagh, M., Ramdan, K., Ajmi, H., Mahri, A.; Phanerozoic Stratigraphy of Saudi Arabia, Saudi Stratigraphic Committee, 2013.

Handy, L.; "Determination of Effective Capillary Pressures for Porous Media from Imbibition Data", PETROLEUM TRANSACTIONS, AIME, VOL. 219, 1960.

Hart, K; Capillary Suction Time Tests on Selected Clays and Shales, Thesis: The University of Texas at Austin, May 1989.

Hatch, C., Wiese, J., Crane, C., Harris, K., Kloss, H.; Water Adsorption on Clay Minerals As a Function of Relative Humidity: Application of BET and Freundlich Adsorption Models, Langmuir 2012, 28, 1790−1803

Hazra, B., Varma, A., Bandopadhyay, A., Chakravarty, S., Buragohain, J., Samad, S., Parsad, A.; FTIR,

XRF, XRD and SEM Characteristics of Permian Shales, India, Journal of Natural Gas Science and Engineering 32 (2016) 239-255.

Hayatdavoudi, A., and Apande, E.; A Theoretical Analysis of Wellbore Failure and Stability in Shales, the University of Louisiana Poster Papers, Chapter 81.

Huadi, F., Aldea, C., Mackereth, B., and Mukhlis, T.; Successful KCl-Free, Highly Inhibitive and Cost-Effective Water-Based Application, Offshore East Kalimantan, Indonesia, paper SPE 132690 prepared for presentation at the IADC/SPE Asia Pacific Drilling Technology Conference and Exhibition held in Ho Chi Minh City, Vietnam, 1-3 November, 2010.

Hensen, E., Smit, B.; Why Clays Swell, J. Phys. Chem. B 2002, 106, 12664-12667

Ismail, I., and Huang, A.; The Application of Methyl Glocoside as Shale Inhibitor in Sodium Chloride Mud, Jurnal Teknologi, June 2009, pp 53-65.

Jinhong, Z., Xiancai, L., Jianxi, Z., Xiandong, L., Jingming, W., Qing, Z., Peng, Y., Interlayer Structure and Dynamics of HDTMA+-Intercalated Rectorite with and without Water: A Molecular Dynamics Study, The Journal of Physical Chemistry, 2012.

Johansen, R., Dunning, H.; Water-Vapor Adsorption on Clays, Clays and Clay Minerals, 1957, 6: 249-258

Josh, M., Esteban, L., Piane, D., Sarout, J., Dewhurst, D., Clennell, M.; Laboratory Characterization of Shale Properties, Journal of Petroleum Science and Engineering, 88–89 (2012) 107–124.

Karger, J., Freude, D.; Mass Transfer in Micro- and Mesopourous Materials, Chem. Eng. Technol. 25 (2002) 8, Wiley-VCH,

Kawano, M., Tomita, K.; Further Investigations on the Rehydration Characterstics of Rectorite, Clays and Clay Minerals, Vol. 40, No. 4, 421-428, 1992.

Keller, L., Holzer, L., Wepf, R., Gasser, P.; 3D geometry and topology of pore pathways in Opalinus clay: Implications for mass transport, Applied Clay Science 52 (2011) 85–95.

Kendal, H.A. and Norton, P (1974), Clay mineralogy solutions to clay problems in Norway. J. Petrol. Technology, v.26, 25-32pp.

Li, K., Horne, R.; "Characterization of Spontaneous Water Imbibition into Gas-Saturated Rocks", paper SPE 62552 prepared for presentation at the 2000 SPE/AAPG Western Regional Meeting held in Long Beach, California, 19-23 June, 2000.

Louks, R., Ruppel, S.; Mississippian Barnett Shale: Lithofacies and depositional setting of a deep-water shale-gas succession in the Fort Worth Basin, Texas, The American Association of Petroleum Geologists, 2006.

Mackay, D., Simandl, G., Ma, W., Redfearn, M., Gravel, J; Indicator mineral-based exploration for carbonatites and related specialty metal deposits - A QEMSCAN® orientation survey, British Columbia, Canada, Journal of Geochemical Exploration 165 (2016) 159–173.

Makhanov, K. Dehghanpour, H., Kuru, E.; "An Experimental Study of Spontaneous Imbibition of Horn

River Shales", paper SPE 162650, 2012.

Militzer, B., Wenk, H., Stackhouse, S., Stixrude, L., First-principles calculation of the elastic moduli of sheet silicates and their application to shale anisotropy, American Mineralogist (2011), Volume 96, 125-137.

Mody, F., Hale, A.; Borehole-Stability Model to Couple the Mechanics and Chemistry of Drilling-fluid/Shale Interactions, Journal of Petroleum Technology, November, 1993.

Mooney, R., Keenan, A., Wood, L.; Adsorption of Water Vapor by Montmorillonite. II. Effect of Exchangeable Ions and Lattice Swelling as Measured by X-Ray Diffraction, Journal of the American Chemical Society (1952), 1370-1374.

Mukhopadhyay, S.; Sample Preparation for Microscopic and Spectroscopic Characterization of Solid Surfaces and Films, Sample Preparation Techniques in Analytical Chemistry, John Wiley & Sons, 2003.

Myers, D.; Invert Muds Help Reduce Sloughing Shale Problems, Oil & Gas Journal, 1993, http://www.ogj.com/articles/print/volume-91/issue-26/in-this-issue/drilling/invert-muds-help-reduce-sloughing-shale-problems.html, Access date: 9/13/2014.

Norrish, K.; The swelling of montmorillonite, Discussions of the Faraday Society (1954), 120-134.

Parfitt, R., Greenland, D.; Adsorption of Water by Montmorillonite-Poly(Ethylene Glycol) Adsorption Products, Clay Minerals (1970) 8, 317

Patel, A., Stamatakis, E., Young, S., and Friedheim, J.; Advances in Inhibitive Water-Based Drilling Fludis-Can They Replace Oil-Based Muds?, paper SPE 106476 prepared for presentation at the 2007 SPE International Symposium on Oilfield Chemistry held in Houston, Texas, USA, 28 February- 2 March, 2007.

Patel, A., Stamatakis, E., Friedheim, J., and Davis, E.; Highly Inhibitive Water-Based Fluid System Provides Superior Chemical Stabilization of Reactive Shale Formations, paper AADE 01-NC-HO-55 prepared for presentation at the AADE 2001 National Drilling Conference held at the Omni Houston Westside, Houston, Texas, 27-29 March, 2001.

Ramseyer, K., Boles, J.; Mixed-layer Illite/Smectite Minerals in Tertiary Sandstones and Shales, San Joaquin Basin, California. Clay, Clay Miner. 1986, 34, 115-124.

Riley, M., Stamatakis, E., Young, S., Hoelsher, K., Stefano, G., Ji, L., Guo, Q., and Friedheim, J.; Wellbore Stability in Unconventional Shale- The Design of a Nano-particle Fluid, paper SPE 153729 prepared for presentation at the SPE Oil and Gas India Conference and Exhibition held in Mumbai, India, 28-30 March, 2012.

Rodriguez, R.; Crandall, D.; Song, X.; Verba, C.; Soeder, D. Imaging Techniques for Analyzing Shale Pores and Minerals; NETL-TRS-6-2014; NETL: Technical Report Series; U.S. Department of Energy, National Energy Technology Laboratory: Morgantown, WV, 2014; p 40

Roehl, E. and Hackett, J.; A Laboratory Technique for Screening Shale Swelling Inhibitors, paper SPE 11117 prepared for presentation at the 57th Annual Fall Technical Conference and Exhibition held in New Orleans, LA, Sept. 26-29.

Santarelli, F., Aquitaine, E., Chenevert, M., and Osisanya, S.; On the Stability of Shales and Its Consequences in Terms of Swelling and Wellbore Stability, paper SPE 23886 prepared for presentation at the 1992 IADC/SPE Drilling Conference held in New Orleans, Louisiana, February 18-21, 1992.

Scholle, P., Ulmer-Scholle, D.; A Color Guide to The Petrography of Carbonate Rocks: Grains, texture, porosity, digenesis, the American Association of Petroleum Geologists, 2003.

Shen, Y., Ge, H., Li, C., Yang, X., Ren, K., Yang, Z., Su, S.; Water Imbibition of Shale and its Potential Influence on Shale Gas Recovery, Journal of Natural Gas Science and Engineering, 35 (2016) 1121-1128

Simpson, J.P., Dearing, H.L. and Salisbury, D.P. (1989), Downhole simulation cell shows unexpected effects of shale hydration on borehole wall. SPE Drilling Engineering, 24-30pp.

Sondergeld, C. H., Ambrose, R. J., Rai, C. S., & Moncrieff, J. (2010, January 1). Micro-Structural Studies of Gas Shales. Society of Petroleum Engineers. doi:10.2118/131771-MS

Sone, H., and Zoback, M.; Mechanical Properties of Shale-Gas Reservoir Rocks – Part 1: Static and Dynamic Elastic Properties and Anisotropy, Geophysics Journal, Vol. 78, No 5, September-October, 2013.

Steiger, R., and Leung, P.; Quantitative Determination of the Mechanical Properties of Shales, SPE Drilling Engineering, September 1992.

Stephens, M., Gomez, S., and Churan, M.; Laboratory Methods to Assess Shale Reactivity with Drilling Fluids, AADE 2009-NTCE-11-04, National Technical Conference & Exhibition, New Orleans, Louisiana.

Stephens, M., Gomez, S., and Churan, M.; Laboratory Methods to Assess Shale Reactivity with Drilling Fluids, AADE 2009-NTCE-11-04, National Technical Conference & Exhibition, New Orleans, Louisiana.

Stephens, M., and He, Wenwu; Drilling Fluids: Tackling Drilling, Production, Wellbore Stability, and Formation Evaluation Issues in Unconventional Resource Development, paper SPE 168710/ URTeC 1576637 prepared for presentation at the Unconventional Resources Technology Conference held in Denver, Colorado, USA, 12-14 August 2013.

Shen, S., Zaidi, S., Mutairi, B., Shehry, A., Sitepu, H., Hamoud, S., Khaldi, F., Edhaim, F.; Quantitative XRD Bulk and Clay Mineralogical Determination of Paleosol Sections of Unayzah and Basal Khuff Clastics in Saudi Arabia, Powder Diffraction 27 (2), June 2012.

Smith, W., Peter, C., Naylor, R., Mukhopadhyay, P., Kalkreuth, F., Macauley, G.; Composition and Depositional Environment of Major Easter Canadian Oil Shales, International Journal of Coal Geology, Volume 19, Issues 1–4, December 1991, Pages 385-438

Skipper, N., Refson, K., McConnell, J.; Computer simulation of interlayer water in 2:1 clays, The Journal of Chemical Physics, 94, 7434 (1991); doi: 10.1063/1.460175.

Stixrude, L., Peacor, R., First-principles study of illite–smectite and implications for clay mineral systems, Nature, Volume 420, November, 2002.

Sun, L., Tanskanen, J., Hirvi, J., Kasa, S., Schatz, T., Pakkanen, T., Molecular Dynamics Study of

Montmorillonite Crystalline Swelling: Roles of Interlayer Cation Species and Water Content, Chemical Physics (2015), 23-31.

Suter, J., Coveney, P., Greenwell, H., Thyveetil, M., Large-Scale Molecular Dynamics Study of Montmorillonite Clay: Emergence of Undulatory Fluctuations and determination of Material Properties, J. Phys. Chem. C 2007, 111, 8248-8259.

Syed, S., Qudaih, R., Talab, I., Janajreh, I.; Kinetics of pyrolysis and combustion of oil shale sample from thermogravimetric data, Fuel (2011), 1631-1637.

Tambach, T. et. al.; Molecular Simulations of Swelling Clay Minerals, J. Phys. Chem. B 2004, 108, 7586-7596.

Tao, L., Xiao, T., Yu, Z., Tao, G., Swelling of K+, Na+ and Ca2+-montmorillonites and hydration of interlayer cations: a molecular dynamics simulation, Chin. Phys. B Vol. 19, No. 10 (2010) 109101.

Tour, T.; Analysis Of Rocks Using X-Ray Fluorescence Spectrometry, The Rigaku Journal, Vol. 6, 1989.

Tang, X., Jiang, Z., Jiang, S., Li, Z.; Heterogeneous Nanoporosity of the Silurian Longmaxi Formation Shale Gas Reservoir in the Sichuan Basin using the QEMSCAN, FIB-SEM and Nano-CT Methods, Marine and Petroleum Geology 78 (2016) 99-109

Tour, T.; Analysis Of Rocks Using X-Ray Fluorescence Spectrometry, The Rigaku Journal, Vol. 6, 1989.

Wilcox. R.D., Fisk, Jr. J.V. and Corbett, G.E., (1987), Filtration method characterizes dispersive properties of shales. SPE Drilling Engineering, vol.2, June, 149-158pp.

Worden, R., Morad, S.; Clay Minerals in Sandstone: Controls on Formation, Distribution and Evolution, Wiley Online Library, 2003.

Washburn, K., Birdwell, J.; Application of Binomial-edited CPMG to Shale Characterization, Journal of Magnetic Resonance, 246, 72-78, 2014
Xradia, VersaXRM-500, User's Guide, January, 2011.

Xu, H., Zhao, T., et. al.; A precise measurement method for shale porosity with low-field nuclear magnetic resonance: a case study of the Carboniferous–Permian strata in the Linxing area, eastern Ordos Basin, China, Fuel, 143, 47-54, 2015

Yang, L., Ge, H., Shen, Y., Ren, K., Sheng, M., Gao, Z., Qin, X., Su, S.; Experimental Research on the Shale Imbibition Characteristics and its Relationship with Microstructure and Rock Mineralogy, paper SPE 176882 prepared for presentation at the SPE Asia Pacific Unconventional Resources Conference held in Australia, 9-11 November, 2015

Young, D. and Smith, D., Simulations of Clay Mineral Swelling and Hydration: Dependence upon Interlayer Ion Size and Charge, Journal of Phys. Chem. B 2000, 104, 9163-9170.

Zalasiewicz, J., Williams, M., Miller, M., Page, A., Blackett, E.; Early Silurian (Llandovery) graptolites from central Saudi Arabia: First documented record of Telychian faunas from the Arabian Peninsula, GeoArabia, Vol. 12, No. 4, 2007.

Zhou, J., Boek, E., Zhu, J., Lu, X., Sprik, M., He, H., Molecular Simulation Study of Hydrated Na-

Rectorite, Langmuir, Feb, 2015, DOI: 10.1021/la503900h.

Zhou, Q., Shen, W., Zhua, J., Zhua, R., He, H., Zhou, J., Yuan, P., Structure and dynamic properties of water saturated CTMA-montmorillonite: molecular dynamics simulations, Applied Clay Science, 2014.

Zhou, Z., and Law, D.; Swelling Clays in Hydrocarbon Reservoirs: the Bad, the Less Bad, and the Useful, 1998.

Zhou, T., Zhang, S., Yang, L., Ma, X., Zou, Y., Lin, H.; Experimental Investigation on Fracture Surface Strength Softening induced by Fracturing Fluid Imbibition and its Impact on Flow Conductivity in Shale Reservoirs, Journal of Natural Gas Science and Engineering, 36 (2016) 893-905

Zhou, Z., Abbas, H., Li, X., Bearinger, D., Frank, W.; Mechanisms of Imbibition during Hydraulic Fracturing in Shale Formations, Journal of Petroleum Science and Engineering, 141 (2016) 125-132

Zoback, M.; Reservoir Geomechanics, Cambridge University Press, New York, 2007

Vitae

Name	:Mohammed Khalid Al-Arfaj
Nationality	:Saudi
Date of Birth	:September 5th, 1983
Email	:mohammed.m0509@gmail.com
Address	:P.O.Box 5293 Dhahran 31311
Academic Background	:B.S. Chemical Engineering, KFUPM, Saudi Arabia, 2006
	MSc. Petroleum Engineering, Heriot-Watt University, Scotland, 2009

- More than 10 year of experience in drilling technology applications (Saudi Aramco): drilling fluids, loss circulation material, cementing and completion.
- More than 20 technical papers in conferences and journals as the main author and co-author
- (February 2016- Present)

  Working as a petroleum engineer in Saudi Aramco (EXPEC ARC)

  Development and field deployment of date seed-based loss circulation material

  Development and field deployment of date tree fiber-based loss circulation material

  Development of high flash oil base for oil-based drilling fluids

  Development and field deployment of a waste vegetable oil-based mud lubricant
- (February 2015- January 2016)

  One-year residency period (Full-time) at KFUPM to work on PhD dissertation
- (July 2013- January 2015)

  Worked as a petroleum engineer in Saudi Aramco (EXPEC ARC)

  Development of date seed-based fluid loss additive for drilling fluids

  Development of testing method for mudcake removal efficiency

  Development of testing method for spotting fluids

  Development of testing method for shale inhibition durability
- (January 2013- June 2013)

  Worked as a drilling engineer in Saudi Aramco (Drilling Technical Department)

Establishment of a drilling fluid database for all fields

Leading stuck pipe avoidance project

- (January 2012- December 2012)

  Worked as a drilling engineer in Saudi Aramco (Drilling & Workover)

  Handling drilling activities for two rigs

  Investigation of liner cement jobs in the North West fields

  Assessment of inhibitive drilling fluids to mitigate shale drilling problems

- (October 2009- December 2011)

  Worked as a Petroleum Engineer in Saudi Aramco (EXPEC ARC)

  Development of Nano-based drilling fluids for shale inhibition

  Development of volcanic ash-based drilling fluid

- (September 2008- September 2009)

  Pursuing MSc. in Petroleum Engineering at Heriot-Watt University

- (July 2006-August 2008)

  Working as a Petroleum Engineer in Saudi Aramco

  Department: EXPEC Advanced Research Center Dept.

  Worked on different projects:

  Evaluation of water and oil swellable packers and the effect of HCl on the swelling process

  Development of high-temperature retarders to mitigate differential cement setting in long deep liners

  Optimization of low density cement that can be utilized to eliminate the need for multi-stage cementing jobs

- (June 2005- August 2005)

  Worked as a process engineer under training in Saudi Aramco (Uthmaniyah Gas Plant)

  Worked on different process problems:

  Used simulators (HYSYS) to simulate different process in the gas plant

  Learned how to run a reactor to de-sulfurize natural gas

  Learned how to use mass balance equations to control the field streams

- Other skills:
    - Computer skills:
        - Programming C++ and Fortran languages
        - Using Eclipse, Petrel, Wellflow, PanSystem
        - Using Molecular Modeling software (Materials Studio and MedeA)
    - Communication skills
        - Conducted several technical presentations in national and international conferences